國立交通大學

電子工程學系電子研究所

博 士 論 文

以亮度／色彩對比為基礎的影像分析技術之研究

A Study of Image Analysis Techniques Based on Luminance/Color Contrast

研　究　生：陳信嘉

指 導 教 授：王聖智　博士


E
S
A
1896

以亮度／色彩對比為基礎的
影像分析技術之研究

A Study of Image Analysis Techniques Based on Luminance/Color Contrast

研 究 生：陳信嘉　　Student: Hsin-Chia Chen

指導教授：王聖智 博士　　Advisor: Dr. Sheng-Jyh Wang

國 立 交 通 大 學

電 子 工 程 學 系　　電 子 研 究 所 博 士 班

博 士 論 文

A Dissertation Submitted to

Department of Electronics Engineering & Institute of Electronics

College of Electrical Engineering and Computer Science

National Chiao Tung University

in Partial Fulfillment of the Requirements

for the Degree of

Doctor of Philosophy

in

Electronics Engineering

June 2006

Hsinchu, Taiwan, Republic of China

中 華 民 國 九 十 五 年 六 月


E
S
A
1896

以亮度／色彩對比為基礎的影像分析技術之研究

研究生：陳信嘉　　指導教授：王聖智博士

國立交通大學電子工程學系電子研究所　博士班

摘要

在本論文中，我們提出以亮度／色彩對比為基礎的客觀視覺評量以估測人類主觀視覺感受評量。針對不同的影像分析應用，如自動面板缺陷檢測應用及彩色切割應用，我們先透過設計視覺實驗得到人類在分析影像時的主觀視覺評量標準，並設計客觀評量因子來估測這些主觀視覺評量，最後再將這些客觀評量因子應用在自動面板缺陷檢測、彩色切割評量技術以及彩色切割技術上。

在傳統的影像分析系統流程中，包含有四個基本的步驟： 1) 影像擷取，2) 影像分析，3) 輸出影像分析結果，及 4) 分析結果評估。具體而言，在一個影像分析系統中，在輸入端我們輸入一張或多張影像進行分析，此系統將針對不同的影像分析應用，使用不同的影像分析技術來分析影像，並輸出分析結果。然後，再根據一些視覺感受評量來對影像分析結果進行評估。在這篇論文中，我們在傳統的影像分析系統流程中，增加兩個重要的分析程序，分別是視覺實驗以及亮度／色彩對比測量。為了得到和人眼主觀視覺分析影像一致之結果，我們針對不同的影像分析應用，分析亮度／色彩對比在人眼視覺感知中所扮演的角色。透過視覺實驗，我們針對不同的影像分析應用，定義合適的亮度／色彩對比，並且粹取出符合人類視覺感受的主觀視覺評量因子。之後，為了量測這些主觀視覺評量因

子，我們以亮度／色彩對比為基礎來發展客觀的視覺評量因子估測方法，並且應用在發展影像分析技術，以此來得到和以人眼分析影像近似的方法和結果。

對於不同的影像分析應用，人眼的主觀視覺評量因子可能不盡相同。在這篇論文中，我們討論了兩種不同的影像分析應用：1) 自動面板缺陷檢測以及 2) 彩色切割應用。在自動面板缺陷檢測的應用中，我們討論人類主觀視覺對低亮度對比的面板缺陷影像的之視覺評量因子及其量測問題。首先，我們先介紹在 Mori 等人發表的論文中所提到的以亮度對比為基礎的主觀視覺因子及其量測公式—SEMU 公式，同時介紹他們得到此一視覺因子的視覺實驗。結合 SEMU 公式，我們提出了一些影像分析技術，試著來偵測不同形態的面板缺陷。其中包括我們提出合適的偵測運算子，如 LOG 運算子，並且討論最佳的自動門檻值設定方法。

在彩色切割應用方面，我們針對包含少量紋理的彩色切割應用，考慮了人眼對於色彩對比的感受。在一張包含少量紋理的彩色影像中，低色彩對比的相鄰像素往往被視為相同的影像區塊，而相鄰高色彩對比的像素位置則為影像區塊的邊界。因此，我們在論文中討論人眼對色彩對比和色差的感受評量。另外，針對彩色切割應用，我們也考慮了人眼對於色彩對比的主觀視覺評量因子，如人眼對於過度切割 (over-segmentation) 的程度感受以及不足切割 (under-segmentation) 的程度感受 … 等等。對此，在論文中，我們透過視覺實驗來驗證這些主觀的視覺評量因子和彩色切割結果品質的關係。之後，我們設計了一些以色彩對比為基礎的客觀視覺評量方法，來估測這些主觀視覺評量因子。同時，我們結合這些設計出來的客觀視覺評量量化估測方法，應用在客觀的彩色切割結果評量以及發展彩色切割演算法的應用上。

最後，我們模擬驗證了所提出的以亮度／色彩對比為基礎的影像分析技術在不同的應用上的分析結果。其結果驗證，我們以亮度／色彩對比為基礎所設計的客觀評量因子和人類的主觀視覺評量因子有很高關聯性。而且，我們也驗證了，在針對不同的影像分析應用所設計的影像分析技術中，亮度／色彩對比的確扮演著不可或缺的角色。因此，如果可以有效率且有效地估測亮度／色彩對比，並且

用亮度／色彩對比為基礎來發展客觀視覺評量，以估測人眼在不同影像分析應用中的主觀視覺評量因子，我們可設計得到近似人類分析影像方法及結果的影像分析技術。

A Study of Image Analysis Techniques Based on Luminance/Color Contrast

Student：Hsin-Chia Chen　　Advisor：Dr. Sheng-Jyh Wang

Department of Electronics Engineering & Institute of Electronics

National Chiao Tung University

Abstract

In this dissertation, a study of image analysis techniques by correlating subjective visual qualities with objective visual quantities based on luminance/color contrast is presented. To mimic the way humans perform image analysis, some subjective visual quantities are considered. To extract and verify the applicability of these visual quantities, subjective experiments are performed first. Then, to measure these subjective visual quantities, some objective quantitative measures based on luminance/color contrast are proposed. With these objective quantitative measures, contrast-based image analysis techniques can be developed for various image analysis applications.

In the flow chart of a conventional image analysis system, four basic parts are included: 1) inputting of images to be analyzed, 2) image analysis with one or more techniques, 3) outputting of analyzed results, and 4) evaluation of the analyzed results. Specifically, given one or more images to be analyzed, different image analysis techniques are adopted for different applications. Then, the analyzed results are evaluated with some evaluation methods according to predefined visual perception requirements. In this dissertation, two more processes are added into an image

analysis system. They are 1) subjective experiments and 2) measurement of luminance/color contrast and/or measurement of visual perception quantities. To mimic the way humans perform image analysis, we need some suitable subjective visual quantities. To extract appropriate visual quantities that may well correspond to humans' perception, subjective experiments are needed. To estimate these subjective visual quantities for different applications, we need to propose effective and efficient objective quantitative measures.

In this dissertation, we consider two different image analysis applications: 1) automatic inspection for visual defects on LCD panels, and 2) color segmentation. For different image analysis applications, the applicable visual quantities will be different. In the automatic defect inspection application, we discuss the suitable visual quantities for the extraction of visual defects with low luminance contrast. Here, we follow Mori's proposal to quantify the degrees of image defects based on the luminance contrast and area size of visual defects. Based on Mori's subjective experiments, which were performed to relate human visual perception with the luminance contrast and area size of visual defects, and the SEMU formula, which was proposed by Mori et al for a quantitative measurement of visual perception, we may effectively quantify the degrees of image defects based on luminance contrast and defect area. The LOG operator is then used to detect several types of visual defects. An optimal thresholding mechanism is also discussed.

For the applications of color segmentation with little texture, we consider segmentation quality, degree of over-segmentation, and degree of under-segmentation as the visual quantities. To verify the correlation among these visual quantities, a few subjective experiments are performed. Here, we use color contrast to quantify these visual quantities. Usually, given a color image, adjacent pixels with low color-contrast are grouped into regions; while adjacent pixels with high color-contrast are regarded

as edges. For color segmentation, we define color-contrast in terms of visible color difference and invisible color difference. Then, some objective quantitative measures based on visible/invisible color difference are proposed to measure these aforementioned subjective visual quantities. In this dissertation, the "intra-region visual error" is proposed to measure the degree of under-segmentation, while the "inter-region visual error" is proposed to measure the degree of over-segmentation. With these visual measures, some image analysis techniques are proposed to perform color segmentation and also the evaluation of color segmentation.

With simulations for these two image analysis applications, some conclusions are drawn. First, the correlations between the luminance/color contrast-based quantitative measures and the visual quantities are really significant. Second, luminance/color contrast may play an important role in the development of image analysis techniques that mimic the way of human perception.

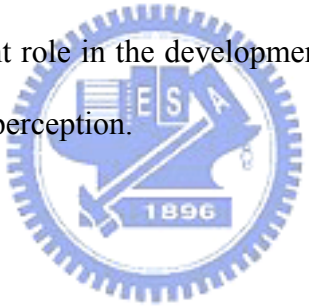

Acknowledgements

我的指導教授 – 王聖智博士，在我的人生中扮演了一個很重要的角色，他不僅是我在求學路上的領航者，亦是我生活上的明師。我在他身上看到了不僅止於學者風範、更有認真做學問的態度以及嚴謹做研究的精神。除了在學問上的深刻著磨，我亦在他身上學到對自我的健康、家庭負責任的態度及精神。如果沒有遇見他，我人生的劇本會完全不同調，非常感謝我敬愛的王老師。

得以在交大求學，我非常的幸運，電子系的蔡中博士、項春申博士、林大衛博士、杭學鳴博士、陳紹基博士、蔣迪豪博士以及電信系的謝世福博士 … 等彥碩是在我的求學期間引領我走學術的殿堂，開拓我的視野，實在有幸得沐春風。

在此，我要特別感謝我的父親母親總是讓我無後顧之憂，尤其家母在我畢業前先一步離我遠去，讓我有子欲養而親不待的感嘆，沒有她的鼓勵、支持及陪伴，我是無法順利完成學業。另外，我要感謝江宜玲小姐，她不但是我的得力助手，更是我精神上的支柱。

另外，趙子毅學長是我生命中另一位貴人，他提供我一個工作的機會，發揮所學的舞台，讓我在等待論文審稿的日子裡，可以有機會了解台灣 IC 設計產業的生態以及台灣 IC 設計公司在國際上的角色定位。

我要感謝的人實在不勝枚舉，交大影像視覺實驗室的郭倫嘉、陳俊宇、錢威融、陳宜賢 … 等人在研究上的相互砥礪。交大通訊多媒體實驗室的張峰誠學長、林郁男學長、吳俊榮學長 … 等人在求學上、研究上、生活上的相互扶持。交大電子所同期的王成業、李瑞梅、涂尚瑋 … 等人在求學上、生活上的相互支持。工業研究院的溫照華課長、鄭尚元課長、李訓銘 … 等人在專案上的相互合作。原相科技公司的林志新、魏守德、蔡彰哲、李泉欣、李宜方 … 等人在工作上的相互激盪。

最後，我要感謝我敬愛的博士班口試委員們，貝蘇章博士、陳永昌博士、黃

仲陵博士、范國清博士、辛正和博士、杭學鳴博士、陳稔博士、陳玲慧博士以及王聖智博士，很感謝您們的意見、愛護及教誨。

To my advisor, parents, and loved ones

Contents

List of Tables

List of Figures

List of Notations

$B(I)$	2nd derivative operator
C_{jnd}	Just noticeable difference
CR	Luminance Ratio
C_W	Luminance Contrast, or called Weber Contrast
ΔE^*_{Lab}	Color difference in CIE L*a*b* color space
$e(i, j)$	Edge weight for each edge in an RAG
$fk(Ri, Rj)$	k=1, 2, 3 denote the edge weight with respective to the PSNR function, the F function and the modified total visual error
$E_{intra}(I)$	Intra-region error
$E_{inter}(I)$	Inter-region error
$E_{total}(I)$	Total visual error
f(A)	The transformation function for the Mura area A

$filter_{LOG}(x)$	1-D LOG filter
$filter_{LOG}^{Round}$	Round-type LOG filter
$filter_{LOG}^{\text{Rectangular}}$	Rectangular -type LOG filter
$MSE(I)$	Mean Square Error
$ME_{\text{int}ra}(I)$	The modified intra-region error
$ME_{\text{int}er}(I)$	The modified intra-region error
$ME_{total}(I)$	Modified Total visual error
Mura	Defects as the visible imperfections of the FOS of a display screen in active use
$N(x;0,\sigma)$	A Gaussian function with zero mean and standard deviation σ
$PSNR(I)$	Peak Signal to Noise Ratio function
$Mura_{Cluster}(x,y)$	Round-type Cluster Mura
SEMU	Semi Mura
SNR	Signal to Noise Ratio
$u(t)$	The step function
$Var_{Estimed\_Noise}$	Variance of AWGN noise produced in the photography process
σ	Standard deviation
$\delta(x)$	The impulse function
$\varphi(x)$	The 2nd derivative of an intensity profile

CHAPTER 1

Introduction

In Section 1.1, the overview of this dissertation is introduced. Then, the organization and contribution of this dissertation is given in Section 1.2.

1.1 Dissertation Overview

As shown in Fig. 1.1, the block diagram within the blue contour shows a conventional flowchart for an image analysis system. In this flowchart, four essential steps are included: 1) inputting of images to be analyzed, 2) image analysis with one or more techniques, 3) outputting of analyzed results, and 4) evaluation of the analyzed results. Specifically, given one or more images to be analyzed, different image analysis techniques are adopted for different applications. The analyzed results are then evaluated with some evaluation methods according to predefined visual perception requirements. Especially, the evaluation methods could be further categorized into 1) objective evaluation methods and 2) subjective evaluation methods.

In this dissertation, two more processes are included: 1) subjective experiments

and 2) measurement of luminance/color contrast and/or measurement of visual perception quantities. To mimic the way humans perform image analysis, we need some suitable subjective visual quantities. For example, in color segmentation applications, subjective visual quantities such as the degree of segmentation quality, the degree of over-segmentation, and the degree of under-segmentation may be considered to be essential. To extract appropriate visual quantities that may well correspond to humans' perception, subjective experiments are necessary. Moreover, subjective experiments may also be useful in discovering the relationships among these selected visual quantities.

On the other hand, to measure these visual quantities for a specific application, we need to propose effective and efficient objective quantitative measures. In this dissertation, we consider the use of luminance/color contrast-based measures to mimic the way humans perform image analysis. In fact, in our study, the luminance/color contrast is used in the blocks of image analysis, evaluation methods, and subjective experiments in Fig. 1.1. For example, in the development of color segmentation algorithms, with proper definitions of color contrast in terms of color difference, we demand that pixels with invisible color difference are to be merged together, while pixels with visible color difference are treated as edges. Based on the visible color difference, some quantitative measures are proposed as the objective counterparts of the subjective visual quantities, which are considered in the subjective experiments. Based on the subjective experiments, the correlations between the subjective visual quantities and the objective quantitative measures are verified. Then, these objective measures can be used for the development of evaluation methods for color segmentation and/or for the development of color segmentation algorithms.

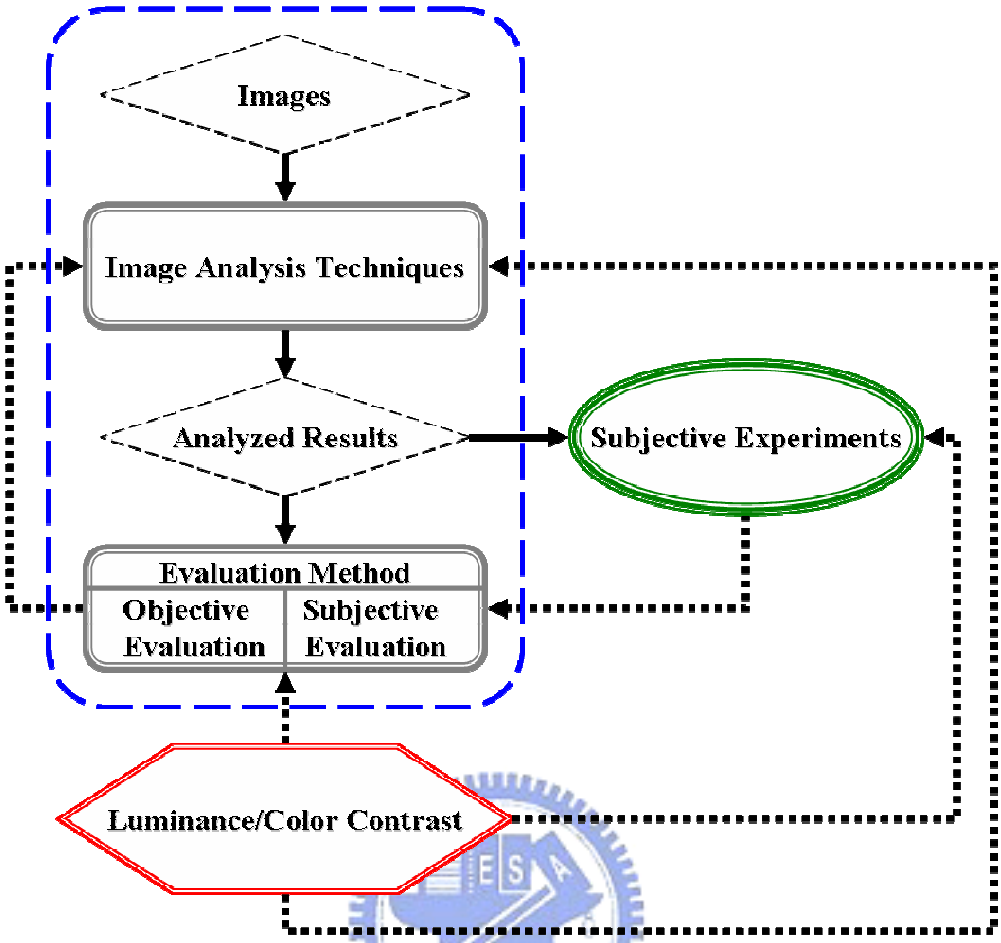

Fig. 1.1 Image Analysis Flowchart Based on Luminance/Color Contrast.

Fig. 1.2 and Fig. 1.3 show two examples for image analysis applications. Fig. 1.2 shows the illustration of a luminance contrast-based auto-inspection process for the detection of visual defects on LCD panels. On the other hand, Fig. 1.3 shows the illustration of a color contrast-based color segmentation process.

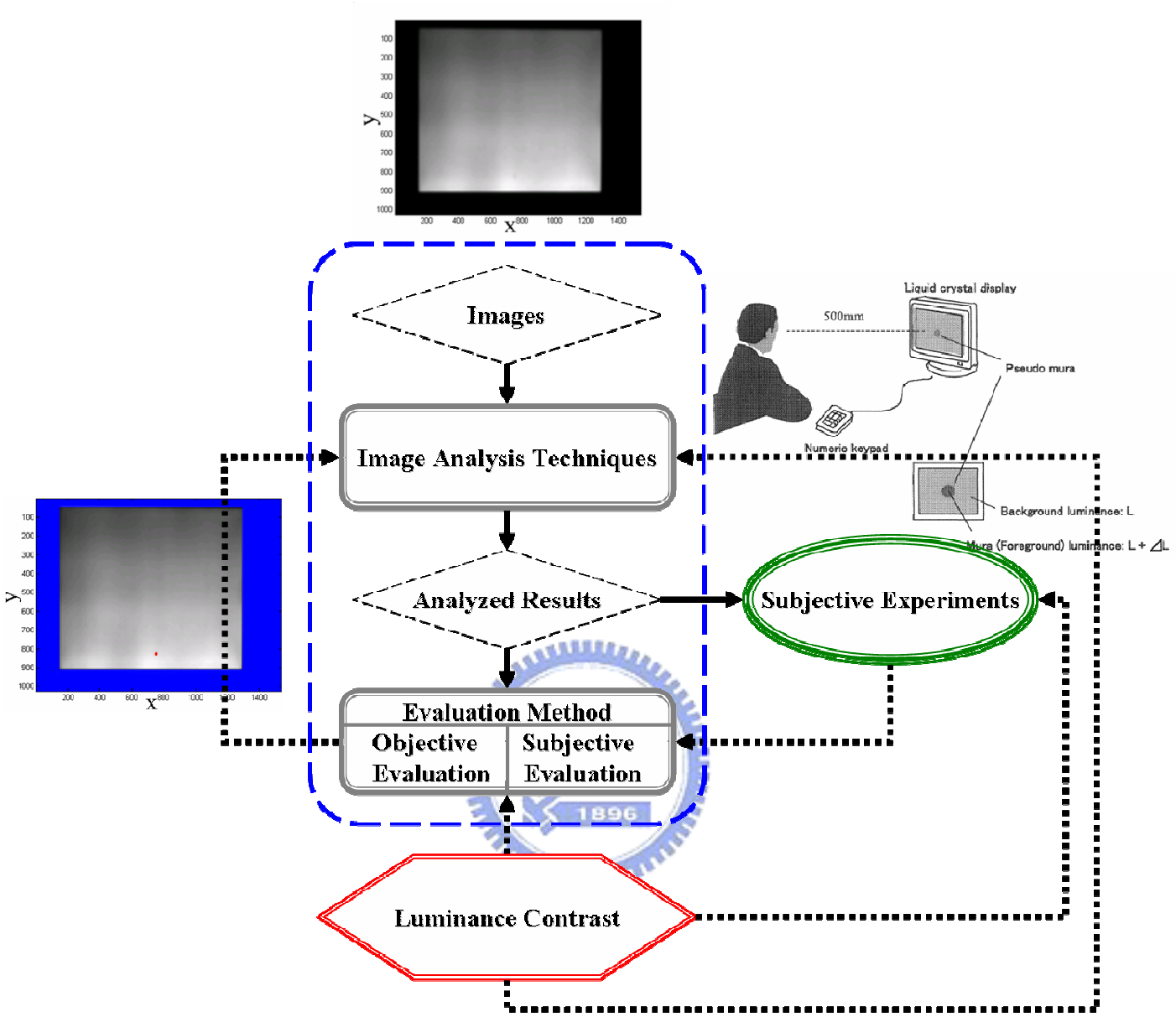

Fig. 1.2 Automatic Inspection Based on Luminance Contrast.

The gray-level image at the top of Fig. 1.2 represents the image of an LCD panel. Compared to a uniform background, the areas with noticeable luminance difference are considered as defects in human's perception. To mimic the way human detects these defects, some luminance contrast-based visual perception formulas, like the SEMU formula explored by Mori et al, can be deduced based on properly designed subjective experiments, as illustrated in the right side of Fig. 1.2. With this SEMU

formula, we develop an optimal threshold mechanism unified with some specified analysis techniques, as explained in Chapter 3 of this dissertation. The analyzed result is then shown in the left side of Fig. 1.2, where the red point indicates a detected Cluster Mura with a very low luminance contrast.

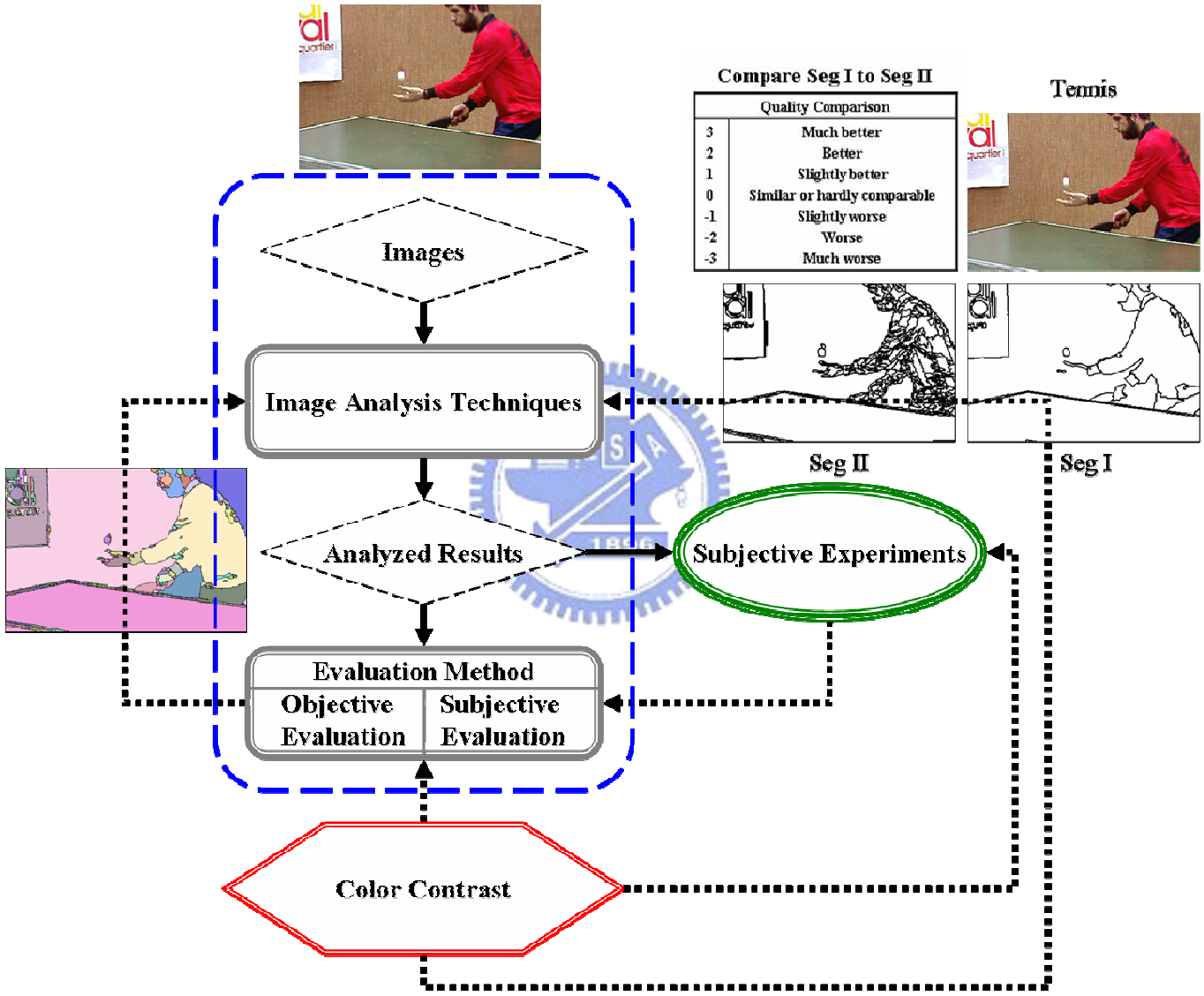

Fig. 1.3 Color Segmentation Based on Color Contrast.

On the other hand, Fig. 1.3 shows the illustration for color segmentation application. The top image shows the input image to be processed. To avoid directly measuring the subjective quality of color segmentation, two subjective visual

quantities, the quantity of missing boundaries and the quantity of fake boundaries, are considered in this dissertation. As shown in the right side of Fig. 1.3, a few subjective experiments are performed to verify the correlations between these two visual quantities and the quality of color segmentation. On the other hand, an objective quantity, named visible color difference, is defined. Intuitively, given a color image, adjacent pixels with invisible color difference are considered to be grouped together, while adjacent pixels with visible color difference are regarded as image edges. Hence, based on the visible color difference, some objective visual quantities, such as the "intra region visual error measure" and the "inter region visual error measure", are proposed to measure the degree of missing boundaries and the degree of fake boundaries. With the subjective experiments, the correlations between the subjective visual quantities and the objective quantitative measures can be verified. With these objective visual quantities, we may propose image analysis techniques for color segmentation and the evaluation color segmentation. For example, in the left side of Fig. 1.3, an image in pseudo colors indicates such a segmented result based on the developed color segmentation algorithm. In this image, pixels painted with the same color are segmented into the same region.

1.2 Organization and Contribution

The following chapters in this dissertation are organized as follows.

- In Chapter 2, some definitions of luminance/color contrast for different image analysis applications are introduced. Also, for the color segmentation issue, some existing image segmentation algorithms and evaluation methods in the literature are introduced.
- In Chapter 3, for the automatic inspection of defects on LCDs, a luminance contrast based formula, named SEMU formula, is introduced. A SEMU-based optimal thresholding mechanism is then proposed to automatically inspect Cluster defects on LCDs.
- In Section 4.1, the definition of a directional color contrast is proposed first. Then, with the directional color contrast, the definition of color contrast in the CIE L*a*b* color space is proposed. Also, a technique that can estimate the directional color contrast of color edges in a color image is proposed. On the other hand, a definition of "visible color difference" in the CIE L*a*b* color space is introduced to represent the effects of color difference in human visual perception. Then, based the defined color contrast, a so-called visible color difference is proposed to differentiate visible color difference from invisible color difference. In Section 4.2, some visual rating experiments are performed to verify the correlation between segmentation quality and degree of over-segmentation and/or degree of under-segmentation. Then, based on the defined "visible color difference" formula in Section 4.1, which are used to estimate the degree of over-segmentation, the degree of under-segmentation, and segmentation quality, some quantitative visual error measures are proposed. These quantitative measures are also used in the evaluation of color

segmentation. In Section 4.3, based on the directional color contrast introduced in Section 4.1, a color segmentation algorithm is proposed. On the other hand, uniting with the proposed quantitative evaluation method mentioned in Section 4.2, a new color segmentation algorithm is proposed.

- Finally, conclusions are drawn in Chapter 5.

CHAPTER 2

Backgrounds

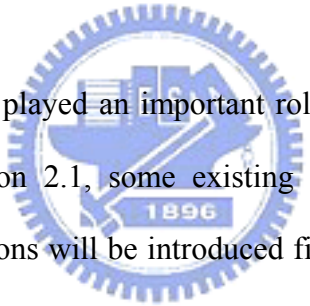

Luminance/color contrast has played an important role in the development of image analysis techniques. In Section 2.1, some existing definitions of luminance/color contrast for different applications will be introduced first. On the other hand, since in this dissertation the evaluation of image segmentation results is especially discussed, the backgrounds for image segmentation algorithms and related evaluation methods are briefly introduced in Section 2.2.

2.1 Luminance/Color Contrast

To measure luminance/color contrast, several definitions of luminance/color contrast have already been proposed for various applications. In Section 2.1.1, we first introduce some existing definitions of luminance contrast. Then, in Section 2.1.2, among a variety of color difference definitions, we introduce the CIE L*a*b* color difference. Based on the CIE L*a*b* color difference, we will propose in the following chapters a few more definitions about color difference.

2.1.1 Luminance Contrast

In this section, we introduce four commonly used definitions related to luminance contrast: 1) Luminance Contrast (Weber Contrast), 2) Luminance Ratio, 3) Peak-to-Peak Contrast (Michelson Contrast, Modulation), and 4) Just Noticeable Difference (JND). The details for each of these four definitions are as follows.

1) *Luminance Contrast, or Weber Contrast*:

To define the relationship between the luminance of an interested area and the luminance of the surrounding area, a measure called Weber contrast is defined in [1]:

$$C_W = (L_S - L_b) / L_b. \quad (2.1)$$

Here, L_S is the luminance of the interested area and L_b is the luminance of the adjacent background. In [1], a thorough technical discussion of this type of measure can be found.

When the background is brighter than the interested area, C_W is negative and ranges from zero to –1. On the contrary, when the background is darker, C_W is a positive number that can be potentially very large. Hence, the sign and value of Cw can be used to describe the relationship between the luminance of an interested area and the luminance of the adjacent background.

2) *Luminance Ratio*:

To specify the difference between bright parts and dark parts in a photo, another measure called Contrast Ratio is often used. This contrast ratio is defined as:

$$CR = L_S / L_b. \quad (2.2)$$

In practice, a logarithmic variation of this CR definition, as expressed in (2.3), is also widely used.

$$\log(CR) = \log(L_S) - \log(L_b). \quad (2.3)$$

In Equation (2.2), the contrast ratio is defined as L_S divided by L_b, where L_S and L_b have the same definitions as that in (2.1). The L_b in the denominator is often a reasonable estimate of the adapted luminance level around this stimulus level in human eyes. Instead of the luminance difference away from the background, the numerator is defined as the luminance of the interested area, Hence, this CR definition has a rather different mathematical behavior from the Weber contrast.

3) *Peak-to-Peak Contrast* (*Michelson Contrast, Modulation*):

To determine the strength of a signal luminance relative to the noise luminance level [1], a measure which evaluates the relation between the spread and the sum of signal and noise is introduced. Here, we have

$$\text{Modulation} = (\text{Lmax} - \text{Lmin}) / (\text{Lmax} + \text{Lmin}) \quad (2.4)$$

In the context of human vision, such kind of noise fluctuation could be caused by scattered lights introduced into the view path by a translucent element, which partly obscures the scene behind it.

4) JND (Abbreviation for *Just Noticeable Difference*) [2]:

For a certain stimulus, the smallest change in the stimulus that can be perceived by human is called the JND. The JND measure is usually used in the study of Psychophysics. Specifically, this definition is often used to indicate a measure in the statistical sense that the probability of being "perceptible" is 50%. For different applications, the definition of the JND measure could be different. Especially in the FPD (Flat Panel Display) visual inspection problem that is to be discussed in this dissertation, the JND over a uniform luminance background is regarded as a gauge of luminance contrast.

2.1.2 CIE L*a*b* Color Difference

On the other hand, for color images, color difference is usually adopted as a gauge of color contrast. Among a variety of color difference definitions, we focus on the CIE L*a*b* color difference. In Section 2.1.2.1, the CIE L*a*b* color space is to be introduced. The color space transformation from the RGB color space to the CIE L*a*b* color space is also described. Then, in Section 2.1.2.2, we introduce the definition of color difference in this CIE L*a*b* color space.

2.1.2.1 CIE L*a*b* Color Space

In the analysis of colors, a proper choice of the color space is a key issue. In this dissertation, we demand three major requirements in the selection of color space: 1) separation of achromatic information from chromatic information, 2) uniform color space, and 3) similar to human visual perception. Among various color spaces, we pick the CIE L*a*b* color space. In this color space, L* represents luminance, while a* and b* represent color components. The definitions for L*, a*, and b* are expressed as follows.

$$L^* = 116 \times \left[f\left(\frac{Y}{Y_n}\right) \right] - 16, \tag{2.5}$$

$$a^* = 500 \times \left[f\left(\frac{X}{X_n}\right) - f\left(\frac{Y}{Y_n}\right) \right], \tag{2.6}$$

$$b^* = 200 \times \left[f\left(\frac{Y}{Y_n}\right) - f\left(\frac{Z}{Z_n}\right) \right], \tag{2.7}$$

$$\begin{cases} f\left(\frac{Y}{Y_n}\right) = \left(\frac{Y}{Y_n}\right)^{1/3}, & \text{for } \frac{Y}{Y_n} > 0.008856; \\ f\left(\frac{Y}{Y_n}\right) = 7.787 \times \left(\frac{Y}{Y_n}\right) + \frac{16}{116}, & \text{for } \frac{Y}{Y_n} \le 0.008856; \end{cases} \tag{2.8}$$

(X_n, Y_n, Z_n): Reference white

The detail about the CIE L*a*b* space can be easily found in many color related books, like [6]. In Figure 2.1, we show an illustration of this CIE L*a*b* color space.

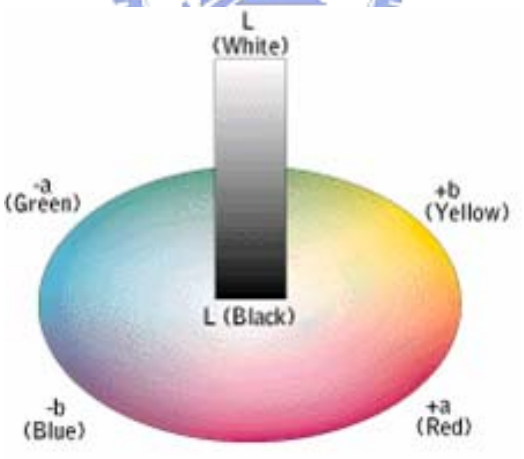

Fig. 2.1 Illustration of the CIE L*a*b* color space [7].

On the other hand, Fig. 2.2 illustrates the color transformation from the CIE L*a*b* color space to the RGB color space. To digitize colors in photos, the (L*,a*,b*) values within an area of interest are first converted to (R_t, G_t, B_t) by using Equations (2.5)(2.6) (2.7)(2.8), and (2.9).

$$\begin{bmatrix} X \\ Y \\ Z \end{bmatrix} = \begin{bmatrix} C_{11} & C_{12} & C_{13} \\ C_{21} & C_{22} & C_{23} \\ C_{31} & C_{32} & C_{33} \end{bmatrix} \cdot \begin{bmatrix} R_t \\ G_t \\ B_t \end{bmatrix} \tag{2.9}$$

In (2.9), R_t, G_t, and B_t are stimulus values captured from the scenery. C_{11}, C_{12}, …, C_{33} are the coefficients of the color transformation from the RGB color space to the XYZ color space.

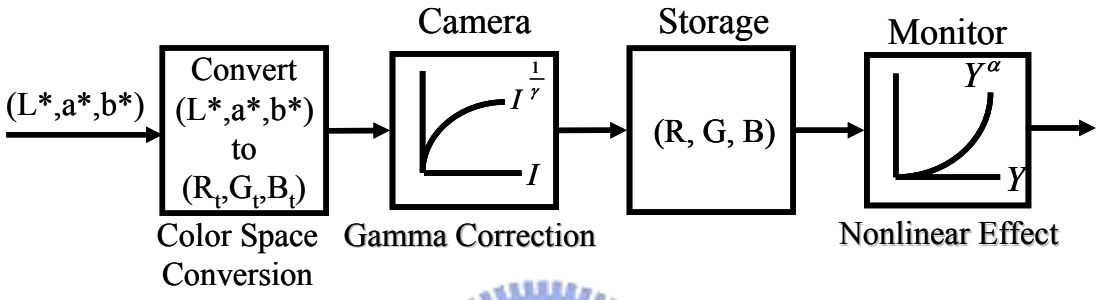

Fig. 2.2 Color space transformation from the CIE L*a*b* space to the RGB color space.

Then, for the compression of data size and the compensation of the nonlinear effect of the monitors, the (R_t, G_t, B_t) values are further mapped to the (R, G, B) values by applying the Gamma correction process expressed in Equation (2.10).

$$(R_t, G_t, B_t) = (R^{\gamma_R}, G^{\gamma_G}, B^{\gamma_B}). \tag{2.10}$$

In Equation (2.10), $\gamma_R, \gamma_G, \gamma_B$ indicate the nonlinear gamma factors for the R, G, and G channels of the output monitor.

2.1.2.2 Color Difference in CIE L*a*b* Color Space

In the CIE L*a*b* space, the differences of color components between Patch X and Patch Y are defined by their differences in lightness (ΔL^*), redness-greenness (Δa^*), and yellowness-blueness (Δb^*). That is,

$$\Delta L^* = L_X^* - L_Y^* \tag{2.11}$$

$$\Delta a^* = a_X^* - a_Y^* \tag{2.12}$$

$$\Delta b^* = b_X^* - b_Y^* \tag{2.13}$$

The overall color difference between these two samples is defined as the Euclidean distance in the CIE L*a*b*. That is,

$$\Delta E_{ab}^* = [(\Delta L^*)^2 + (\Delta a^*) + (\Delta b^*)]^{1/2} \tag{2.14}$$

The differences in color can also be defined by the differences in lightness (ΔL^*), chroma (ΔC_{ab}^*), and hue (ΔH_{ab}^*) [8]. In mathematics, we have

$$\Delta L^* = L_A^* - L_B^* \tag{2.15}$$

$$\Delta C_{ab}^* = (a_A^{*2} + b_A^{*2})^{1/2} - (a_B^{*2} + b_B^{*2})^{1/2} \tag{2.16}$$

$$\Delta H_{ab}^* = [(\Delta E_{ab}^*)^2 - (\Delta L^*)^2 - (\Delta C_{ab}^*)^2]^{1/2} \tag{2.17}$$

or

$$\Delta E_{ab}^* = [(\Delta L^*)^2 + (\Delta C_{ab}^*) + (\Delta H_{ab}^*)]^{1/2}. \tag{2.18}$$

2.2 Introduction of Image Segmentation

In Section 2.2.1, we will introduce some existing image segmentation algorithms first. Then, evaluation methods for color segmentation are introduced in Section 2.2.2.

2.2.1 Image Segmentation Algorithms

In recent years, plenty of efforts have been focusing on the segmentation of color images. In general, current image segmentation algorithms can be roughly classified into three major categories: 1) image domain-based techniques; 2) feature space-based techniques; and 3) physics-based techniques [13]. For image domain-based techniques, like [14], the similarity of neighboring pixels or the discontinuity of local information is used as the gauge for segmentation. Adjacent pixels with small intensity/color variations are merged together, while pixels with large enough variations are split apart. For feature space-based techniques, like [26], the data distribution of the entire image plays a crucial role. Clustering or grouping techniques are usually applied over the data distribution to allot image data into groups. On the other hand, for physics-based techniques, the adopted mathematical tools are basically the same as the former two kinds of techniques, while an underlying physical model is used to account for the reflection properties of colored matter [40].

2.2.1.1 Image Domain-Based Approaches

In general, for image domain-based techniques, the similarity of neighboring pixels or the discontinuity of local information is used as the gauge for segmentation. These image domain-based methods could be roughly classified into two kinds of methods: 1) edge-based methods and 2) region-based methods. Edge-based methods usually split apart pixels with large enough data variations, while region-based methods

merge together adjacent pixels with small intensity/color variations.

2.2.1.1.1 Edge-Based Methods

As mentioned above, edge-based methods usually split apart pixels with large enough data variations. So far, plentiful methods have been proposed to detect image boundaries/edges. For example, in [16], to detect boundaries in a given image, three criteria are introduced by the author: 1) good detection, 2) good localization, and 3) single response to a single edge. To have good boundary detection, the detector maximizes the signal-to-noise ratio; on the other hand, to have good localization of boundaries, the detected edge points should be as close to the position of the true edge as possible. With these three criteria, the author finds the optimal detector based on numerical optimization. In [14] and [18], the authors proposed a boundary detection scheme based on "edge flow". This scheme utilizes a predictive coding model to identify the direction of change in colors and textures at each image location at a given scale. An edge flow vector at each image location is then constructed. By propagating the edge flow vectors, the boundaries can be detected at the image locations where two opposite directions of flow are encountered in a stable state. On the other hand, in [17] and [19], the gradient vector of intensity/color data is used as a gauge to locate boundaries. Usually, the locations with large gradient values are regarded as the locations of edges.

2.2.1.1.2 Region-Based Methods

Different from edge-based methods, region-based methods merge adjacent pixels with small intensity/color variations into regions. In [15] and [23], colors in an image are first quantized into several representative classes. These image pixels are then replaced by the corresponding color-class labels. Then, a criterion using the class-map

is proposed to estimate the data variations in local windows. A region growing method is used to segment the image based on the estimated data variations. In [20][21][22][25], image gradient is used as a gauge to estimate image boundaries/edges. By applying the watershed transform on the gradient magnitude, primitive regions can be produced. Then, region competition, region growing, and/or region merging are used to produce the final segmentation results.

2.2.1.2 Feature Space-Based Approaches

For feature space-based techniques [26], the data distribution of the entire image plays a crucial role. Clustering or grouping techniques are usually applied over the data distribution to allot image data into groups. In [26] and [33], given a color image, a neighborhood is modeled as a distribution of colors. Then, the authors tried to show that the increase in the accuracy of the representation causes higher-quality results for low-level vision tasks on complicated natural images, especially as the size neighborhood increases. In [27][30][32], the authors proposed a general non-parametric technique to analyze a complex multimodal feature space and to delineate arbitrarily shaped clusters in the feature space. A recursive mean shift procedure is used to detect the modes of the distribution. Based on the estimated modes of the distribution, an image segmentation algorithm is performed by classifying images pixels into corresponding clusters. On the other hand, in [29] and [34], the authors treated image segmentation as a graph partitioning problem and proposed a so-called “normalized cut” method to segment the graph. The normalized cut method measures the overall dissimilarity between different groups as well as the overall similarity within the groups. In [31], image segmentation is formulated as a data clustering problem based sparse proximity data. Dissimilarities of pairs of textured regions are computed based on a multiscale Gabor filter representation. Then,

an optimization framework, which uses statistical tests as a measure of homogeneity, is proposed for unsupervised texture segmentation. In [35], the authors extended the general idea of a histogram to the homogeneity domain. Then, uniform regions are identified via multi-level thresholding on the homogeneity histogram. On the other hand, in [36][37][38], based on statistical frameworks with the assumption of Gaussian/Non-Gaussian densities, image analysis techniques, such as expectation maximization, independent component analysis, or Data-Driven Markov Chain Monte Carlo, are applied for image segmentation.

2.2.1.3 Physics-Based Approaches

For physics-based techniques, the adopted mathematical tools are basically the same as the former two kinds of techniques, while an underlying physical model is used to account for the reflection properties of colored matter [40]. In [13] and [40], several photometric invariant similarity measures are proposed to assist image analysis techniques in handling undesired imaging conditions, such as shading, shadows, illumination changes, and highlights.

2.2.2 Evaluation Methods for Image Segmentation

Color segmentation is a crucial step in image analysis and pattern recognition. The performance of color segmentation may significantly affect the quality of an image understanding system. So far, hundreds of color segmentation algorithms have already been developed to deal with various kinds of image-related applications [13][41]. For these color segmentation algorithms, the automatic setting of controlling parameters is usually a difficult task. Currently, these control parameters are often adjusted by the users in an interactive and tiresome manner. Moreover, the selection of control parameters is also image-dependent. For most color segmentation algorithms, there exists no parameter setting that is universally applicable.

On the other hand, it is well known that performance evaluation of segmentation algorithms is critical and essential in the development of image understanding systems. However, as compared with the tremendous efforts spent in the development of segmentation algorithms, relatively fewer efforts have been made on the subject of image segmentation evaluation [42][43][44][45][46]. As shown in Fig. 2.3, Zhang classified existing evaluation methods for image segmentation into three categories [42][43]: 1) analytical methods; 2) discrepancy methods; and 3) goodness methods. Analytical methods directly evaluate segmentation algorithms by analyzing their principles, requirements, utilities and complexity, etc [42][43]. Due to the lack of a general theory for image segmentation, analytical methods work well only for some particular models or for some desirable properties of the algorithms. Moreover, these analytical methods themselves are seldom used alone. On the contrary, both discrepancy methods and goodness methods evaluate the performance of segmentation by judging the quality of segmentation results directly. Especially, discrepancy methods measure the difference between the segmentation result and a

reference result, which is usually an expected result or a ground truth [47][48]. On the other hand, as illustrated in Fig. 2.3, goodness methods evaluate the segmentation results directly with certain quality measures, without the use of any reference result.

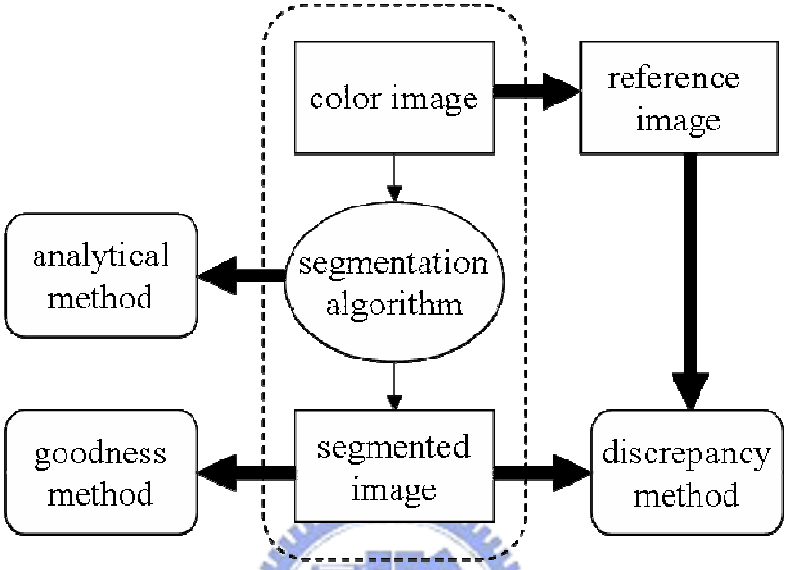

Fig. 2.3 Approaches for Evaluating Image Segmentation [42][43].

Among these three evaluation categories, the third type of methods, the goodness methods, is considered a more practical approach due to its direct evaluation of segmentation results without any user-dependent ground truth [49][50]. In this dissertation, we'll focus on this type of evaluation methods. Moreover, we believe that, some evaluation principles and formulas in these evaluation methods can be used to facilitate the development of segmentation algorithm. Hence, some goodness measures that had been proposed before are to be used in the development of a segmentation algorithm in this dissertation.

So far, several goodness methods have already been proposed [42][43][49][50]. One type of method is to evaluate segmented results with the use of the "Peak Signal to Noise Ratio" (PSNR) function, which is defined as follows:

$$PSNR\ (f) = 10\ \mathbf{log}_{10}\left(\frac{255^{2}}{MSE\ (I)}\right), \text{ and} \tag{2.19}$$

$$MSE\ (f) = \sum_{x=1}^{N}\sum_{y=1}^{M}\left(f(x,y) - f'(x,y)\right)^{2} / (N \times M), \tag{2.20}$$

where I is an $N \times M$ color image $f(x,y)$, and $f'(x,y)$ is denoted as the segmented result, with the color of each segmented region being filled with the average color of that region. Then, with a specified region number, the desired segmented results are defined to be the results with the maximal PSNR value, or equally with the minimum MSE value. In general, this type of method tends to measure the within-region color difference between the original color image and the segmented result. However, due to the lack of consideration regarding the color contrast between adjacent regions, this type of method tends to prefer over-segmented results, which include many small regions. This is because a larger value of MSE would be expected when we merge several small regions into a large one.

To avoid producing overly segmented results, the factor of region area is considered in the approach proposed by Liu and Yang [49]. In their approach, an evaluation function named F function is defined as:

$$F(I) = \frac{1}{1000\ (N \times M)}\sqrt{R} \times \sum_{i=1}^{R}\frac{e_i^{2}}{\sqrt{A_i}}, \tag{2.21}$$

where I is the image to be segmented, R is the number of regions in the segmented image, e_i is the color error of the ith region, A_i is the area of the ith region, and N, M represent the length and width of the image. Here, e_i is defined as the sum of the Euclidean distance in the RGB color space between the color vectors in the original image and the color vectors in the segmented image, in the ith region. Consequently, with a smaller F-function value, the segmented result is regarded to be better.

Although these methods take the factor of region area into account to avoid the

segmented results from including too many small regions, the relation between color difference and region area is not clearly treated. Hence, these F-function based methods may include both over-segmented regions and under-segmented regions at the same time. Furthermore, since these evaluation functions only consider the color differences within regions but ignore the color contrast between regions, they may cause some undesired circumstances. For example, the segmented result with each pixel being labeled as an independent region may be treated as a "perfect" result without any color difference error.

Based on Equation (2.21), two further improved evaluation functions are proposed in [50] that are defined as:

$$F'(I) = \frac{1}{10000\ (N \times M)} \times \sqrt{\sum_{A=1}^{Max} [R(A)]^{1+1/A}} \times \sum_{i=1}^{R} \frac{e_i^2}{\sqrt{A_i}}, \qquad (2.22)$$

and

$$Q(I) = \frac{1}{10000\ (N \times M)} \times \sqrt{R} \times \sum_{i=1}^{R} \left[\frac{e_i^2}{1 + \log A_i} + \left(\frac{R(A_i)}{A_i} \right)^2 \right], \qquad (2.23)$$

where $R(A_i)$ represents the number of regions with the area size A_i. In both equations, the areas of regions are considered to punish these segmentation results with too many small regions. Similarly, the number of segmented regions is also included, aiming to achieve segmented results with an appropriate number of homogeneous regions.

For the above evaluation functions, two primary requirements are adopted to define "preferred" segmentation results: smaller color difference and fewer segmented regions. However, color difference and the number of segmented regions are two very different measures in their physical meanings. The trade-off between these two measures would be very difficult. Moreover, the preferred number of segmented regions could be very different from image to image. When this image-dependent measure is involved in a single evaluation function, it would be rather difficult to

perform segmentation evaluation without having the prior knowledge of the image contents in advance.

In summary, although several goodness functions have already been proposed, most of them are not directly based on human visual perception. Instead, most goodness methods combine several existing measures together to formulate their evaluation functions. The selection and combination of measures are usually subjective. The adjustment of weighting coefficients is often troublesome. Moreover, for most evaluation methods, the quality of segmentation is usually represented in a single function, which mixes together several weakly related measures. Without knowing the erroneous information about the segmented result under evaluation, these approaches could be very unreliable.

CHAPTER 3

Visual Inspection for Mura on LCDs Based on Luminance Contrast

3.1 Introduction of Automatic Inspection for Mura on LCDs

Recently, Liquid Crystal Displays (LCDs) have received increasing market attention because of the decreasing prices and the improved visual quality. Among several characteristics regarding the visual quality of LCDs, the front-of-screen (FOS) quality of LCDs is essential. Most existing FOS quality tests depend on the perception of human eyes. However, human inspection needs higher labor power and usually causes inefficient and inconsistent inspection. Instead of human inspection, automatic inspection that employs efficient algorithms over photographed images could be a reasonable and reliable way to evaluate the FOS quality of LCDs.

So far, several efforts have been spent on the fulfillment of defect classification

and the establishment of quality evaluation standards [2][9]. For example, the Video Electronics Standards Association (VESA) has been carrying activities related to the standards for classifying defects [9], and the Semiconductor Equipment and Materials International (SEMI) has spent a lot of efforts on the standardization of defect quantification [2]. However, even though there is a high demand of automatic inspection of FOS quality, there are relatively few efforts spent on the development of defect detection algorithms [3][10][11][12].

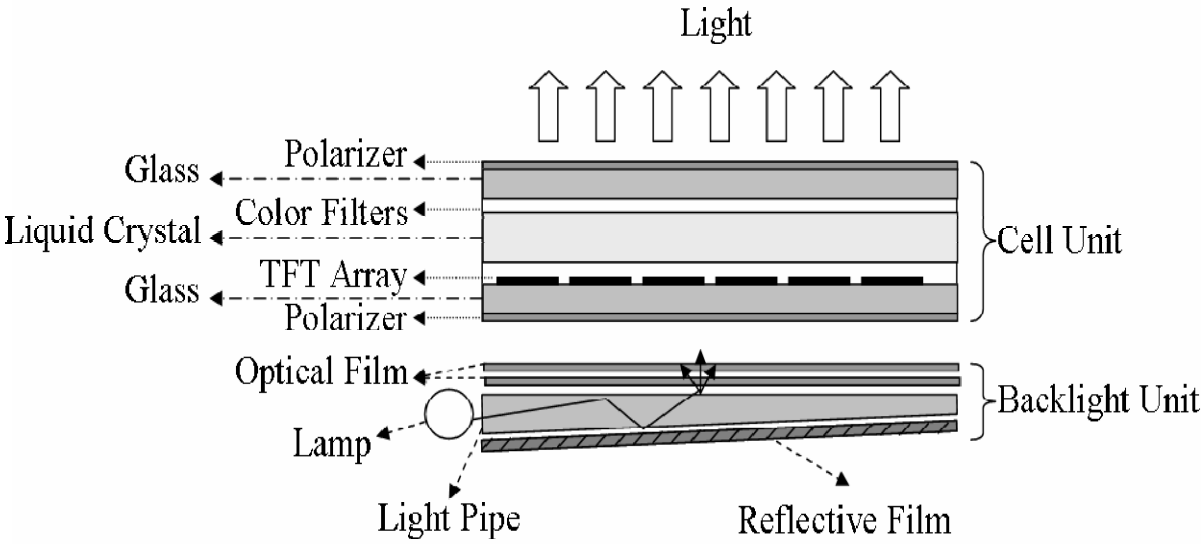

Fig. 3.1 Cross-section of an active matrix TFT-LCD.

In this chapter, we focus on the development of detection algorithms for the inspection of the FOS quality of an active matrix thin-film transistor liquid crystal display (AM TFT-LCD). Fig. 3.1 illustrates the cross-section of an AM TFT-LCD. Basically, an LCD display includes two essential components: Cell Unit and Backlight Unit. In the cell unit, there are mainly five elements: liquid crystal, thin-film-transistor (TFT) array, color filters, glasses, and polarizer. In general, the functionality of cell unit is to make the RGB color switching at each pixel controllable. On the other hand, in the backlight unit, there are four basic elements: lamp, light pipe,

reflective film and optical film. Generally, the functionality of backlight unit is to produce uniform light.

In the inspection of FOS quality, the so-called Mura defects greatly influence the FOS quality [9]. The Mura defects are defined as the visible imperfections of the FOS of a display screen in active use. Mura defects usually appear as a low contrast, non-uniform brightness regions, typically larger than a single pixel [2]. As shown in Table 3.1 Mori et al [10] listed several causes of Mura defects in TFT-LCD. Usually, the manufacturing performance of each component in the cell unit or in the backlight unit would affect the appearance of Mura defects. A superior manufacture process produces fewer Mura defects. Usually, the non-uniformity in various kinds of components induces different kinds of Mura defects.

Table 3.1 Causes of Mura defects on TFT-LCD [10]

Basic Unit	Causes of Mura
Cell unit	(1) Non-uniform gap between glasses
	(2) Non-uniform color of color filter
	(3) Non-uniform density of liquid crystal
	(4) Non-uniform thickness of TFT array layer
Backlight unit	(5) Wrinkled optical filter
	(6) Non-uniform lamp's rays

3.1.1 SEMU Formula Based on Just Noticeable Difference

As mentioned above, Mura indicates the defects as the visible imperfections on the FOS of a display screen. To make standard for the quantification of Mura phenomenon, a committee in SEMI defines a measurement index for Mura in the inspection of FPD (Flat Panel Display) image quality. To define Mura, an ergonomic approach is used to investigate human eye's sensitivity with respect to Mura by exploring the relation between Mura's area and contrast. Also, an index, named SEMU (Semi Mura), is defined to express the degree of Mura defects. This SEMU index is defined to be the ratio of the target's contrast over the contrast at JND. To deduce the SEMU formula, a subjective experiment had been conducted in [3], as shown in Fig. 3.2. In this experiment, a special LCD panel was produced to display 256 gradations in the luminance range between 43 cd/m^2 and 54 cd/m^2. A program created synthesized Mura and displayed the Mura at the center of the LCD panel. The observer looked at the screen with both eyes without any artificial pupil. The viewing direction is normal to the center of the LCD panel and the viewing distance is 500 mm. The experiments were performed in a darkroom and the observer could freely adjust the luminance of the displayed Mura by using a numeric keypad. The test began with the gray level of the synthesized Mura set to the same level as that of the background. Then, the observer adjusted the luminance of the Mura to the level where the Mura region was just perceptible and also to another level where the Mura can be clearly detected. The contrast values of the synthesized Mura at both levels were recorded. The contrast at the first level provided the data for the JND (Just Noticeable Difference) contrast, while the contrast at the second level provided the data for the "Dist (Distinct difference)" contrast.

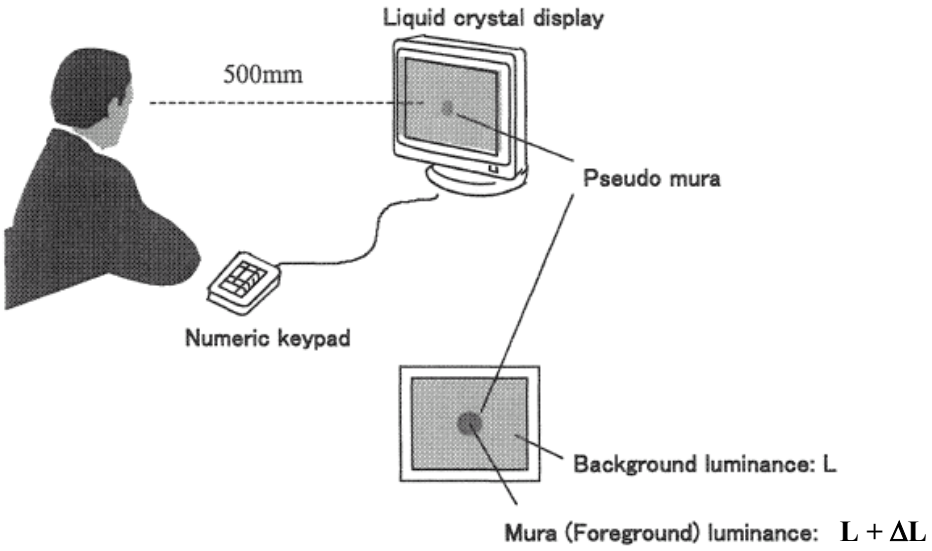

Fig. 3.2 Experimental conditions and equipment used in the subjective evaluations in [3].

Assume the background luminance is denoted as L and the Mura luminance is denoted as L + ΔL. In this experiment, the contrast of the Mura was defined to be the value of ΔL/L. Various sizes of circle-type and rectangle-type Muras were used in the experiments. The observers include 8 experts, who regularly conduct Mura inspections and analysis, and 8 college students with normal vision (with near vision strength (500mm) of 1.2 or greater for both eyes).

Fig. 3.3 shows the experimental results for Muras larger than 1 pixel, where the horizontal axis is $1/A^{0.33}$ and the vertical axis is the value of contrast. The observers' JND data are plotted as " •", while the Dist data are plotted as "o". The bold line was determined by the linear regression of the JND data. This line indicates a strong correlation between the size of Mura and the perceived contrast value of Mura. In this experiment, the larger the area of the Mura is, the smaller the JND contrast becomes. In other words, Muras are more visible as their area becomes larger. In mathematics, the linear relationship between JND contrast (C_{jnd}) and $A^{0.33}$ was expressed in [3] as

$$C_{jnd} = 1.97/A^{0.33} + 0.72. \quad (3.1)$$

This equation indicates the important characteristics of the "just noticeable

difference" for LCD Muras.

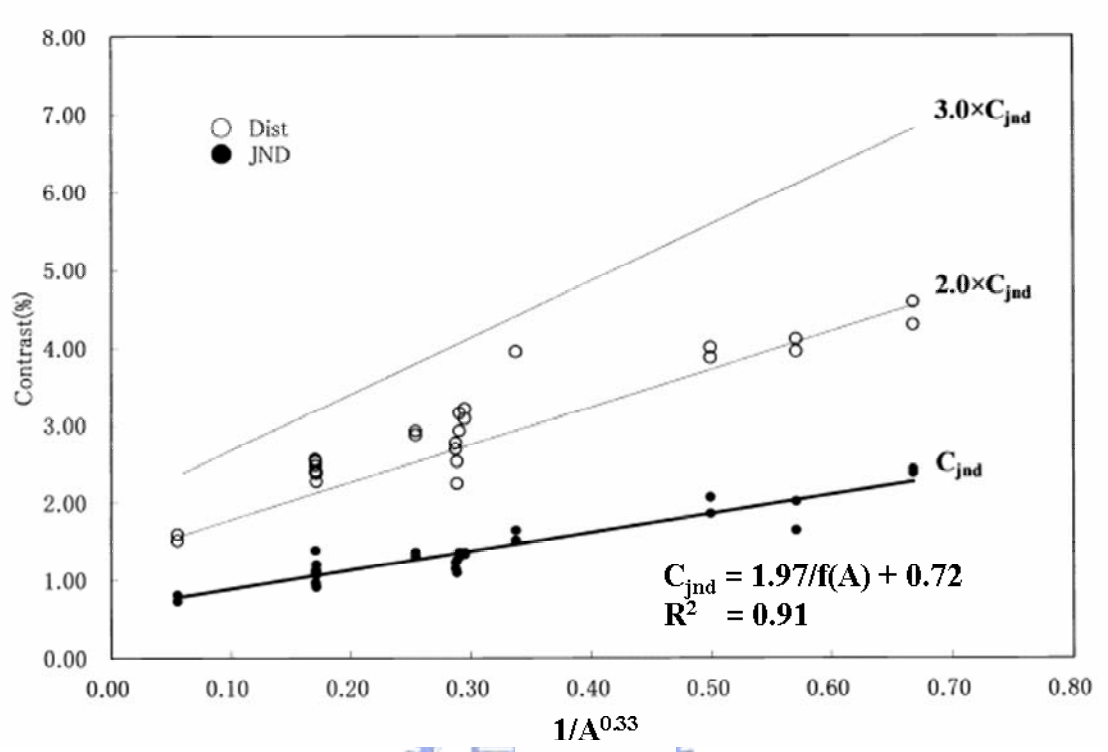

Fig. 3.3 JND and Dist result of the subjective evaluation in [3].

$f(A) = A^{0.33}$, A: Mura area (mm^2)

Fig. 3.3 also shows the straight lines for 2.0×Cjnd and 3.0×Cjnd. The Dist contrast data is around the 2.0×Cjnd line. This indicates that not only the JND level but also the visible contrast level has the linear relationship between the contrast level and $A^{0.33}$. Hence, the level of Mura defects can be described accordingly.

To evaluate the blemish degree of Cluster Mura defect, the SEMU formula is defined as:

$$SEMU \equiv \frac{|C_x|}{C_{jnd}} = \frac{|C_x|}{(\frac{1.97}{A^{0.33}} + 0.72)}, \tag{3.2}$$

where C_x is the average contrast of Mura, C_{jnd} is the just noticeable contrast of Mura, and A is the area of Mura [2]. A larger value of SEMU indicates a more serious

blemish. In [4] and [5], some modified versions of this SEMU formula have been further proposed. In these modified SEMU formulae, the contrast and the area of Mura defects are still the main factors. Similar to Equation (3.2), either a larger contrast of Mura or a larger area of Mura will cause a higher degree of blemish.

As mentioned above, Mura defects appear as low contrast, non-uniform brightness regions. They are typically larger than a single pixel when the screen is at a constant gray level. Moreover, various kinds of Mura defects are caused by different reasons. It would be difficult to develop a single universal algorithm to detect all kinds of Mura defects. In this dissertation, we consider two major kinds of Mura defects, Cluster Mura and Vertical-Band Mura. These two types of Mura are common in the FOS of LCDs. In Section 3.2, we'll introduce the photography of the FOS image first. Then, in Section 3.3, the proposed techniques in the detection of Cluster Mura are discussed. In Section 3.4, on the other hand, we discuss the proposed techniques for the detection of Vertical-Band Mura.

3.2 Photography of FOS Images

Fig. 3.4(a) shows the prototype of our automatic inspection system. In this system, we have an LCD panel that is under test, a CCD camera to capture the FOS image of the LCD panel, and a computer to execute Mura detection algorithms. In the inspection process, the LCD panel under test is vertically placed on the apparatus. Each time, the LCD panel is driven by a pattern generator to display a certain gray level image pattern. Then, the camera will capture an FOS image for this specific pattern. The FOS image is transmitted to the computer for storage and then is inspected by a set of Mura detection algorithms.

At markets, 15-inch and 17-inch LCD panels are the mainstream for desktop displays and notebook displays. In fact, the manufacture processes in these two types of LCD panels are quite similar. Hence, the appearances of Mura defects are also similar. Both types of LCD panels can be inspected by this prototype system. Moreover, to mimic the performance of human inspection, the specifications of the CCD camera are chosen to have a more than 12-bit dynamic range and a spatial resolution of 1532 × 1024 pixels.

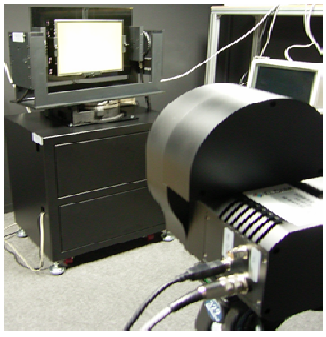

(a) Inspection prototype

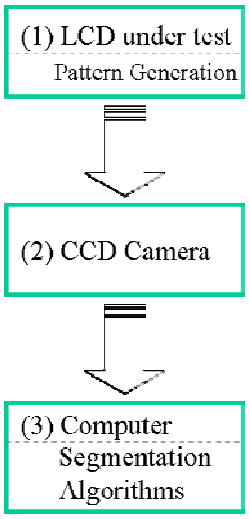

(b) Flowchart of LCD inspection

Fig. 3.4 The prototype of the LCD inspection system.

3.2.1 Aliasing

In the photography process, aliasing usually occurs when the lens of camera is well focused on the center of the FOS. Fig. 3.5(a) shows an image with aliasing. Fig. 3.5(b) shows the enlarged image of the portion inside the red rectangular in Fig. 3.5(a). As shown in Fig. 3.5(b), the lattice-like pattern occurs when the camera lens is in focus. This lattice-like pattern will not only increase the difficulty in automatic inspection but also influence the inspection results of Mura defects.

To eliminate the aliasing effect, several anti-aliasing approaches have already been published or patented [51][52]. These approaches usually require additional accessories and may cause image blurring. Among these approaches, we adopt the de-focusing approach, which may eliminate the aliasing effect without additional accessories. In this approach, we focus the camera lens on the FOS of LCD first, followed by slightly de-focusing the lens till the lattice-like pattern disappears. Although this method still causes some degree of blurring in the FOS image, this method demands no extra expense. In Fig. 3.5(c), we show the de-focused image of Fig. 3.5(a). It can be easily seen that the lattice-like pattern is suppressed.

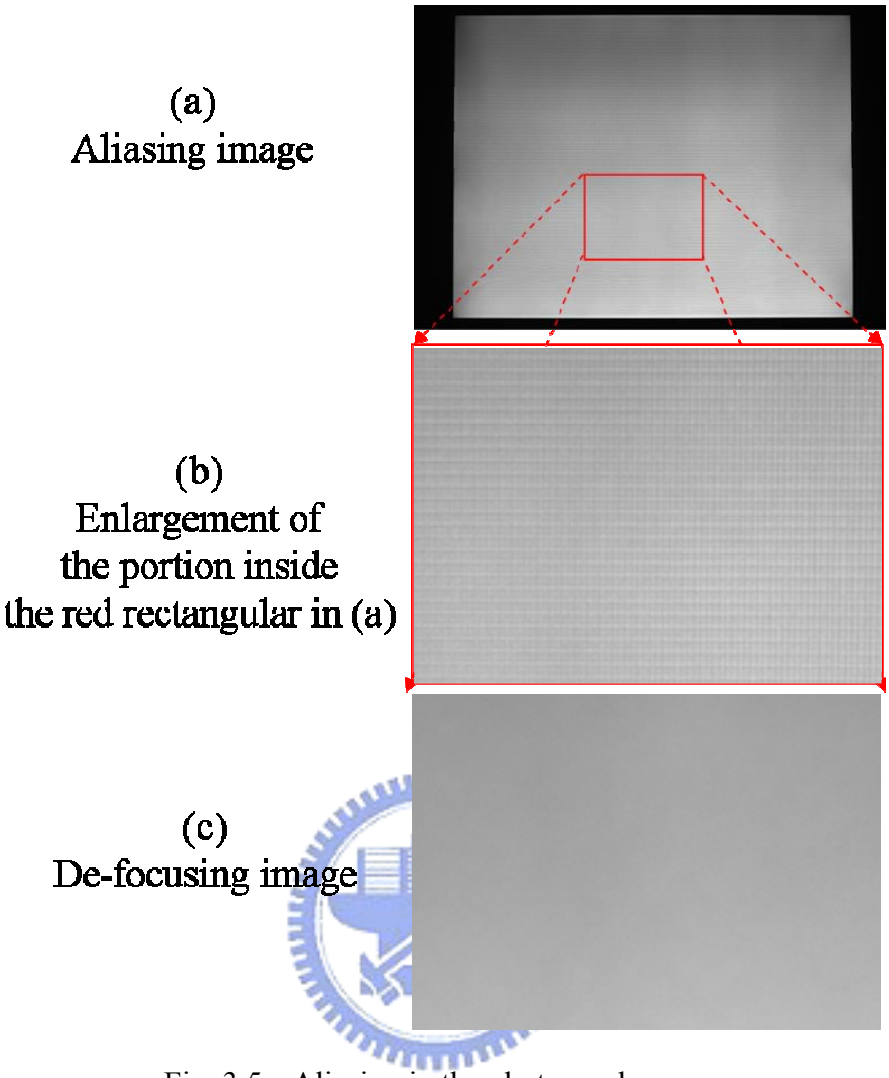

Fig. 3.5 Aliasing in the photography process.

3.2.2 Cluster Mura and V-Band Mura

Among several kinds of Mura defects, the detection of two major kinds of Mura defects, Cluster Mura and Vertical Band (V-Band) Mura, will be taken into account in this dissertation. As mentioned before, Mura defects appear as non-uniform brightness regions in the FOS of an LCD panel. Nevertheless, not all kinds of Mura defects appear in a similar manner. For example, Cluster Mura usually appears as a cluster of several points locating within a small area. As shown in Fig. 3.6(a)(c), a round-type Cluster Mura defect locates at (x=750, y=820), while a rectangular-type Cluster Mura defect appears as a narrow region ranging from (x=200, y=720) to (x=600, y=720). On the other hand, a V-Band Mura usually appears as a wide vertical strip with either brighter or darker brightness with respect to the uniform background. As shown in Fig. 3.6(e), a V-Band Mura is centered around x=850. The cause of V-Band Mura usually comes from non-uniform thickness of components, such as non-uniform thickness of the glasses in the cell unit. In comparison, Cluster Muras usually appear within a local area, while V-Band Muras usually occupy a larger area. The appearance model of a Cluster Mura is quite different from that of a V-Band Mura. It would be impractical to detect both types of Muras based on a single algorithm.

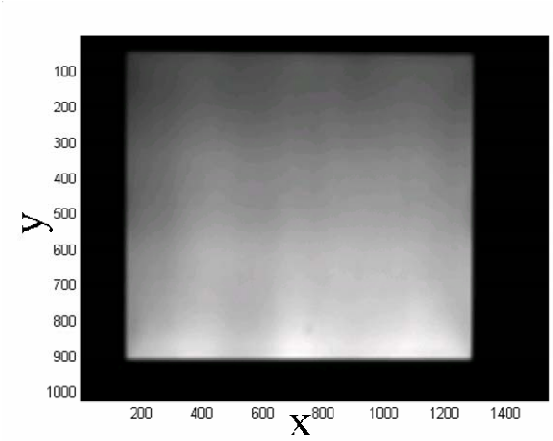

(a) Round-type Cluster Mura

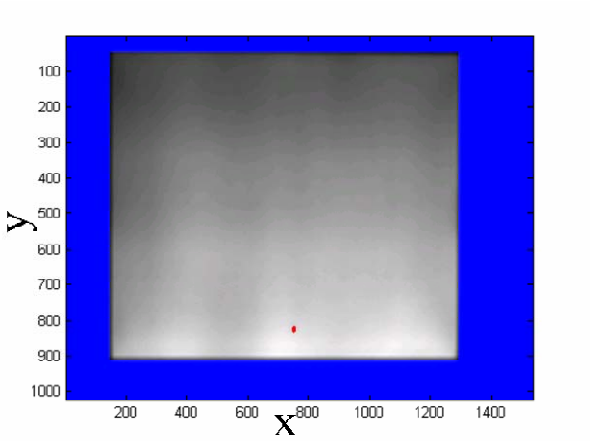

(b) Detection result of (a)

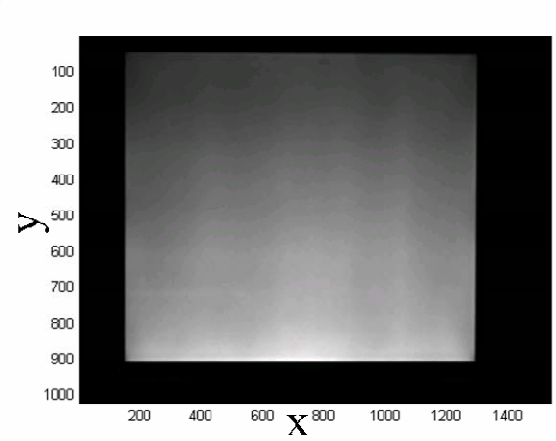

(c) Rectangular-type Cluster Mura

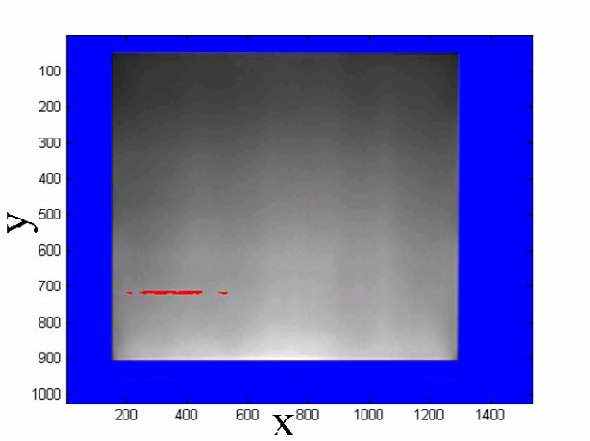

(d) Detection result of (c)

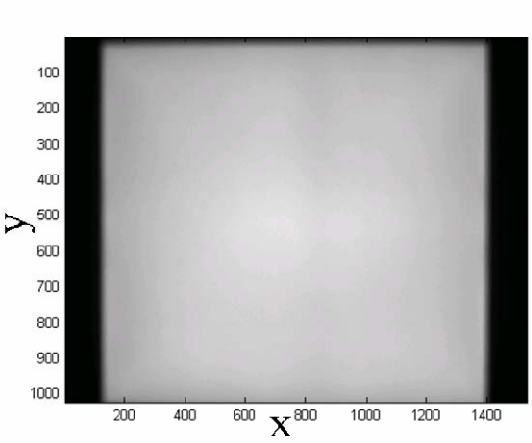

(e) V-Band Mura

Fig. 3.6 Cluster Mura and V-Band Mura.

In the following sections, we will present the use of two different approaches to deal with these two kinds of Mura defects. These two different approaches actually share the same kernel: a Laplacian of Gaussian (LOG) filter. This LOG filter, which compares the intensity of the target with the intensity of the surroundings, will be demonstrated to be very useful in the development of Mura detection algorithms. To detect Cluster Mura defects, an approach based on 2-D LOG filters will be presented in Section 3.3. To detect V-Band Mura, on the other hand, an approach based on 1-D LOG filters will be presented in Section 3.4.

3.3 Inspection of Cluster Mura

3.3.1 Cluster Mura Detection

In practice, there are two types of Cluster Mura defects: round-type Cluster Mura and rectangular-type Cluster Mura. In the selection of operators to detect these two types of Muras on a constant luminance level, two requirements are demanded: 1) having fewer parameters and 2) being less influenced by the shading of the luminance level. Therefore, to detect round-type Cluster Mura defects, we use a 2-D round-type LOG filter as shown in Fig. 3.7(a). The kernel function of this LOG filter is chosen to be the 2st derivative of a Gaussian function. In mathematics, this kernel function can be formulated as

$$filter_{LOG}^{Round}(x,y) = \left(\nabla_{xx} + \nabla_{yy}\right) N(x,y;0,\sigma_x,\sigma_y), \tag{3.3}$$

where $N(x,y;0,\sigma_x,\sigma_y)$ denotes a 2-D Gaussian function with zero mean and standard deviations σ_x and σ_y. If we set $\sigma_x = \sigma_y = \sigma$, then there is only one parameter to be assigned by users. In Section 3.3.2, we will discuss the rule of parameter setting.

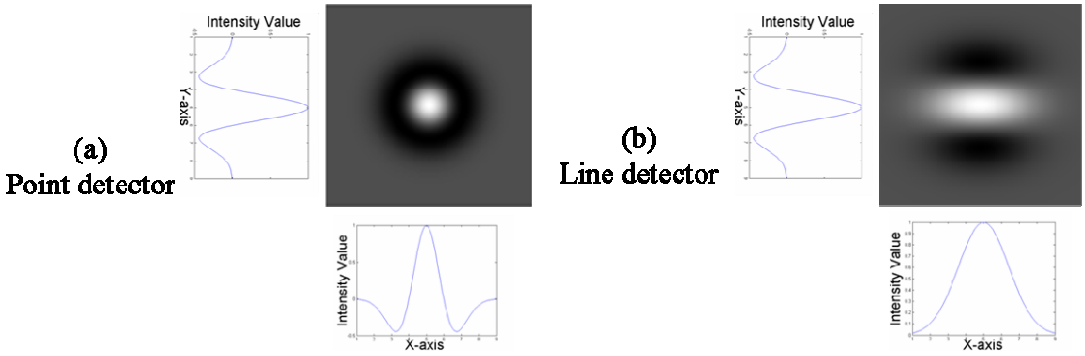

Fig. 3.7 2-D LOG filters for point detection and line detection.

On the other hand, to detect rectangular-type Cluster Muras, we adopt a 2-D rectangular-type LOG filter, as shown in Figure 3.7(b). The corresponding formula of

this rectangular -type LOG filter can be formulated as

$$filter_{LOG}^{\text{Rectangular}}(x,y) = \left(\nabla_{yy}\right) N(x,y;0,\sigma_x,\sigma_y). \tag{3.4}$$

Similarly, in Equation (3.4), there are two parameters, σ_x and σ_y. If the ratio of these two parameters, $r = \sigma_x / \sigma_y$, is fixed, then there is only one parameter left to be assigned by users.

With the round-type LOG filters and the rectangular-type LOG filters, the round-type Cluster Mura defects and the rectangular-type Cluster Mura can be detected. The detection result of Fig. 3.6(a) is given in Fig. 3.6(b), in which the blue region denotes the area of no interest while the red area denotes the detection result of Cluster Mura. Similarly, the detection result of Fig. 3.6(c) is given in Fig. 3.6(d).

3.3.2 Optimal Threshold Based on the SEMU Formula

To evaluate the blemish degree of the Cluster Mura defects, the SEMU formula [2] mentioned in Section 3.1.1 is defined as

$$SEMU \equiv \frac{|C_x|}{C_{jnd}} = \frac{|C_x|}{(\frac{1.97}{A^{0.33}} + 0.72)}, \tag{3.5}$$

where C_x is the average contrast of Mura, C_{jnd} is the just noticeable contrast of Mura, and A is the area of Mura. As indicated in this equation, either a larger contrast or a larger area will cause a higher degree of blemish.

On the other hand, as mentioned in Section 3.3.1, to detect round-type Cluster Muras, the round-type LOG filters are adopted. As illustrated in Fig. 3.8, we assume additive white Gaussian noise (AWGN) is involved in the photography process.

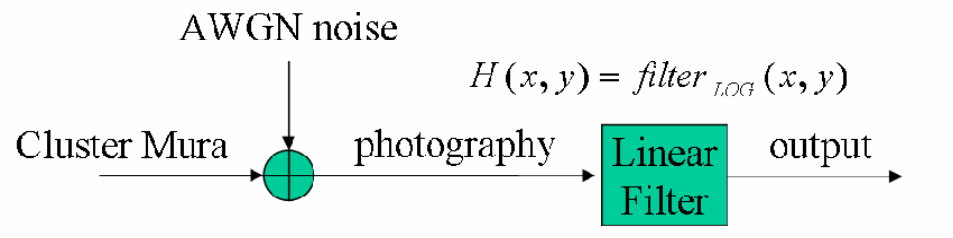

Fig. 3.8 Cluster Mura and photography process.

Hence, the filtered image of a Cluster Mura defect could be described as

$$Output(x,y) = Mura_{Cluster}(x,y) \otimes filter_{LOG}^{Round}(x,y). \tag{3.6}$$

Assume the round-type Cluster Mura is modeled as

$$Mura_{Cluster}(x,y) = h \times u\left(1 - \frac{x^2 + y^2}{r^2}\right). \tag{3.7}$$

where r is the radius of the round-type Cluster Mura, and $u(t)$ is the step function defined as

$$u(t)=\begin{cases}0, & t<0\\ 1, & t\geq 0\end{cases}. \tag{3.8}$$

Combining Equation (3.6) with Equation (3.7), we could derive

$$\begin{aligned} Output(x,y)\big|_{x=y=0} &= Mura_{Cluster}(x,y)\otimes filter_{LOG}(x,y)\Big|_{\sigma_x=\sigma_y=\sigma,\,x=y=0}\\ &= \frac{-hr^2}{4\sigma^4}\exp(-\frac{r^2}{2\sigma^2}). \end{aligned} \tag{3.9}$$

On the other hand, the variance of the filtered noise can be estimated to be

$$Var_{Filtered\_Noise}=\left(Var_{Estimated\_Noise}\right)\int\int\left|H(u,v)\right|^2 dudv, \tag{3.10}$$

where $Var_{Estimed\_Noise}$ denotes the variance of the AWGN noise produced in the photography process and $H(x,y)$ represents the round-type LOG filter.

If combining Equation (3.3) and Equation (3.10), we can have

$$Var_{Filtered\_Noise}=\frac{Var_{Estimated\_Noise}}{32\pi\sigma^7}. \tag{3.11}$$

By optimizing the Signal to Noise Ratio (SNR), which is defined as

$$\text{SNR}\equiv\frac{(\text{Output})^2}{Var_{\_Filtered\_noise}}, \tag{3.12}$$

we can derive the relationship between the radius of the round-type Cluster Mura and the standard deviation of the optimal LOG filter. The relationship is found to be

$$r=\frac{1}{\sqrt{2}}\sigma. \tag{3.13}$$

This radius corresponds to the size of the "matched" Mura that can produce the maximal output after the LOG filtering.

As mentioned before, to evaluate the blemish degree of Cluster Mura, the SEMU formula is suggested in [2]. If we assume the SEMU value to be a constant *S*, the relation between Mura's contrast and Mura's area can be derived. That is, if we define

$$\frac{h}{(\frac{1.97}{A^{0.33}}+0.72)}=S\,, \tag{3.14}$$

then we have

$$Output(x,y)\big|_{x=y=0}=-\left(0.2126\sigma^{-8/3}+0.09\sigma^{-2}\right)\exp(-1/4)S\,. \tag{3.15}$$

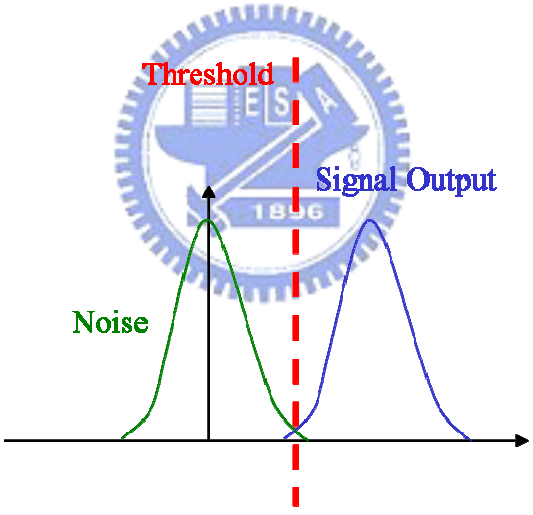

Fig. 3.9 Optimal threshold.

According to the Bayesian formula, the optimal threshold for the detection of Mura is shown in Fig. 3.9. Once the constant *S* is fixed and the standard deviation of the Gaussian function is determined, the optimal threshold can be decided as expressed in Equation (3.16),

$$threshold=\frac{1}{2}\times-\left(0.2126\sigma^{-8/3}+0.09\sigma^{-2}\right)\exp(-1/4)S\,. \tag{3.16}$$

3.4 Inspection of V-Band Mura

3.4.1 V-Band Mura Detection

Unlike Cluster Muras, a V-Band Mura usually appears with a large area. In general, as the size of filters increases, the computation time increases dramatically. Therefore, the use of a 2-D LOG filter whose shape "matches" the shape of V-Band Mura is no longer a suitable way for efficient inspection. In this dissertation, we take a different approach to detect V-Band Mura defects. Fig. 3.10(b) shows the FOS image with three contours, where the pixels with similar intensity values are drawn in the same color. The pixels with red color have larger intensity values than the pixels with brown color, while the pixels with brown color have larger intensity values than the pixels with black color. In Fig. 3.10(b), we can see that the tendency of the intensity variation along the vertical direction is approximately the same at any horizontal coordinate. Basically, with a fixed horizontal coordinate, the intensity in the center area tends to be larger than the intensities on the two sides. Due to this similarity in the intensity variation along the vertical direction, the operation of intensity integration along the vertical direction will not affect the tendency of intensity variation along the horizontal direction.

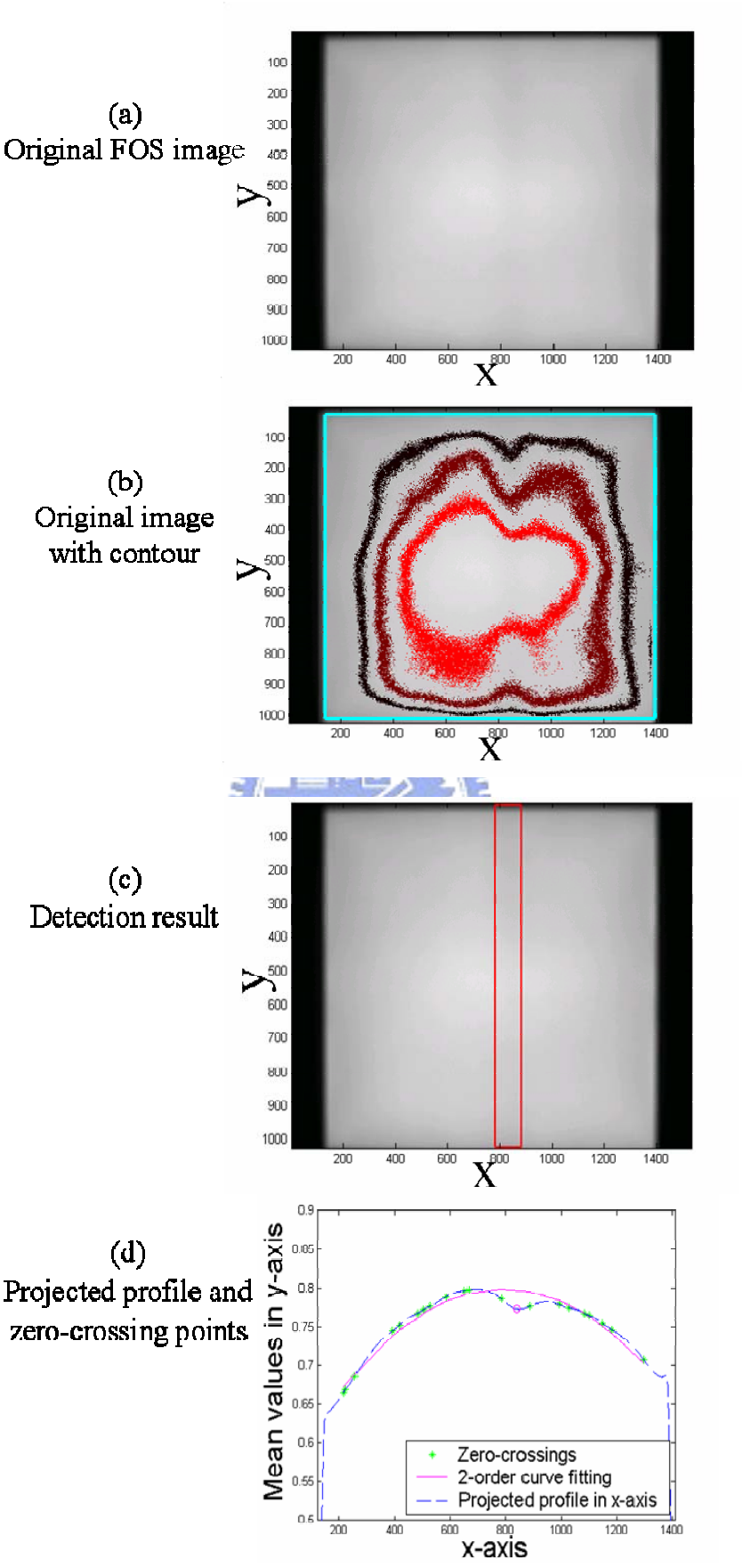

Fig. 3.10 V-Band Mura detection.

Hence, in our approach, the projection method is applied first along the vertical direction. As shown in Fig. 3.10(d), the blue dotted line represents the intensity profile projected along the y-axis. With this projected intensity profile, we can easily see that the profile around x=850 have a significant variation. To detect this significant variation, we first estimate a smooth curve from the original profile. To estimate the smooth curve, some specific sample points are needed. Since the zero-crossing points of the 2nd derivative of the intensity profile represent the locations of the profile with no significant curvature variation. Therefore, we use these zero-crossing points as the sample points in our proposed algorithm in order to estimate the smooth curve from the original intensity profile.

To extract zero-crossing points, we use a 1-D LOG filter to estimate the 2nd derivative of the profile. With a 1-D LOG filter formulated in Equation (3.17), we can apply this filter over the projected profile to estimate the 2nd derivative of the profile. Then, zero-crossing points can be detected, as represented in green points in Fig. 3.10(d).

$$filter_{LOG}(x) = (\nabla_{xx})N(x;0,\sigma_x). \tag{3.17}$$

With these zero-crossing points, a 2nd-order curve fitting method is adopted to generate a smooth intensity profile, shown as the pink curve in Fig. 3.10(d). Comparing this smooth curve to the original curve, we define the fractions with a large deviation from the original curve to be the locations of V-Band Mura defects. Fig. 3.10(c) shows the detection result of V-Band Mura in Fig. 3.10(a), with the red box circling the area of V-Band Mura.

3.4.2 FOS Surface Reconstruction

To verify the V-Band detection approach, we reconstruct an imaginary FOS image based on an approximated smooth intensity profile. In Fig. 3.11(c), with these zero-crossing points extracted by the 1-D LOG filter, Spline interpolation is adopted to estimate the smooth intensity profile, which is represented as the red curve in Fig. 3.11(c). With this smooth intensity profile, we can reconstruct the smoothed FOS surface, as shown in Fig. 3.11(b).

To conclude this chapter, we suggest the use of 2-D round-type/rectangular-type LOG filters to detect round-type/rectangular-type Cluster Mura defects. With 2-D LOG filters, the optimal threshold is analyzed based on the SEMU formula which is based on luminance contrast. Also, we propose a curvature based approach to detect V-Band Mura defects. In the curvature based approach, a 1-D LOG filter is used to generate a smooth curve that represents the curvature tendency of the 1-D projected profile. With this smooth curve, V-Band Mura defects with a large deviation of luminance contrast can be detected easily. In simulation, the results demonstrate the LOG filters are very useful in the development of detection algorithms for the inspection of Mura defects.

(a)
Original FOS image

(b)
Reconstructed image

(c)
Projected profile,
zero-crossing points,
and Spline interpolation

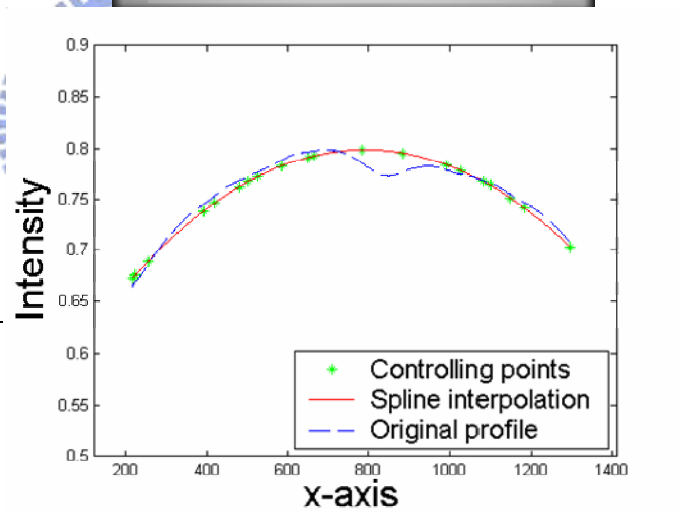

Fig. 3.11 FOS surface reconstruction.

CHAPTER 4

Development and Evaluation of Color Segmentation Algorithms Based on Color Contrast

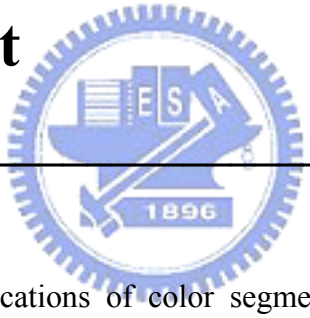

In this chapter, for the applications of color segmentation with little texture, the definitions of color contrast and visible color difference are introduced first. In Section 4.1, the definition of a directional color contrast is proposed In Section 4.1 first. Then, with the directional color contrast, the definition of color contrast in the CIE L*a*b* color space is proposed. Also, a technique that can estimate the directional color contrast of color edges in a color image is proposed. On the other hand, a definition of "visible color difference" in the CIE L*a*b* color space is introduced to represent the effects of color difference in human visual perception. Then, based the defined color contrast, a so-called visible color difference is proposed to differentiate visible color difference from invisible color difference. In Section 4.2, some visual rating experiments are performed to verify the correlation between

segmentation quality and degree of over-segmentation and/or degree of under-segmentation. Then, based on the defined "visible color difference" formula in Section 4.1, which are used to estimate the degree of over-segmentation, the degree of under-segmentation, and segmentation quality, some quantitative visual error measures are proposed. These quantitative measures are also used in the evaluation of color segmentation. In Section 4.3, based on the directional color contrast introduced in Section 4.1, a color segmentation algorithm is proposed. On the other hand, uniting with the proposed quantitative evaluation method mentioned in Section 4.2, a new color segmentation algorithm is proposed.

4.1 Color Contrast and Visible Color Difference

In Section 4.1.1, we'll introduce the definition of directional luminance contrast and directional color contrast in the CIE L*a*b* color space. On the other hand, we introduce a new definition of color difference, called visible color difference in Section 4.1.2. Based on the visible color difference, new measurements are to be proposed for a quantitative evaluation of color segmentation in the next section.

4.1.1 Color Contrast in CIE L*a*b* Color Space

For color segmentation, we define directional luminance contrast in Section 4.1.1.1 for image domain-based color segmentation algorithms. Then, directional color contrast in the CIE L*a*b* color space is discussed in Section 4.1.1.2.

4.1.1.1 Definition of Directional Contrast

For color segmentation applications, data variation in a local area is usually used as the gauge for segmentation. Pixels with a small data variation are grouped together, while pixels with a large data variation are detected as boundaries. To measure data

variation, the derivative information is commonly used. Nevertheless, a direct use of derivative values may not faithfully reflect the way humans perceive object boundaries. Fig. 4.1(a) shows an intensity profile extracted from a real image. Basically, each edge on this profile comprises three major factors: 1) edge height, 2) edge slope, and 3) noise irritation. Among these three factors, edge height is more related to the way human perceives edges than the other two [26]. However, all these three factors influence the measurement of the derivative information around an edge. For example, the values of the 1st differentiation are plotted in Fig. 4.1(b). In the middle of Fig. 4.1 (a), there appear two apparent edges: a sharp edge around x = 40 and a smooth edge around x = 50. Even though these two edges have similar edge height, their 1st derivatives are quite different. Furthermore, the noise fluctuation around x = 80 generates a 1st derivative value that is as large as the 1st derivative value around x = 50. These two examples imply that a direct use of the 1st derivative information could be very risky if we aim for accurate segmentation.

In this dissertation, we name the edge height as edge contrast. It is defined as the intensity or color difference between the high-curvature points on the two sides of the boundary, as shown in Fig. 4.2. To detect these high-curvature points, we use a 2nd derivative operator to estimate the curvature of the profile. As shown in Fig 4.2, we treat the extreme points on the 2nd derivative profile as the high-curvature points. In our approach, the 2nd derivative operator is designed as

$$B(x) = \delta(x) - N(x;0,\sigma). \tag{4.1}$$

Here, $\delta(x)$ denotes the impulse function:

$$\delta(x) = \begin{cases} 1, & x = 0 \\ 0, & \text{otherwise} \end{cases}, \tag{4.2}$$

while $N(x;0,\sigma)$ denotes a Gaussian function with zero mean and standard deviation σ.

By convoluting a profile I(x) with this operator, we have

$$\begin{aligned}\varphi(x) &= I(x) \otimes B(x) \\ &= I(x) - I(x) \otimes N(x;0,\sigma).\end{aligned} \tag{4.3}$$

Basically, $\varphi(x)$ can be imagined as the 2nd derivative of the profile $I(x)$. Moreover, the local extremes of $\varphi(x)$ correspond to the high-curvature points of $I(x)$. Fig. 4.1(c) shows the contrast information extracted from Fig. 4.1(a) using Equation (4.3) with σ = 2.0, which is determined empirically. It is obvious that Fig. 4.1(c) offers much more reliable information than Fig. 4.1(b).

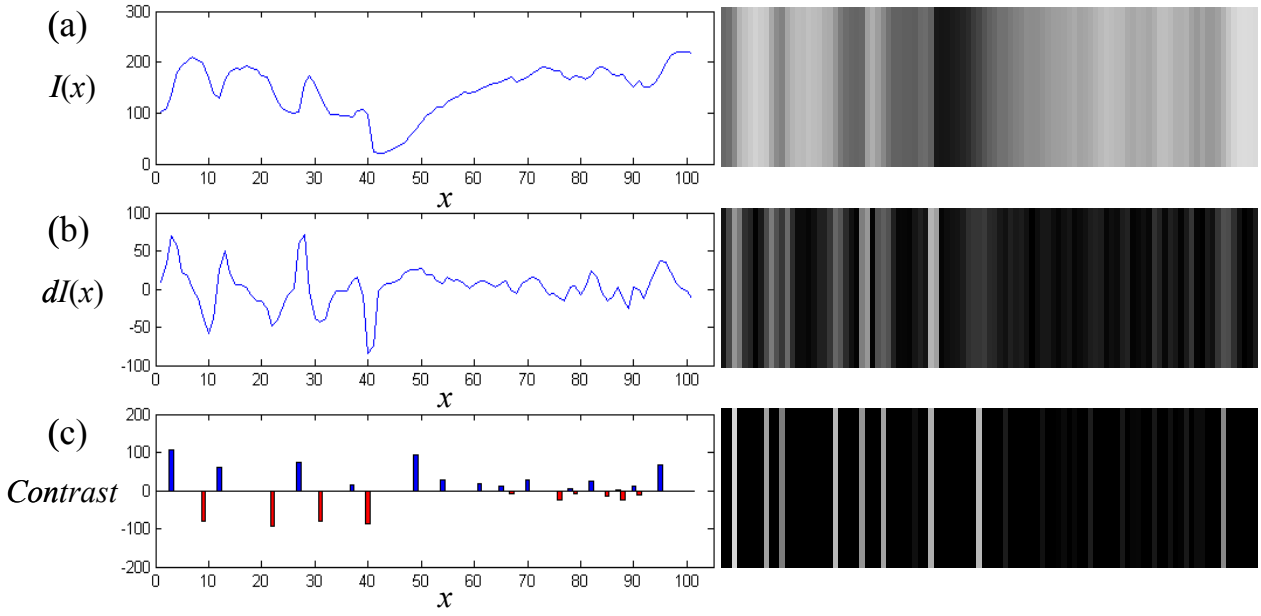

Fig. 4.1 (a) An intensity profile extracted from a real image. (b) The estimated 1st derivative information. (c) The estimated contrast information with σ = 2.0.

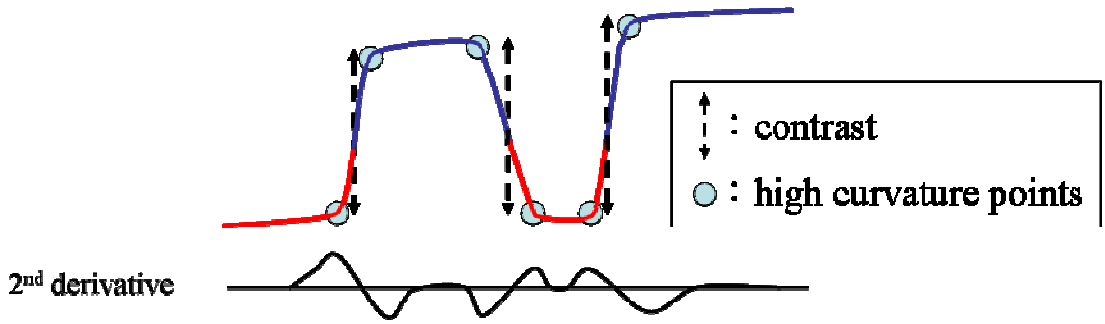

Fig. 4.2 The definition of contrast in one dimension.

Since the 2nd derivative is orientation-dependent, the contrast information at an image pixel can be measured along various orientations. In this dissertation, we propose a contrast-based color segmentation algorithm which is to be introduced in Section 4.3.1. In that algorithm, we detect boundaries by checking the relations between each pixel and its eight neighbors. Hence, four directional operators are used at each pixel to measure the curvature information at that pixel. These four directions are 0°, 45°, 90° and 135°, respectively. All these four directional contrast data are then grouped together in subsequent processes.

4.1.1.2 Definition of Color Contrast in CIE L*a*b* Color Space

In color image segmentation, a proper choice of color space is also a crucial issue. In the selection of color space, we choose the CIE L*a*b* color space due to three major properties of this color space: 1) separation of achromatic information from chromatic information, 2) uniform color space, and 3) similar to human visual perception [53]. Here, L* represents the luminance component, while a* and b* represent two color components. The formulae for converting an RGB image into the (L*, a*, b*) coordinates can be found in many color-related articles, like [53] and [54].

In the CIE L*a*b* color space, the Euclidean distance between the color $\left(L_1^*, a_1^*, b_1^*\right)$ and the color $\left(L_2^*, a_2^*, b_2^*\right)$ is defined as

$$\Delta E^*_{Lab} = \sqrt{\left(L_2^* - L_1^*\right)^2 + \left(a_2^* - a_1^*\right)^2 + \left(b_2^* - b_1^*\right)^2} \,. \tag{4.4}$$

This is approximately equivalent to the perceptual difference between these two colors [26][53]. By incorporating this color difference formula into our contrast definition, we define the color contrast across an edge as

$$\text{color contrast} \equiv \sqrt{\text{contrast}_{L^*}^{\,2} + \text{contrast}_{a^*}^{\,2} + \text{contrast}_{b^*}^{\,2}} \tag{4.5}$$

To further explore the correlation between color contrast and the luminance level or color level, we performed a subjective experiment. In our experiment, 10 observers are involved and the patterns are displayed over a calibrated ViewSonic PT775 monitor. Here, the values of luminance/color contrast are coarsely quantized into eleven steps: 0, 5, 10, 15, …, 50. In the experiment, a set of 11 step images with different contrast values but the same level value is used as reference. Each time, a step image with randomly specified contrast and level values is generated and is placed on the right side of each reference pattern for comparison, as shown in Fig. 4.3. The observers are asked to choose one or two reference patterns whose perceptual contrast is most similar to the randomly generated step image. Totally, 131 testing images are examined and the averaged results are shown in Fig. 4.4(a)-(d). It can be seen that our color contrast definition is roughly equivalent to the perceived color contrast and is weakly correlated with luminance/color levels. This implies that a single global threshold may work reasonably well over the whole image to suppress perceptually faint edges.

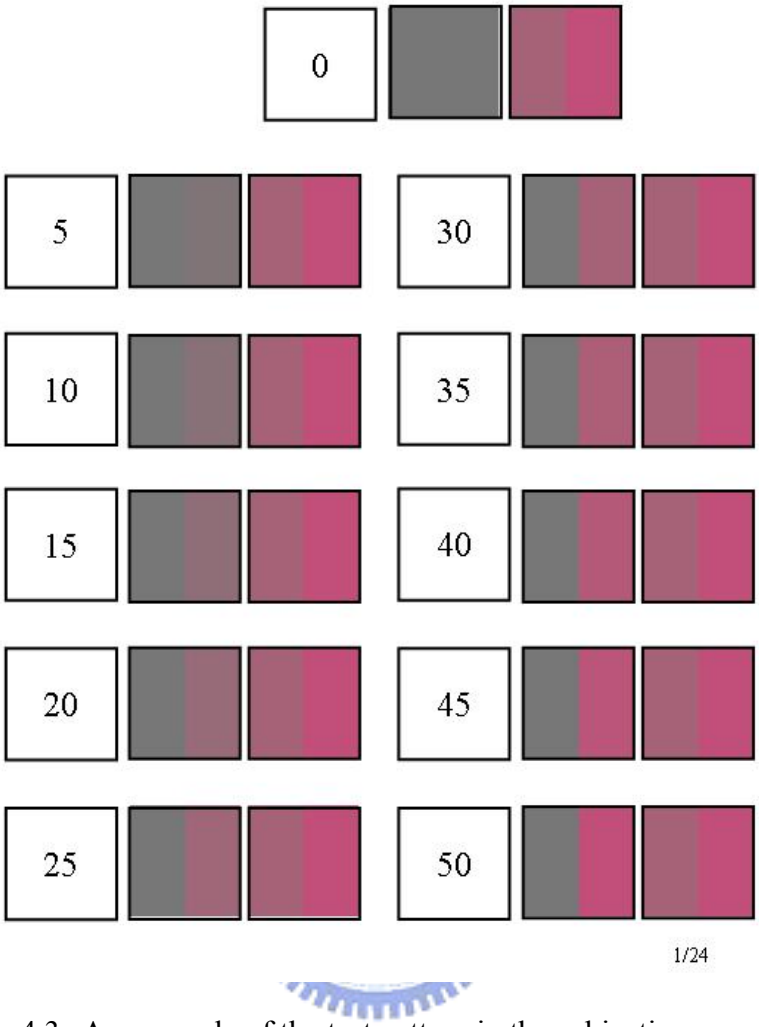

Fig. 4.3 An example of the test pattern in the subjective experiment.

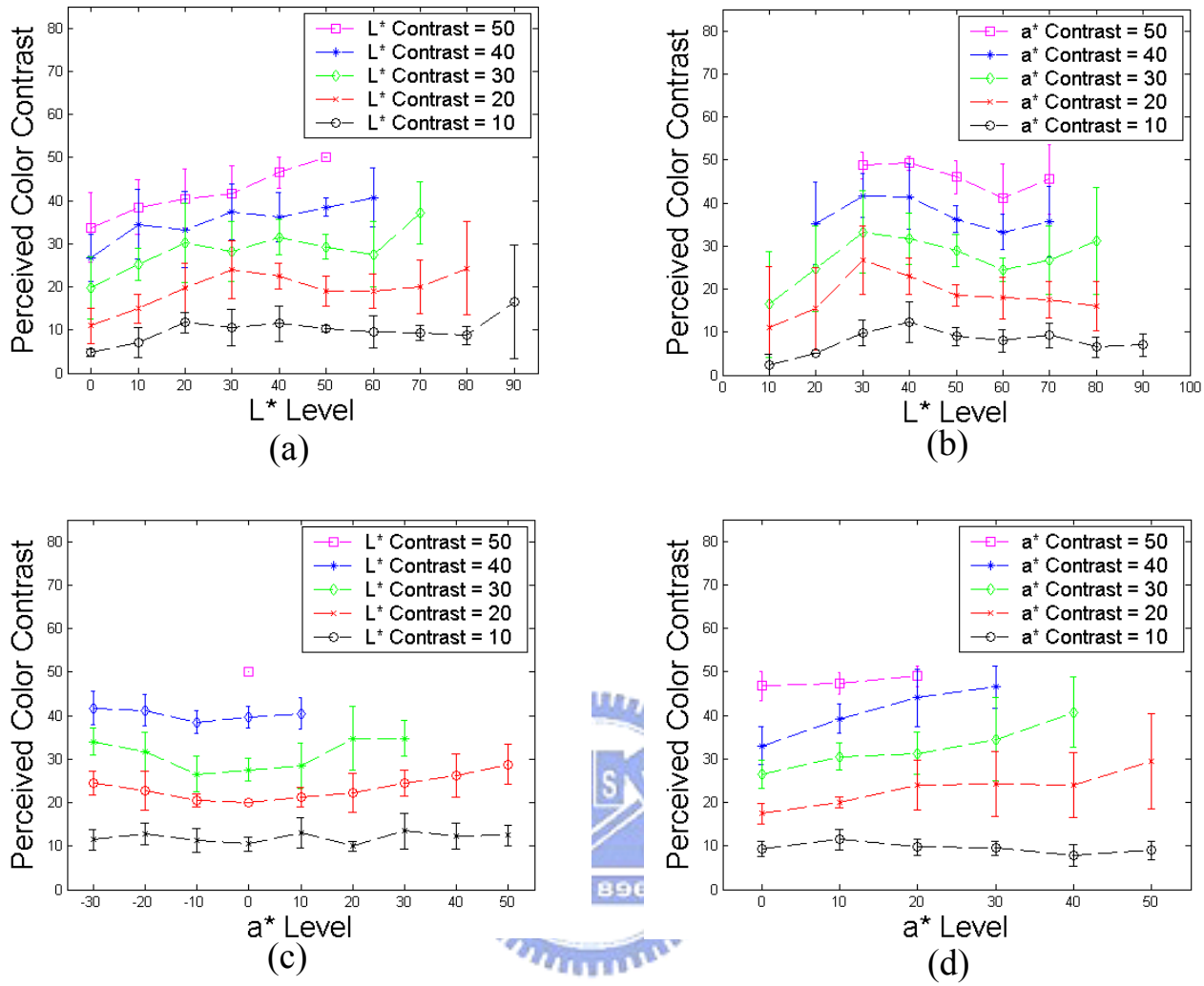

Fig. 4.4 Subjective experiment results for color contrast perception.

(a) Perceived color contrast versus luminance level for 5 different L* contrasts.

(b) Perceived color contrast versus luminance level for 5 different a* contrasts.

(c) Perceived color contrast versus color level for 5 different L* contrasts.

(d) Perceived color contrast versus color level for 5 different a* contrasts.

4.1.2 Definition of Visible Color Difference

In this section, for the evaluation of color segmentation, we introduce a new color contrast definition named "visible color difference", which is used to mimic the way human perceives color difference. Among various definitions regarding color difference [55], we choose the aforementioned CIE ΔE*Lab definition as the basis of color difference. As mentioned in the literature [53][55], the value of ΔE*Lab is perceptually analogous to humans' visual perception of color difference. This color difference definition is defined over the CIE L*a*b* color space, which is a roughly perceptually uniform color space. As aforementioned, the ΔE*Lab color difference between two colors, $\left(L_1^*, a_1^*, b_1^*\right)$ and $\left(L_2^*, a_2^*, b_2^*\right)$ in the CIE L*a*b* color space is defined as

$$\begin{aligned}\Delta E_{Lab}^* &\equiv \left\| \left(L_1^*, a_1^*, b_1^*\right) - \left(L_2^*, a_2^*, b_2^*\right) \right\|_{L^*a^*b^*} \\ &= \sqrt{\left(L_1^* - L_2^*\right)^2 + \left(a_1^* - a_2^*\right)^2 + \left(b_1^* - b_2^*\right)^2}\end{aligned} \tag{4.6}$$

Moreover, as indicated in [56], the values of ΔE*Lab could be roughly classified into three different levels to reflect three different degrees of color difference perceived by humans. As listed in Table 4.1, the color difference is hardly perceptible when ΔE*Lab is smaller than 3; is perceptible but still not distinct when ΔE*Lab is between 3 and 6; and is distinct when ΔE*Lab is larger than 6 [56]. Hence, in this dissertation, we define a color difference is "visible" if its ΔE*Lab value is larger than 6.

Table 4.1: The effect of color difference in the CIE L*a*b* color space on human visual perception [56]

ΔE^*_{Lab}	*Effect*
< 3	*Hardly perceptible*
3 < 6	*Perceptible, but not distinct*
> 6	*Distinct*

4.2 Quantitative Evaluation for Color Segmentation Based on Visible Color Difference

In Section 4.2.1, to extract visual perception factors for color segmentation, we'll perform a series of visual rating experiments. Based on these visual rating experiments, we'll introduce a visible color difference-based quantitative evaluation for color segmentation in Section 4.2.2.

4.2.1 Visual Rating Experiments for Color Segmentation Evaluation

As aforementioned, existing color segmentation algorithms can be roughly classified into three major categories: 1) image domain-based approaches; 2) feature space-based approaches; and 3) physics-based approaches [13]. For image domain-based approaches, most methods could be further classified into two groups: 1) edge-based methods and 2) region-based methods. To select appropriate color segmentation algorithms for the visual rating experiments, the segmentation algorithms are picked based on three criteria:

1) diverseness: these algorithms represent different types of image segmentation algorithms;
2) visibility: these algorithms had been presented to the vision community through a refereed publication; and
3) availability: the codes of these algorithms are readily available.

Based on these three criteria, we pick three different kinds of segmentation algorithms for our visual rating experiments. For edge-based approaches, we picked Ma and

Manjunath's Edge Flow algorithm [14]; for region-based approaches, we picked Deng and Manjunath's JSEG algorithm [15]; and for feature space-based approaches, we picked Comaniciu and Meer's Mean Shift algorithm [27]. Since physics-based approaches are much less popular than the others, this type of approaches is not considered in our experiments.

To mimic the way humans evaluate segmentation results, we consider the degree of "visible" missing boundaries and the degree of "visible" fake boundaries. To explore how missing boundaries and fake boundaries affect the perceived quality of image segmentation, a few visual rating experiments are made. In our experiments, 20 observers are involved. To acquire more accurate experiment results with less sensitivity to contexts, the stimulus-comparison method is used [57]. In the stimulus-comparison method, any two of the subjects should be compared. Hence, this type of approach is very time-consuming. To avoid heavy time consumption but without sacrificing the diversity of color images, 6 different color images are used. These six images are shown in Figs. 4.5(a)-(f) and are named "Fruit", "Lena", "House", "Tower", "Room", and "Table Tennis", respectively. On the other hand, since the attributes of segmentation results produced by different algorithms are quite different, it would be fairly difficult to compare segmentation results among different algorithms. For example, one algorithm may generate segmentation results with inaccurately located boundaries, while another algorithm may generate segmentation results with accurate boundaries but with some extra fake boundaries. Hence, in this dissertation, we only focus on the comparison of segmentation results produced by the same algorithm, but with different settings of the control parameters.

$(W_{idth}, H_{eight}) = (256,190)$

(a)

$(W_{idth}, H_{eight}) = (352,240)$

(b)

$(W_{idth}, H_{eight}) = (256,256)$

(c)

$(W_{idth}, H_{eight}) = (256,384)$

(d)

$(W_{idth}, H_{eight}) = (256,256)$

(e)

$(W_{idth}, H_{eight}) = (256,256)$

(f)

Fig. 4.5 Six test images.

(a) “Fruit”. (b) “Lena”. (c) “House”.
(d) “Tower”. (e) “Room”. (f) “Table Tennis”.

In the experiments, the segmented results of “Fruit” and “Lena” are produced by the Edge Flow algorithm [14]. The “Fruit” image is less textured, while the “Lena” image includes slight texture over the hat fringe region. On the other hand, the segmented results of “House” and “Tower” are produced by the JSEG algorithm [15], while the segmented results of “Room” and “Table Tennis” are produced by the Mean-Shift algorithm [27]. Table 4.2 shows the summary of these 6 color images and the corresponding segmentation algorithms.

Table 4.2: Color images versus the applied segmentation algorithms

Color image / Segmentation algorithm	Fruit	Lena	House	Tower	Room	Table Tennis
Edge-Flow algorithm [14]	◎	◎				
JSEG algorithm [15]			◎	◎		
Mean-Shift algorithm [27]					◎	◎

For each image, 9 segmentation results are produced by one of the three algorithms with 9 different settings. Then, every two of these nine segmentation results are displayed in a random order on an LCD (Liquid Crystal Display) monitor for comparisons, as shown in Fig. 4.6. That is, for each color image, there are $C_2^9 = 36$ segmentation pairs to be compared. Totally, for all 6 color images, there are $6 \times 36 = 216$ segmentation pairs to be compared. For each pair, 20 observers are asked to subjectively compare the right segmentation result, named Seg I, with the left segmentation result, named Seg II, in terms of the perceived segmentation quality, together with the perceived degree of missing boundaries and the perceived degree of fake boundaries. Here, we use the seven-grade scales with a set of categories defined in semantic terms (e.g. much better, better, slightly better).

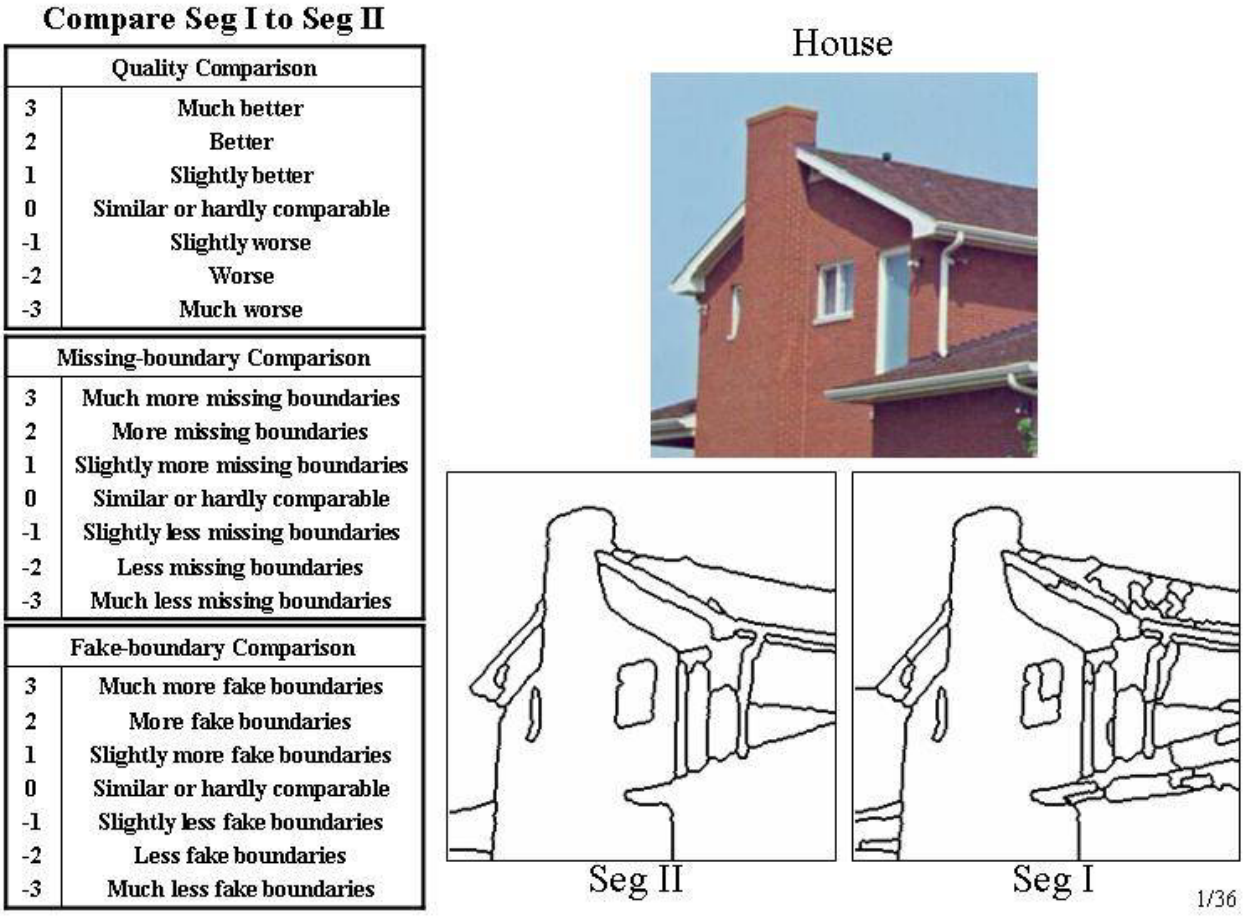

Fig. 4.6 One of the 36 comparison patterns for the "House" image.

The experiment results for Figs. 4.5(a)-(f) are shown in Figs. 4.7(a)-(b). In Fig. 4.7(a), the 9 triangles represent the averaged segmentation quality versus the averaged degree of missing boundaries for the 9 segmentation results of the "Fruit" image. The term "averaged" means that value is computed based on the grades from all 20 observers. Similarly, the asterisks, pentagrams, squares, circles, and plus-signs represent the averaged segmentation quality versus the averaged degree of missing boundaries for the segmentation results of "Lena", "House", "Tower", "Room", and "Table Tennis", respectively. In Fig. 4.7(a), it seems there is no apparent correlation between the perceived segmentation quality and the degree of missing boundaries. On the other hand, Fig. 4.7(b) shows the plot of the averaged segmentation quality versus

the averaged degree of fake boundaries for the segmentation results of the 6 color images. Similarly, the correlation between the segmentation quality and the degree of fake boundaries is not apparent.

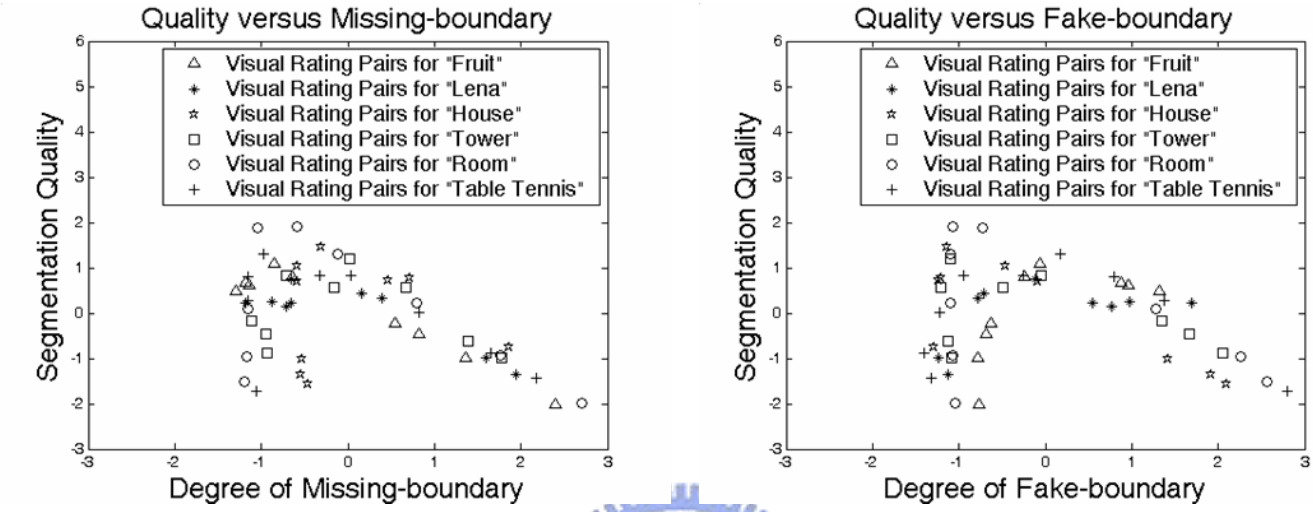

(a) (b)

Fig. 4.7 Results of the visual rating experiments.

(a) Segmentation quality versus the degree of missing-boundary for Figs. 4.5(a)-(f).

(b) Segmentation quality versus the degree of fake-boundary for Figs. 4.5(a)-(f).

To measure the correlation between the averaged segmentation quality and the averaged degree of missing-boundary/fake-boundary, we calculate the correlation coefficient, which is defined as

$$r = \frac{\sum (X - \bar{X})(Y - \bar{Y})}{\sqrt{\sum (X - \bar{X})^2} \sqrt{\sum (Y - \bar{Y})^2}}, \tag{4.7}$$

where $\bar{X}$ is the mean of the scores on the X variable, while $\bar{Y}$ is the mean of the scores on the Y variable. In Table 4.3, we list the correlation coefficient representing the correlation between the segmentation quality and the degree of missing-boundary/fake-boundary. As listed in Table 4.3, we can see that the correlation between the segmentation quality and the degree of missing boundaries is

not always significant at the 0.05 level for these 6 images. Neither is the correlation between the segmentation quality and the degree of fake boundaries. Here, the level of significance is defined as a small value which is larger than or equal to a rejection probability yielded by a statistical hypothesis test [58].

Table 4.3: Averaged segmentation quality vs. Missing-boundary and/or Fake-boundary

Color Image / Correlation	Fruit	Lena	House	Tower	Room	Table Tennis
Quality vs. Missing-boundary	-0.954**	-0.840**	0.001	-0.206	-0.432	-0.496
Quality vs. Fake-boundary	0.642	0.509	-0.788*	-0.396	-0.434	-0.114
Quality vs. Missing-boundary + Fake-boundary	-0.944**	-0.797*	-0.994**	-0.964**	-0.994**	-0.920**

* correlation is significant at the 0.05 level (two-tailed) [59].

** correlation is significant at the 0.01 level (two-tailed) [59].

Since the correlation between the averaged segmentation quality and the averaged degree of missing-boundary/fake-boundary is not strong, we try to explore the correlation between the averaged segmentation quality and the combination of missing-boundary and fake-boundary. In Fig. 4.8(a), the horizontal axis represents the degree of missing boundaries, increasing from left to right; while the vertical axis represents the degree of fake boundaries, increasing from bottom to top. Each of the 9 segmentation results for Fig. 4.5(a) is represented by a square pattern in Fig. 4.8(a). The color of the square patterns denotes the normalized averaged grade of segmentation quality, increasing from dark red to white. It can be seen that the best quality scores usually occur at the lower-left corner of the figure. This means the preferred segmentation results are these results with both a lower degree of missing boundaries and a lower degree of fake boundaries. Similarly, the simulation results for Figs. 4.5(b)-(f) are shown in Figs. 4.8(b)-(f), respectively. All these figures reveal the same phenomenon. To confirm this phenomenon, we plot the averaged segmentation

quality versus the averaged degree of missing boundaries plus the averaged degree of fake boundaries for all 6 color images, as shown in Fig. 4.8(g). In Fig. 4.8(g), we can easily see that the correlation between the visual quality of color segmentation and the combination of these two visual errors is strong. To verify the strong correlation between the segmentation quality and the degree of missing boundaries plus fake boundaries, we calculate the corresponding correlation coefficients. As listed in Table 4.3, it can be seen that the correlation coefficients between the segmentation quality and the combined degree of missing boundaries and fake boundaries is significant at the 0.05 level, or even at the 0.01 level, for all 6 images. Moreover, since the sign of the correlation coefficient is negative, it implies that the preferred segmentation result is a segmentation result with a lower degree of missing boundaries plus a lower degree of fake boundaries. Hence, once if we can find some reasonable measures to estimate the degree of missing boundaries and the degree of fake boundaries, we may use these measures to evaluate the segmentation quality in a reasonable and practical way.

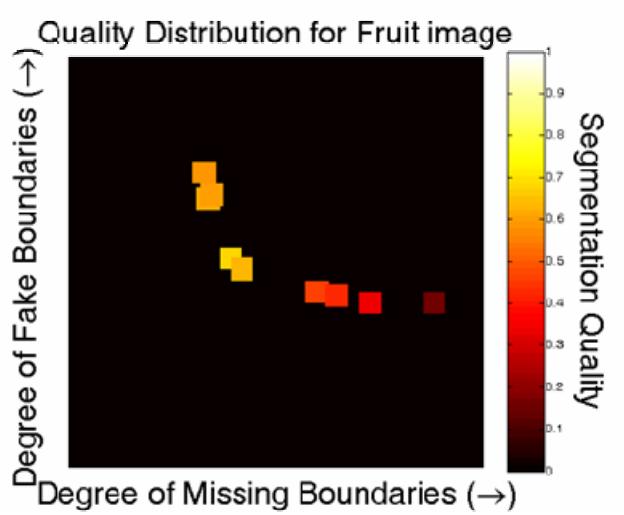
Quality Distribution for Fruit image
Degree of Fake Boundaries (→)
Degree of Missing Boundaries (→)
Segmentation Quality

(a)

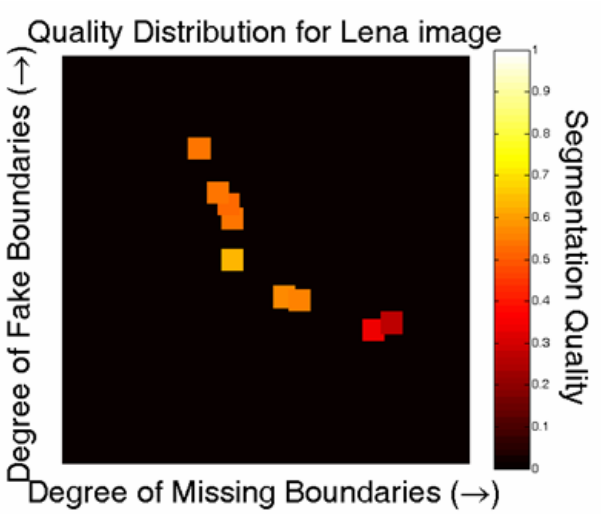
Quality Distribution for Lena image
Degree of Fake Boundaries (→)
Degree of Missing Boundaries (→)
Segmentation Quality

(b)

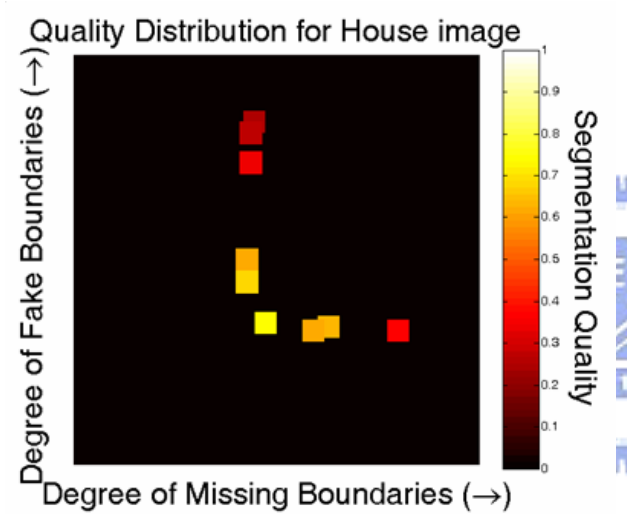
Quality Distribution for House image
Degree of Fake Boundaries (→)
Degree of Missing Boundaries (→)
Segmentation Quality

(c)

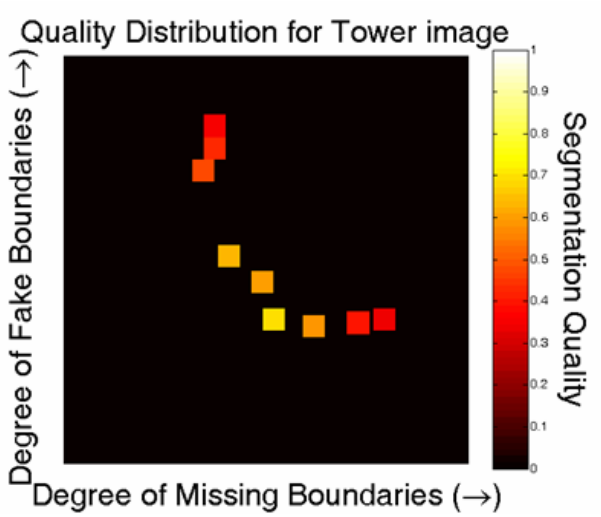
Quality Distribution for Tower image
Degree of Fake Boundaries (→)
Degree of Missing Boundaries (→)
Segmentation Quality

(d)

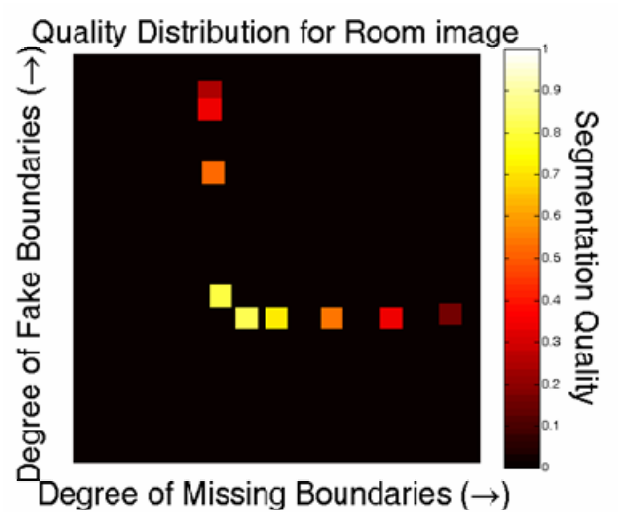
Quality Distribution for Room image
Degree of Fake Boundaries (→)
Degree of Missing Boundaries (→)
Segmentation Quality

(e)

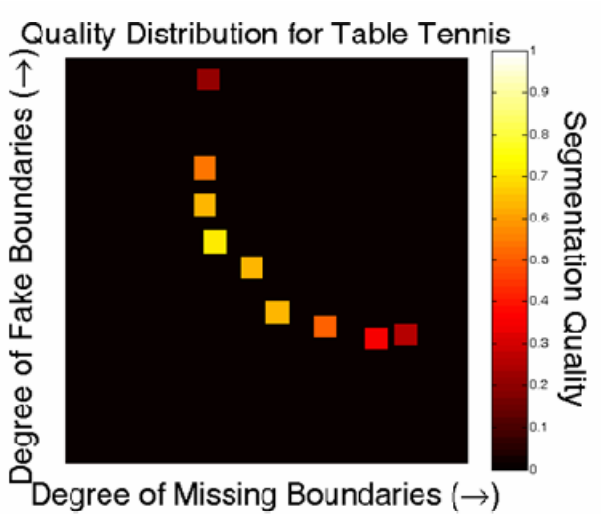
Quality Distribution for Table Tennis
Degree of Fake Boundaries (→)
Degree of Missing Boundaries (→)
Segmentation Quality

(f)

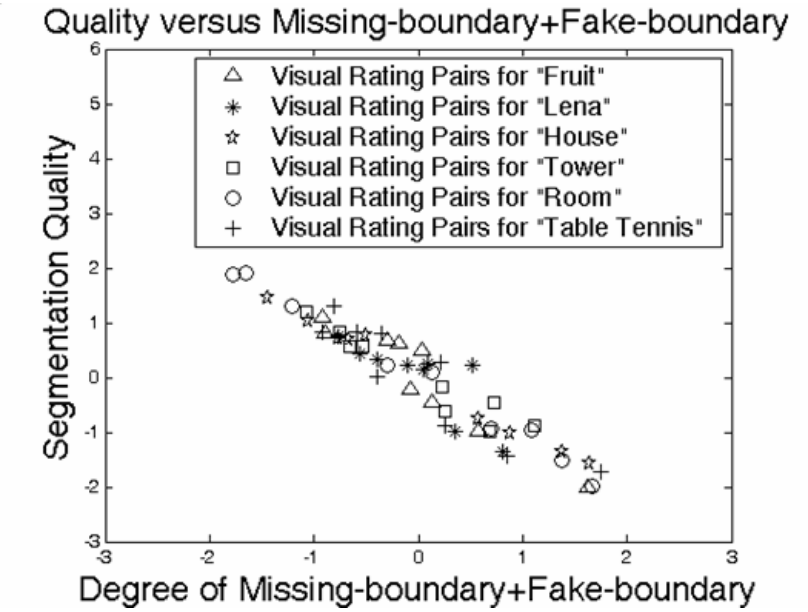

(g)

Fig. 4.8 Segmentation quality with respect to the degree of missing boundary and the degree of fake boundary.

(a) “Fruit”. (b) “Lena”. (c) “House”. (d) “Tower”. (e) “Room”. (f) “Table Tennis”. (g) The quality of segmentation versus the degree of missing-boundary plus the degree of fake-boundary.

4.2.2 Quantitative Evaluation for Color Segmentation

In Section 4.2.2.1, we first propose visible color difference-based quantitative measures of visual errors. To avoid directly evaluating the subjectively perceived quality of color segmentation, two objective visual quantities, the quantity of missing boundaries and the quantity of fake boundaries, are considered. To explore how missing boundaries and fake boundaries affect the perceived quality of color segmentation, a few visual rating experiments were made. On the other hand, to fit for human's visual perception on color difference, the visible color difference has been defined in Section 4.1.2. Based on these experiments and the definition of visible color difference, two measures, named intra-region visual error and inter-region visual error, are proposed to estimate the degrees of missing boundaries and fake boundaries, respectively. With these two measures, a scheme by using the Inter-Region-Error/Intra-Region-Error plot for the evaluation of color segmentation is proposed. Then, in Section 4.2.2.2, we'll demonstrate the use of the Inter-Region-Error/Intra-Region-Error plot for color Segmentation. Also, in Section 4.2.2.3, we'll demonstrate the use of the Inter-Region-Error/intra-Region-Error plot for the performance comparison of various color segmentation algorithms.

4.2.2.1 Quantitative Measures of Visual Errors Based on Visible Color Difference

To estimate the degree of missing boundaries and fake boundaries, some appropriate quantitative measures are formulated in this section. In general, for quantitative methods, three basic types of measures are considered: 1) intra-region measure; 2) inter-region measure; and 3) region-shape measure [42][43]. Usually, intra-region measures are designed to measure the homogeneity within segmented regions, while

inter-region measures are designed to measure the heterogeneity between adjacent regions. On the other hand, region-shape measures are usually designed to measure the regularity of region shape. Intuitively, the former two types of measures may be closely linked to the way humans evaluate the quality of segmentation at the discrimination level, while the third type of measures is more likely to be linked to the evaluation at the recognition level. Moreover, the intra-region measure which evaluates the homogeneity within segmented regions can be adopted to estimate the degree of missing boundaries, while the inter-region measure which evaluates the heterogeneity between adjacent regions can be used to estimate the degree of fake boundaries. Hence, in this dissertation, we focus on the discussion of intra-region measure and inter-region measure. In Section 4.2.2.1.1, 4.2.2.1.2, and 4.2.2.1.3, some new quantitative measures, which are based on the preference of having less visual errors for the evaluation of color segmentation, are introduced. Also, some experiment results deduced in Section 4.2.1 demonstrate that the combination of the degree of missing boundaries and the degree of fake boundaries is closely related to humans' subjective evaluation over segmentation performance. Therefore, if we can formulate some appropriate measures to estimate the degrees of missing boundaries and fake boundaries, we may find some quantitative and effective ways to evaluate color segmentation algorithms.

4.2.2.1.1 Intra-region Visual Error

To evaluate the degree of missing boundaries, a measure, named "intra-region visual error", is designed. In each segmented region, these pixels with ***visible*** color difference away from the average color of that region are regarded as pixels with visible color errors. Intuitively, a properly segmented region should contain as few visible color errors as possible. Any missing boundary will cause the increase of intra-region visual errors. Given an $N \times M$ color image $f(x,y)$, we first denote $\hat{f}(x,y)$ as the segmented color image, with the color of each segmented region being filled with the average color of that region. We then define the intra-region error as:

$$\mathrm{E}_{\mathrm{intra}}(I) = \frac{\sum_{x=1}^{N}\sum_{y=1}^{M} u(\left\| f(x,y) - \hat{f}(x,y) \right\|_{L^*a^*b^*} - th)}{N \times M}, \tag{4.8}$$

where $\| \|_{L^*a^*b^*}$ denotes the color difference in the CIE L*a*b* space, *th* denotes the threshold for visible color difference, and u(.) denotes the step function that is defined as

$$u(x) = \begin{cases} 1 & x \geq 0 \\ 0 & \text{otherwise} \end{cases}. \tag{4.9}$$

In this dissertation, we choose the threshold "*th*" to be 6 based on the reason explained in Section 4.1.2

In Equation (4.8), given a segmented result, we calculate the total amounts of the pixels with visible color errors in order to estimate the degree of missing boundaries. When a segmented region contains more missing boundaries, the average color of that region will has a larger color difference from the original colors of those pixels. Once the color difference is large enough to be visible, the number of the pixels will be counted in Equation (4.8). Hence, as the degree of missing boundaries increases, there will be more pixels with visible color errors in Equation (4.8).

In Table 4.4, for each of the 6 color images, we confirm that the correlation between the intra-region visual error and the degree of missing boundaries is significant at the 0.01 level and the sign of the correlation is positive. This implies that, given a segmentation result, the intra-region visual error could be an effective way to estimate the perceived degree of missing boundaries.

Table 4.4: Missing-boundary vs. Intra-region visual error

Color Image / Correlation	Fruit	Lena	House	Tower	Room	Table Tennis
Missing-boundary vs. Intra-error	0.978**	0.980**	0.901**	0.980**	0.866**	0.918**

** correlation is significant at the 0.01 level (two-tailed) [59].

4.2.2.1.2 Inter-region Visual Error

On the other hand, the second measure, named "inter-region visual error", is designed to evaluate the degree of fake boundaries. Given a color segmentation result, we take into account these boundary pixels with ***invisible*** color difference across the boundary. Intuitively, these pixels are not supposed to be detected as boundaries. Hence, as more fake boundaries appear in the segmented image, more inter-region visual errors are expected. In this dissertation, we define the inter-region visual error of a segmented image as:

$$\mathrm{E}_{\mathrm{inter}}(I) = \frac{\sum_{i=1}^{R}\sum_{\substack{j=1 \\ j\neq i}}^{R} w_{ij} \times u\left(th - \left\|\hat{f}_i - \hat{f}_j\right\|_{L^*a^*b^*}\right)}{N \times M}, \tag{4.10}$$

where R denotes the number of segmented regions, and w_{ij} denotes the joined length between Region i and Region j. Here, w_{ij} is equal to zero if Region i and Region j are not connected.

Similarly, in Equation (4.10), given a segmented result, we calculate the total amounts of the boundary pixels with invisible color errors to measure the degree of fake boundaries. Actually, when two adjacent regions contain an invisible boundary, the color difference between the average colors of the adjacent regions will be small. Therefore, once the average color difference between any two adjacent regions is too small to be visible, the joined boundary pixels will be counted. Hence, if the degree of fake boundaries increases, more boundary pixels with invisible color errors will be counted in Equation (4.10).

In Table 4.5, for each of the 6 color images, we confirm that the correlation between inter-region visual error and the perceived degree of fake boundaries in the visual rating experiments is also significant at the 0.01 level and the sign of the correlation is positive. This implies that the inter-region visual error could be an effective measure for the perceived degree of fake boundaries.

Table 4.5: Fake-boundary vs. Inter-region visual error

Color Image / Correlation	Fruit	Lena	House	Tower	Room	Table Tennis
Fake-boundary vs. Inter-error	0.961**	0.964**	0.988**	0.991**	0.982**	0.853**

** correlation is significant at the 0.01 level (two-tailed) [59].

4.2.2.1.3 The Inter-Region Error/Intra-Region Error Plot

With these two newly designed measures, we can estimate the degrees of missing boundaries and fake boundaries, respectively. Even though each of these two measures is still image-dependent, the alliance of both measures may provide an effective way for segmentation evaluation.

In Fig. 4.9, we show the plot of intra-region visual error versus inter-region visual error. As the given image is under-segmented, more boundaries are missing and the intra-region visual error increases. On the contrary, as the image is over-segmented, more fake boundaries appear and the inter-region error increases. These two measures are complementary to each other. With these two measures, the segmentation can be evaluated in a reasonable way. These two measures are also closely related in physical meaning. This makes the trade-off between these two measures much easier.

In this dissertation, we focus on the evaluation of color segmentation for these images without complex texture. In Section 4.2.2.2, the use of the Inter-Region-Error/Intra-Region-Error plot in the evaluation of color segmentation is to be introduced. First, the evaluation of segmentation results for a given segmentation algorithm is described. Then, the evaluation method for the comparison of various segmentation algorithms is presented in Section 4.2.2.3.

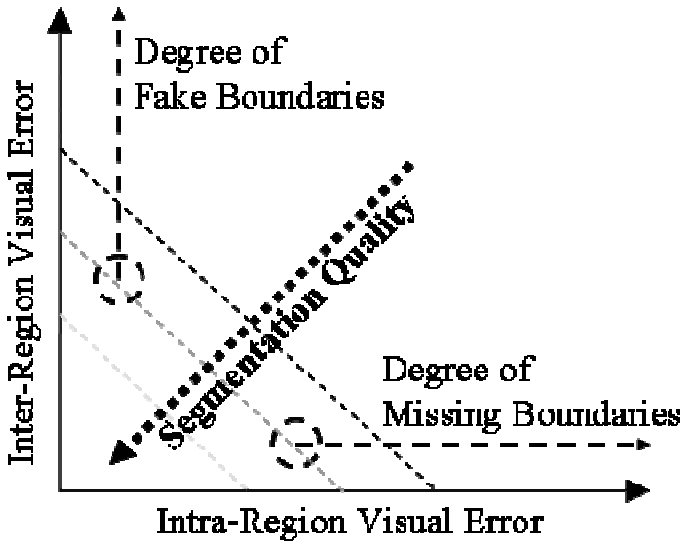

Fig. 4.9 Inter-Region-Error/Intra-Region-Error plot.

4.2.2.1.4 Ratio of Intra-region Visual Error to Inter-region Visual Error

As shown in Figs. 4.8(a)-(f), the preferred segmented results are usually located at the lower-left corner in the plot of the quality segmentation versus the sum of the degree of missing boundaries and the degree of fake boundaries. Since the defined intra-region visual error is proportional to the degree of missing boundaries and the inter-region visual error is proportional to the degree of missing boundaries, a preferred segmentation result is expected to locate at the lower-left corner of the Inter-Region-Error/Intra-Region-Error plot, as shown in Fig. 4.9. Analogous to the phenomenon that perceived segmentation quality is closely correlated with the sum of the degree of missing boundaries and the degree of fake boundaries, we assume the visual quality of a segmentation result can be evaluated based on a linear combination of intra-region visual error and inter-region visual error. That is, for I_j^i, the jth segmentation result of the ith image, we define its total visual error E_j^i as

$$E_j^i = \alpha_j^i E_{\text{intra}}\left(I_j^i\right) + \beta_j^i E_{\text{inter}}\left(I_j^i\right). \tag{4.11}$$

The total visual error E_j^i may also be normalized with respect to α_j^i and we have

$$\hat{E}_j^i = E_{\text{intra}}\left(I_j^i\right) + \lambda_j^i E_{\text{inter}}\left(I_j^i\right). \tag{4.12}$$

In Equation (4.12), the coefficient λ_j^i is to balance the contributions of visual error from $E_{\text{intra}}(I_j^i)$ and $E_{\text{intra}}\left(I_j^i\right)$. For different image contents and different segmentation algorithms, λ_j^i's are expected to be different. Based on the results of the visual experiments we made in Section 4.2.1, we may perform linear fitting over

perceived segmentation quality, measured intra-region errors, and measured inter-region error to estimate the value of λ. Table 4.6 shows the estimated values of λ for these 6 color images. In general, as the value of λ increases, the preferred segmented results are the results with more intra-region visual errors; while as the value of λ decreases, the preferred segmented results are the results with more inter-region visual errors. We can easily see that for different images and different algorithms the values of λ are quite different. Nevertheless, for each segmentation algorithm, the values of λ are basically between 1 and 10, except the value of λ for the Edge Flow algorithm with the Fruit image

Table 4.6: Optimal Values of λ for Different Images

Color Image	Fruit	Lena	House	Tower	Room	Table Tennis
λ_i	0.586	1.36	9.05	7.70	3.18	5.34
Segmentation algorithm	Edge Flow	Edge Flow	JSEG	JSEG	Mean Shift	Mean Shift

To further investigate the impact of coefficient λ over the performance of the proposed evaluation scheme, we discuss the correlation of the averaged segmentation quality and the total visual error with respect to λ's. As shown in Fig. 4.10, the 9 triangles denote the minus values of the correlation coefficients for the segmented results of "Fruit", with λ = 1, 2, …, 9, respectively. Similarly, the asterisks, pentagrams, squares, circles and plus-signs denote the minus correlation coefficients for the segmented results of "Lena", "House", "Tower", "Room" and "Table Tennis", respectively. It can be seen that the λ's in Table 4.6 correspond to the λ that causes the maximal correlation. For example, for the case of the "Room" image, the minus value of the correlation coefficient reaches its local maximum around λ = 3. Moreover, for most images, the value of the correlation coefficient remains large even if λ is

changed. The averaged values of the minus correlation coefficients are represented in the black solid line. It can be seen that, with λ ranging from 2 to 7, the correlation of the averaged segmentation quality and the total visual error remains significant at the 0.05 level. Hence, in this dissertation, we use the averaged value of λ's in Table 4.6, as calculated in Equation (4.13), to be a typical choice of λ.

$$\lambda \equiv \frac{1}{6}\sum_{i=1}^{6}\lambda_i = 4.54\,. \tag{4.13}$$

Of course, this typical choice of λ is only a rough estimate and may not work for all types of images. How to automatically choose an appropriate value of λ for a given image deserves further investigation in the future.

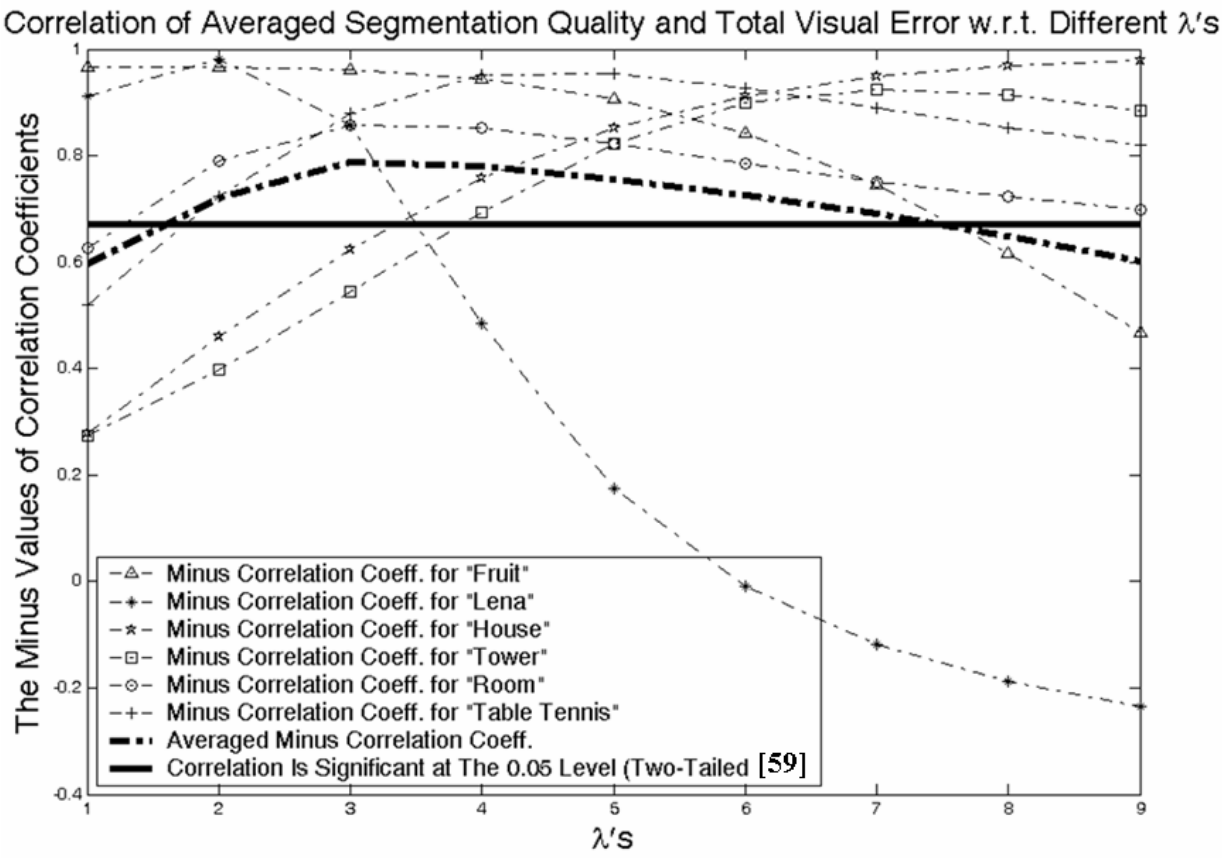

Fig. 4.10 The correlation plot of averaged segmentation quality and total visual error with respect to different λ's.

4.2.2.2 Color Segmentation Evaluation Based on Inter-Region-Error/Intra-Region-Error Plot

In this section, the use of the Inter-Region-Error/Intra-Region-Error plot in the evaluation of color segmentation is introduced. Also, the automatic selection of parameter settings for a given segmentation algorithm is described.

Fig. 4.11(a) shows the "Fruit" image. Figs. 4.11(b)-(f) show several segmentation results of Fig. 4.11(a) produced by the Edge-Flow algorithm [14], with different parameter settings. Subjectively, Fig. 4.11(c) is preferable. In comparison with Fig. 4.11(c), Fig. 4.11(b) has a higher degree of fake boundaries, while Figs. 4.11(d)-(f) have higher degrees of missing boundaries. As shown from left to right in Fig. 4.11(s), the five blue circles represent the "intra-region visual error" versus "inter-region visual error" pairs of Figs. 4.11(b)-(f), respectively. It can be seen that, with similar intra-region errors, Fig. 4.11(b) has larger inter-region error values than that of Fig. 4.11(c). On the other hand, with similar inter-region errors, Figs. 4.11(d)-(f) have larger intra-region error values than that of Fig. 4.11(c). Hence, in the selection of parameter setting, the sum of $E_{intra}(I)$ and $E_{inter}(I)|_{\lambda=4.54}$ may serve as a suitable measure for the evaluation of segmentation performance. As the sum reaches a smaller value, the parameter setting is expected to achieve better segmentation. In Fig. 4.11(s), we use the quality straight line, $E_{intra}(I) + E_{inter}(I)|_{\lambda=4.54}$ to illustrate this idea. Here we use gray straight quality lines to denote the lines $E_{intra}(I) + E_{inter}(I)|_{\lambda=4.54}$ = constant. It can be easily seen that Fig. 4.11(c) does have the smallest sum if compared with the other four.

In Figs. 4.11(g) and 4.11(m), we show another two examples of color images. Figs. 4.11(h)-(l) show the segmentation results of Fig. 4.11(g) produced by the JSEG algorithm [15], while Figs. 4.11(n)-(r) show the segmentation results of Fig. 4.11(m) produced by the Mean-Shift algorithm [27], all with different parameter settings.

Similarly, in Fig. 4.11(s), from left to right, the "intra-region error" versus "inter-region error" pairs of Figs. 4.11(h)-(l) are represented in five magenta triangles; while the error pairs of Figs. 4.11(n)-(r) are represented in five red crosses. It can be easily seen that Fig. 4.11(j) has the smallest error sum if compared with Figs. 4.11(h)-(l); while Fig. 4.11(p) has the smallest error sum if compared with Figs. 4.11(n)-(r). In perception, the segmented results in Fig. 4.11(j) and Fig. 4.11(p) do appear to be the most preferable results among these candidates.

Similarly, In Figs. 4.12(a), 4.12(g) and 4.12(m), we show the other three color images. Figs. 4.12(b)-(f) show the segmentation results of Fig. 4.12(a) produced by the Edge-Flow algorithm [14]; Figs. 4.12(h)-(l) show the segmentation results of Fig. 4.12(g) produced by the JSEG algorithm [15]; and Figs. 4.12(n)-(r) show the segmentation results of Fig. 4.12(m) produced by the Mean-Shift algorithm [27]; all with different parameter settings. Similarly, in Fig. 4.12(s), from left to right, the "intra-region error" versus "inter-region error" pairs of Figs. 4.12(b)-(f) are represented in five blue circles; the error pairs of Figs. 4.12(h)-(l) are represented in five magenta triangles; and the error pairs of Figs. 4.12(n)-(r) are represented in five red crosses. It can be easily seen that Fig. 4.12(d) has the smallest error sum if compared with Figs. 4.12(b)-(f); Fig. 4.12(j) has the smallest error sum if compared with Figs. 4.12(h)-(l); and Fig. 4.12(p) has the smallest error sum if compared with Figs. 4.12(n)-(r). In perception, the segmented results in Fig. 4.12(d), Fig. 4.12(j) and Fig. 4.12(p) do appear to be the most preferable results among these candidates.

In summary, we use the above three simulation results to demonstrate how the Inter-Region-Error/Intra-Region-Error plot can be used to automatically select the parameter setting based on the performance of segmentation results. In fact, $E_{intra}(I)$ and $E_{inter}(I)$ can be combined in various forms based on user's requirements. So far, we found that the simple form $E_{intra}(I) + E_{inter}(I)$ performs pretty well when applied to

various types of color images.

(a)

(b)

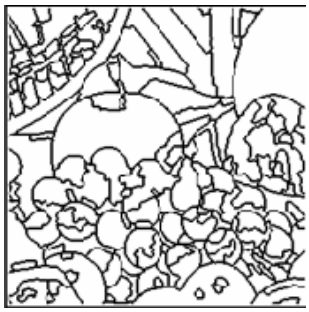

(c)

(d)

(e)

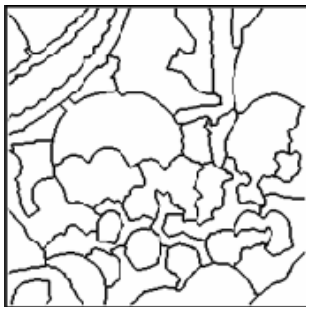

(f)

(g)

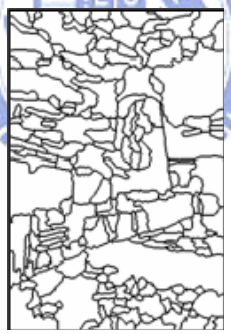

(h)

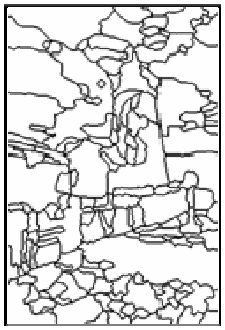

(i)

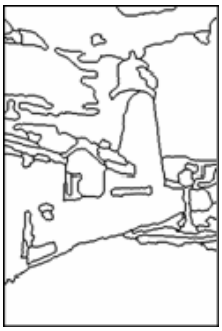

(j)

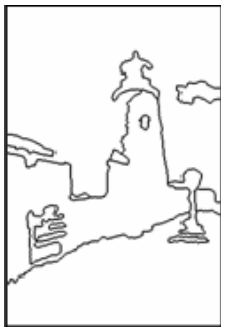

(k)

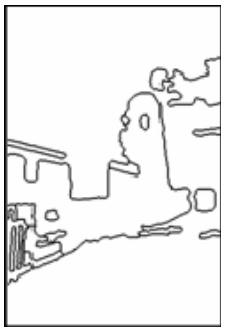

(l)

(m) (n) (o)

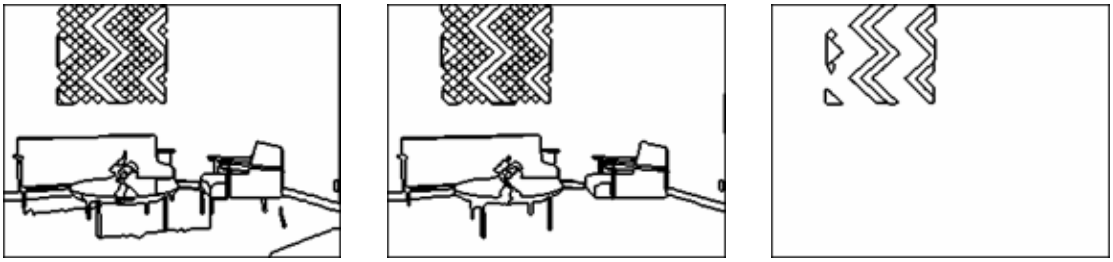

(p) (q) (r)

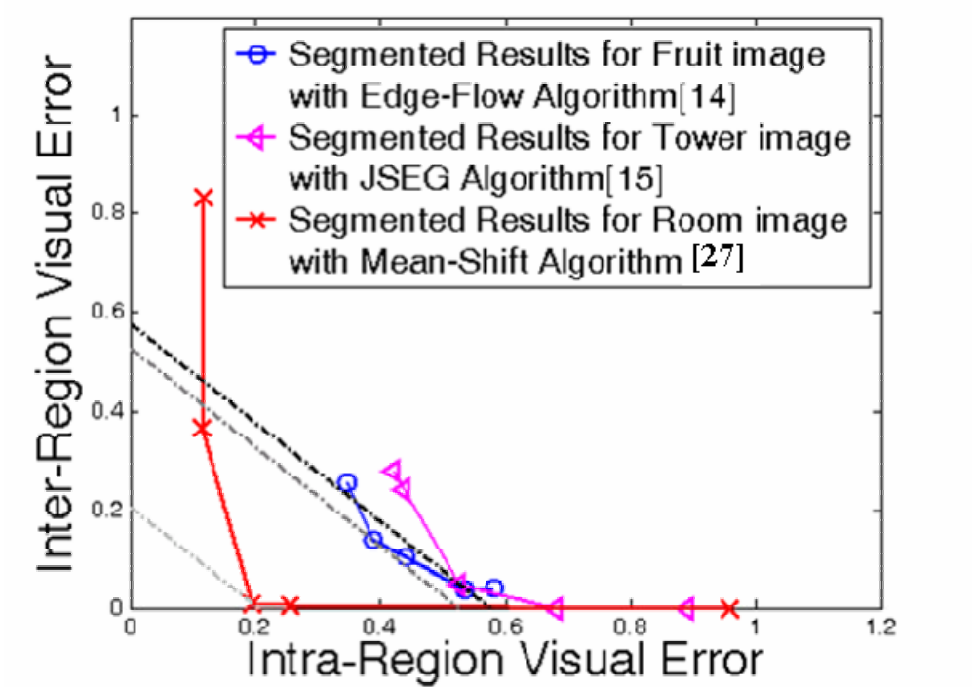

(s)

Fig. 4.11 Evaluation of segmentation results.

(a) The Fruit image. (g) The Tower image. (m) The Room image.
(b)-(f) Segmented results of a by using the Edge-Flow algorithm [14].
(h)-(l) Segmented results of g by using the JSEG algorithm [15].
(n)-(r) Segmented results of m by using the Mean-Shift algorithm [27].
(s) The Inter-Region-Error/Intra-Region-Error plot of b-f, h-l, and n-r.

(a)

(b)

(c)

(d)

(e)

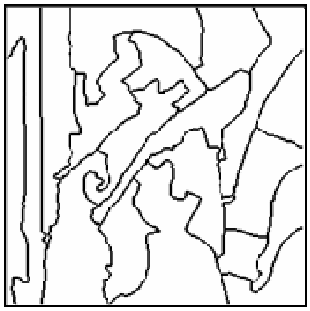

(f)

(g)

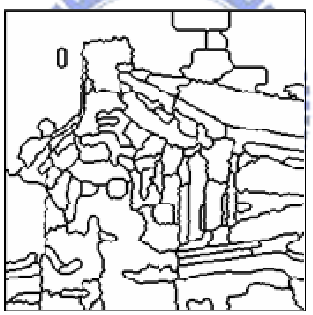

(h)

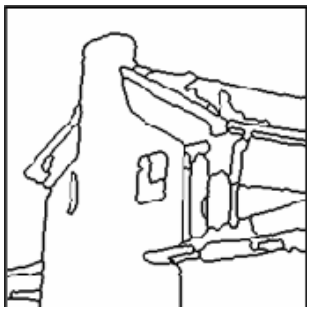

(i)

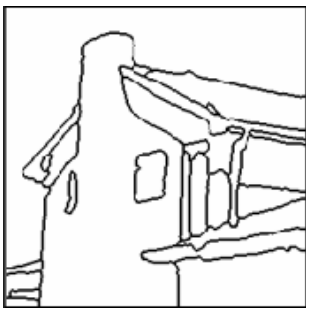

(j)

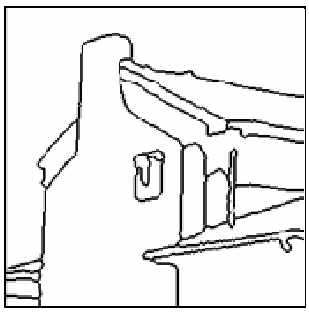

(k)

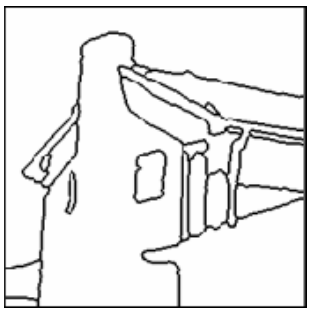

(l)

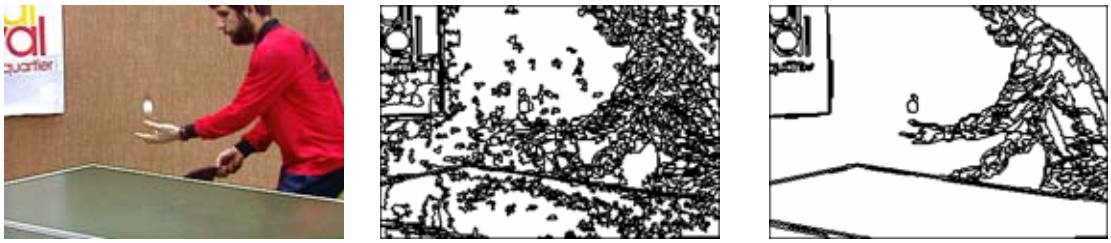

(m) (n) (o)

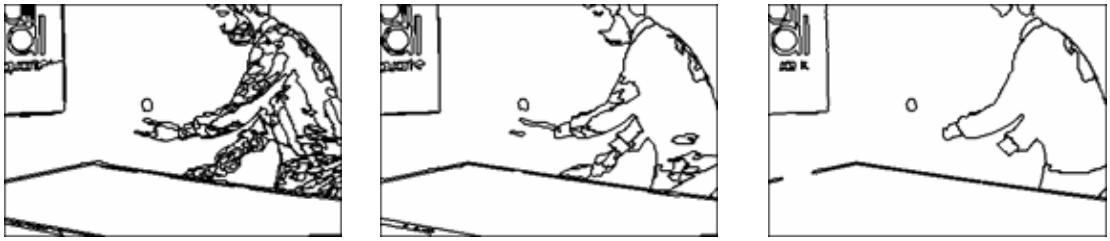

(p) (q) (r)

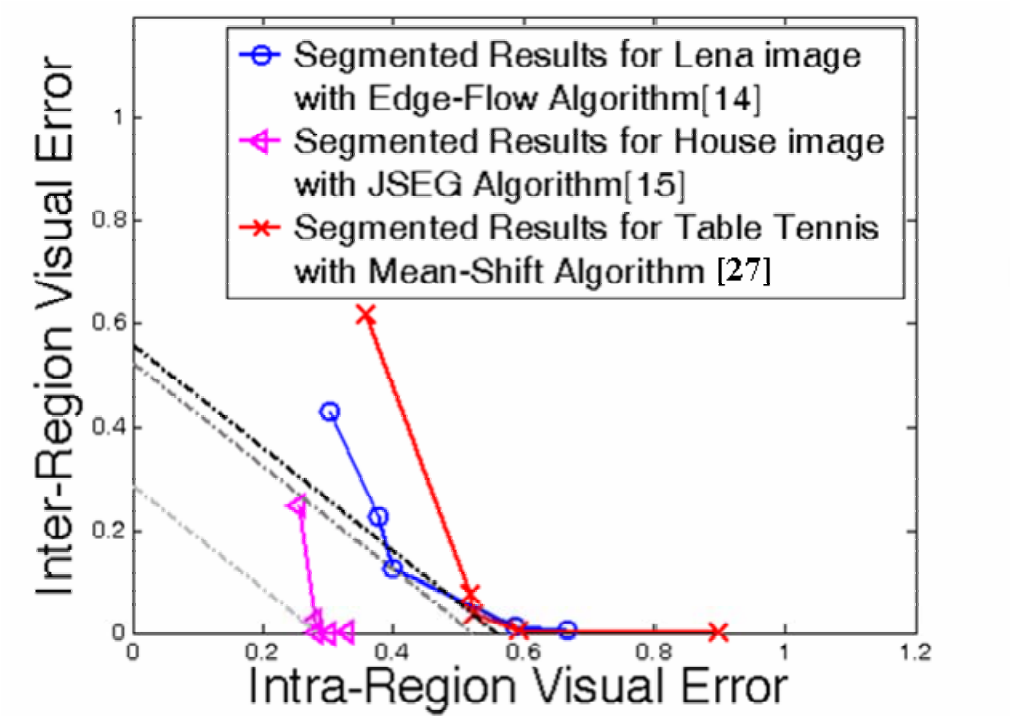

(s)

Fig. 4.12 Evaluation of segmentation results.

(a) The Lena image. (g) The House image. (m) The Table Tennis image.
(b)-(f) Segmented results of a by using the Edge-Flow algorithm [14].
(h)-(l) Segmented results of g by using the JSEG algorithm [15].
(n)-(r) Segmented results of m by using the Mean-Shift algorithm [27].
(s) The Inter-Region-Error/Intra-Region-Error plot of b-f, h-l, and n-r.

In Table 4.7, we compare the proposed evaluation measure, $E_{intra}(I) + E_{inter}(I)|_{\lambda=4.54}$, with three existing evaluation measures in the literature. These three measures are the $F(I)$ measure in [49], the $F'(I)$ measure in [50], and the $Q(I)$ measure in [50]. In Table 4.7, the five segmentation results shown in Fig. 4.11(b)-(f) are used as the test inputs for the comparison. Here, the "averaged visual quality" denotes the subjective evaluation results based on the visual experiment mentioned in Section 4.2.1, with a larger number indicating a better rating of perceived quality. The other four rows indicate the evaluation scores based on the proposed measure, $E_{intra}(I) + E_{inter}(I)|_{\lambda=4.54}$, the $F(I)$ measure, the $F'(I)$ measure, and the $Q(I)$ measure, respectively. For these four evaluation measures, a smaller number indicates a better rating of the measurement. Moreover, the numbers in parentheses indicate the ranking of these five test inputs based on the applied evaluation measure. According to the subjective visual experiment results, Fig. 4.11(c) is ranked as the best segmentation results among Figs. 4.11(b)-(f). As shown in Table 4.7, the proposed evaluation measure does pick Fig. 4.11(c) as the best segmentation with the smallest visual errors, while all the other three evaluation measures pick Fig. 4.11(f) as the best segmentation result. Similarly, in Tables 4.8~4.12, we show the comparisons over the other five color images. All these tables illustrate that the proposed evaluation measure $E_{intra}(I) + E_{inter}(I)$ does provide a reasonable and reliable way for the evaluation of color segmentation.

Table 4.7: Evaluation Comparison for the Fruit image

Segmented Result / Evaluation	Fig. 4.11(b)	Fig. 4.11(c)	Fig. 4.11(d)	Fig. 4.11(e)	Fig. 4.11(f)
Averaged Visual Quality	0.488 (3)	1.100 (1)	0.806 (2)	-0.225 (4)	-0.469 (5)
$E_{intra}(I) + E_{inter}(I)\|_{\lambda=4.54}$	0.600 (4)	0.528 (1)	0.542 (2)	0.572 (3)	0.625 (5)
$F(I)$	0.753 (5)	0.730 (4)	0.440 (3)	0.379 (2)	0.285 (1)
$F'(I)$	0.075 (5)	0.073 (4)	0.044 (3)	0.038 (2)	0.029 (1)
$Q(I)$	0.201 (5)	0.183 (4)	0.154 (3)	0.143 (2)	0.128 (1)

Table 4.8: Evaluation Comparison for the Tower image

Segmented Result / Evaluation	Fig. 4.11(h)	Fig. 4.11(i)	Fig. 4.11(j)	Fig. 4.11(k)	Fig. 4.11(l)
Averaged Visual Quality	-0.469 (4)	-0.181 (3)	0.569 (1)	0.556 (2)	-0.625 (5)
$E_{intra}(I) + E_{inter}(I)\|_{\lambda=4.54}$	0.702 (4)	0.677 (2)	0.576 (1)	0.681 (3)	0.893 (5)
$F(I)$	1.090 (5)	0.987 (4)	0.194 (3)	0.091 (1)	0.184 (2)
$F'(I)$	0.109 (5)	0.099 (4)	0.019 (3)	0.009 (1)	0.018 (2)
$Q(I)$	0.354 (5)	0.330 (4)	0.153 (2)	0.092 (1)	0.180 (3)

Table 4.9: Evaluation Comparison for the Room image

Segmented Result / Evaluation	Fig. 4.11(n)	Fig. 4.11(o)	Fig. 4.11(p)	Fig. 4.11(q)	Fig. 4.11(r)
Averaged Visual Quality	-0.963 (4)	0.100 (3)	1.869 (1)	1.306 (2)	-1.988 (5)
$E_{intra}(I) + E_{inter}(I)\|_{\lambda=4.54}$	0.950 (4)	0.479 (3)	0.205 (1)	0.262 (2)	0.959 (5)
$F(I)$	1.021 (5)	0.540 (4)	0.389 (2)	0.392 (3)	0.076 (1)
$F'(I)$	0.102 (5)	0.054 (4)	0.039 (2)	0.039 (2)	0.008 (1)
$Q(I)$	0.155 (5)	0.094 (2)	0.085 (1)	0.107 (3)	0.135 (4)

Table 4.10: Evaluation Comparison for the Lena image

Segmented Result / Evaluation	Fig. 4.12(b)	Fig. 4.12(c)	Fig. 4.12(d)	Fig. 4.12(e)	Fig. 4.12(f)
Averaged Visual Quality	0.219 (3)	0.231 (2)	0.765 (1)	-0.999 (4)	-1.363 (5)
$E_{intra}(I) + E_{inter}(I)\|_{\lambda=4.54}$	0.733 (5)	0.606 (3)	0.525 (1)	0.602 (2)	0.673 (4)
$F(I)$	0.902 (5)	0.769 (4)	0.614 (3)	0.224 (2)	0.173 (1)
$F'(I)$	0.090 (5)	0.077 (4)	0.061 (3)	0.022 (2)	0.017 (1)
$Q(I)$	0.175 (5)	0.173 (4)	0.149 (3)	0.127 (2)	0.113 (1)

Table 4.11: Evaluation Comparison for the House image

Segmented Result / Evaluation	Fig. 4.12(h)	Fig. 4.12(i)	Fig. 4.12(j)	Fig. 4.12(k)	Fig. 4.12(l)
Averaged Visual Quality	-1.363 (5)	1.050 (2)	1.469 (1)	0.725 (4)	0.769 (3)
$E_{intra}(I) + E_{inter}(I)\|_{\lambda=4.54}$	0.502 (5)	0.303 (2)	0.286 (1)	0.303 (2)	0.333 (4)
$F(I)$	0.473 (5)	0.194 (4)	0.125 (3)	0.100 (1)	0.116 (2)
$F'(I)$	0.047 (5)	0.019 (4)	0.013 (3)	0.001 (1)	0.012 (2)
$Q(I)$	0.148 (5)	0.072 (4)	0.059 (2)	0.050 (1)	0.064 (3)

Table 4.12: Evaluation Comparison for the Table Tennis image

Segmented Result / Evaluation	Fig. 4.12(n)	Fig. 4.12(o)	Fig. 4.12(p)	Fig. 4.12(q)	Fig. 4.12(r)
Averaged Visual Quality	-1.713 (5)	0.794 (3)	1.306 (1)	0.831 (2)	-0.894 (4)
$E_{intra}(I) + E_{inter}(I)\|_{\lambda=4.54}$	0.977 (5)	0.595 (2)	0.560 (1)	0.598 (3)	0.897 (4)
$F(I)$	6.320 (5)	2.195 (4)	1.738 (3)	0.704 (2)	0.218 (1)
$F'(I)$	0.632 (5)	0.220 (4)	0.174 (3)	0.070 (2)	0.022 (1)
$Q(I)$	1.124 (5)	0.576 (4)	0.462 (3)	0.268 (2)	0.184 (1)

In summary, in this dissertation, we describe a new evaluation scheme based on the visible color difference for color segmentation. To avoid directly evaluating the subjective quality of color segmentation, we estimate the degrees of missing boundaries and fake boundaries first. With the combination of these two quantities, we could approach the subjective evaluation of color segmentation. Also, based the definition of visible color difference, we design two measures, the intra-region visual

error and inter-region visual error, to estimate the degrees of missing boundaries and fake boundaries, respectively. We found the measures based on these two types of visible color differences have significant correlation with the degree of missing boundaries and the degree of fake boundaries. With these two measures, an evaluation scheme is proposed to evaluate the segmentation results and help the automatic selection of parameters for a given segmentation algorithm. The simulation results have demonstrated the potential of this approach in providing reliable and efficient evaluations over color segmentation. Moreover, given that the proposed measures of segmentation quality are designed to fit for subjective evaluations of segmentation quality, these measures are particularly applicable to tasks such as content-based image retrieval.

4.2.2.3 Performance Comparison of Color Segmentation Algorithms Based on Inter-Region-Error/Intra-Region-Error Plot

The performance comparison between different segmentation algorithms is also an important issue in image segmentation. In the evaluation of segmentation algorithms, an objective and quantitative evaluation is essential. In this section, we demonstrate how to use the Inter-Region-Error/Intra-Region-Error plot to compare the performance of various segmentation algorithms.

Fig. 4.13(a) shows a color image and several segmented results produced by the JSEG algorithm [15] and the Mean-Shift algorithm [27]. In Fig. 4.13(h), the red circles denote the inter-region error and the intra-region error pairs of 7 segmentation results produced by the JSEG algorithm, while the blue crosses represent the error pairs of 7 segmentation results produced by the Mean-Shift algorithm. Fig. 4.13(b)(c)(d) show three of these seven segmentation results produced by the JSEG algorithm, while Fig. 4.13(e)(f)(g) show three of these seven segmentation results produced by the Mean-Shift algorithm. With these sample pairs, a 2^{nd}-order curve fitting is adopted to estimate the tendency between the inter-region error and the intra-region error in Fig. 4.13(h). Here, the red curve shows the performance tendency of the JSEG algorithm, while the blue curve shows the performance tendency of the Mean-Shift algorithm. With these two tendency curves, it can be easily seen that with a similar intra-region error, the segmentation results produced by the Mean-Shift algorithm have smaller inter-region errors. That is, with a similar intra-error value, the segmentation results produced by the JSEG algorithm tend to be more over-segmented. Similarly, with a similar inter-region error, the segmentation results produced by the Mean-Shift algorithm tend to have smaller intra-region errors.

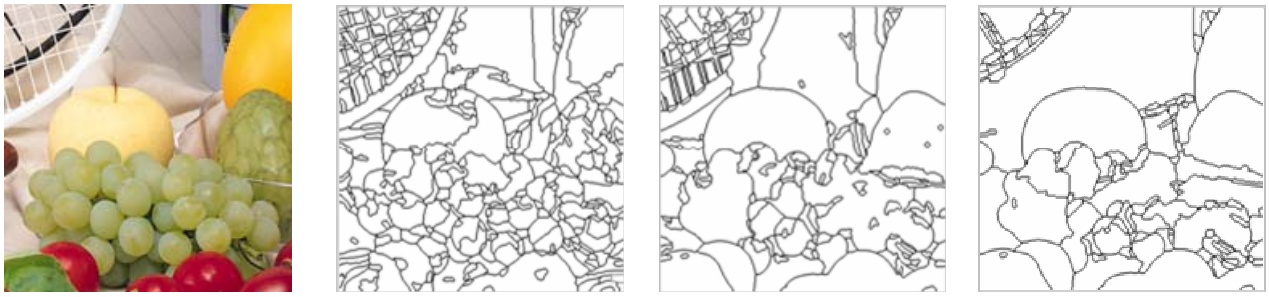

(a) (b) (c) (d)

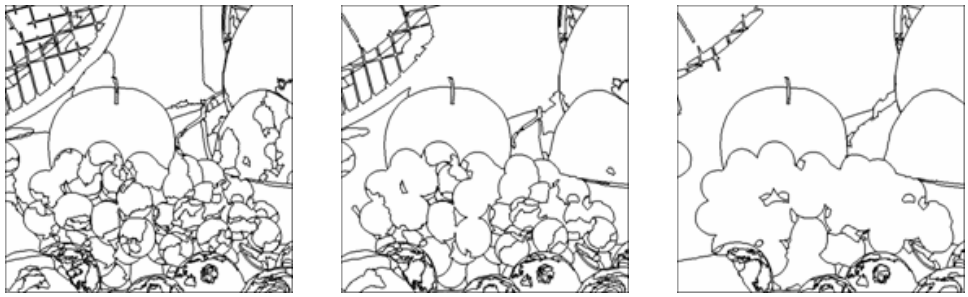

(e) (f) (g)

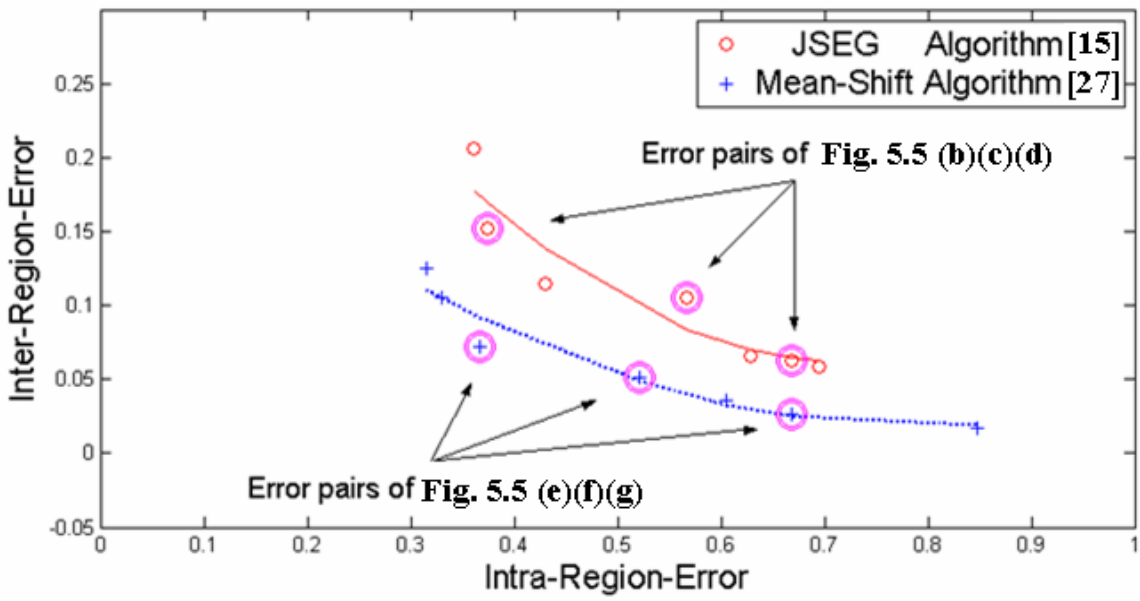

(h)

Fig. 4.13 Comparison with different algorithms.

(a) Original image.

(b)(c)(d) Segmentation results using the JSEG algorithm [15].

(e)(f)(g) Segmentation results using the Mean-Shift algorithm [27].

(h) Comparison of the JSEG algorithm and the Mean-Shift algorithm.

4.3 Color Segmentation Algorithms Based on Color-Contrast and Visible-Color-Difference

In Section 4.3.1, we'll introduce a color-contrast based color segmentation algorithm, which is an image domain-based approach. On the other hand, we'll also propose in Section 4.3.2 a visible-color-difference based color segmentation, which unites with quantitative visual measures

4.3.1 Color Segmentation Algorithm Based on Color Contrast

As mentioned in Section 2.2, for image domain-based color segmentation approaches, the gauge of segmentation is usually based on data variation in a local area. Similarity-based algorithms group together pixels with small data variation, while discontinuity-based algorithms detect places with large data variation. To measure data variation, the derivative information is commonly used. Nevertheless, as aforementioned, direct uses of derivative values may not faithfully reflect the way human perceives object boundaries. Basically, each edge on this profile comprises three major factors: 1) edge height, 2) edge slope, and 3) noise irritation. Among these three factors, edge height is closely related to the way human perceives edges. In Section 4.1.1.1, we define edge contrast in terms of edge height, which is the intensity or color difference between the high-curvature points on the two sides of the boundary. To detect these high-curvature points, we use a 2nd derivative operator B(x) to estimate the curvature of the profile.

$$B(x) = \delta(x) - N(x;0,\sigma). \tag{4.14}$$

By convoluting a profile I(x) with this operator, we have

$$\varphi(x) = I(x) \otimes B(x)$$
$$= I(x) - I(x) \otimes N(x;0,\sigma). \quad (4.15)$$

Basically, $\varphi(x)$ can be imagined as the 2nd derivative of the profile $I(x)$. The local extremes of $\varphi(x)$ correspond to the high-curvature points of $I(x)$.

Since the 2nd derivative is orientation-dependent, the contrast information at an image pixel has to be measured along various orientations. As aforementioned, we detect boundaries by checking the relations between each pixel and its eight neighbors. Hence, four directional operators are used at each pixel to measure the curvature information at that pixel. These four directions are 0°, 45°, 90° and 135°, respectively. Based on directional contrast information and a single-threshold scheme over the estimated color contrast, the flowchart of the proposed algorithm is illustrated in Fig. 4.14.

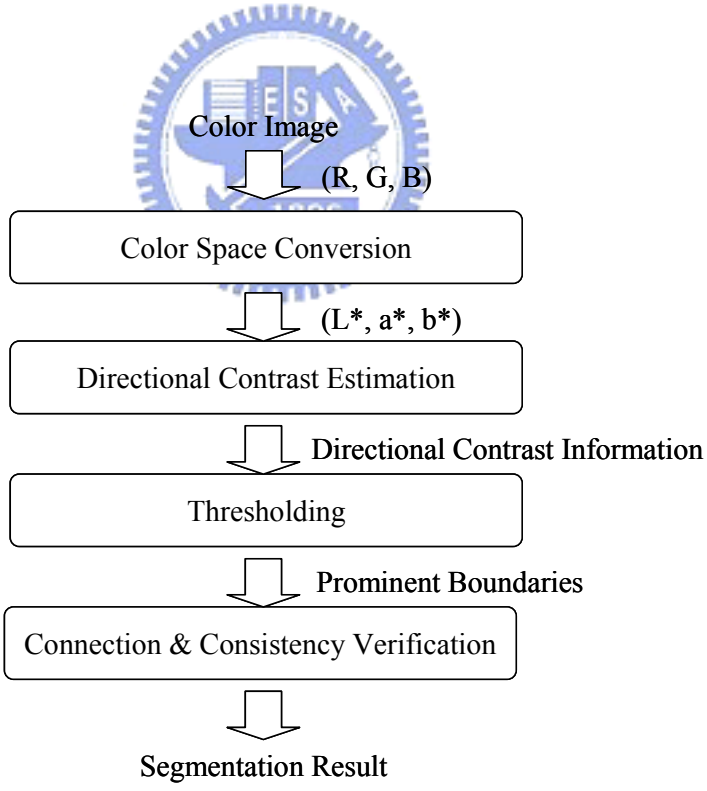

Fig. 4.14 Flow chart of the proposed algorithm.

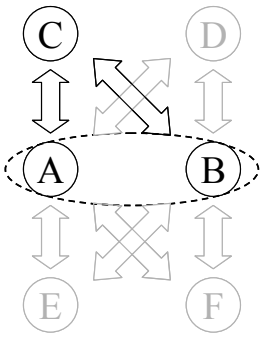

Fig. 4.15 Illustration of consistency verification.

In the flowchart, the color space conversion is applied first. Then four directional operators are applied to each component of (L*,a*,b*) to extract directional contrast. A single threshold is then applied over the estimated color contrast to detect boundaries. These directional data are merged together via the connection-and-verification process. In the connection-and-verification process, horizontal boundaries and vertical boundaries are checked first. Any two neighboring pixels without a boundary between them are connected together. Then, these 45° and 135° boundaries are checked to remove logically inconsistent connections.

Here we use Fig. 4.15 to illustrate the meaning of a logically consistent connection. Take the triplet of Pixel-A, Pixel-B and Pixel-C as an example. Let "=" denote there is no boundary between two neighboring pixels; "≠" denote there is a boundary between two neighboring pixels; and "∩" denote the logical AND. We have that

If A=B ***is true,***

then either (A=C)∩(B=C) ***or*** (A≠C)∩(B≠C) ***has to be true.***

Otherwise, the connection between Pixel-A and Pixel-B is logically inconsistent.

In this verification step, all logically inconsistent connections are disconnected. Surviving connections are then merged together to produce the final segmentation result.

Fig. 4.16(a) shows a color image. The segmented result of the proposed algorithm is shown in Fig. 4.16(b), represented in pseudo colors with $\sigma = 1.4$ and contrast-threshold = 23. Even though these two parameters are determined empirically, the parameter setting process is quite simple. Usually, a larger σ is used to better suppress noise, while a smaller σ value is used to distinguish tiny details. Similarly, a larger value of threshold is used to extract objects of larger intensity variations, while a small value of threshold is used to distinguish object details. In comparison, the parameter setting process is usually troublesome in many existing segmentation algorithms. Take the Deng and Manjunath's algorithm [15] as an example, as we choose a small quantization threshold, many tiny details are revealed but the uniform background is split into several regions, as shown in Fig. 4.16(c). On the contrary, as we increase the value of quantization threshold, the background is merged together, but many tiny objects, like the palm in Fig. 4.16(e), are mistakenly merged. These two algorithms were performed on a PC with an Intel Pentium III CPU, running at 800 Mhz and with 256 MB memory. Given a 512×512 color image, the CPU time is around 1 to 2 minutes for Deng and Manjunath's algorithm, is around 10 to 20 seconds and for our proposed algorithm, without performing code optimization.

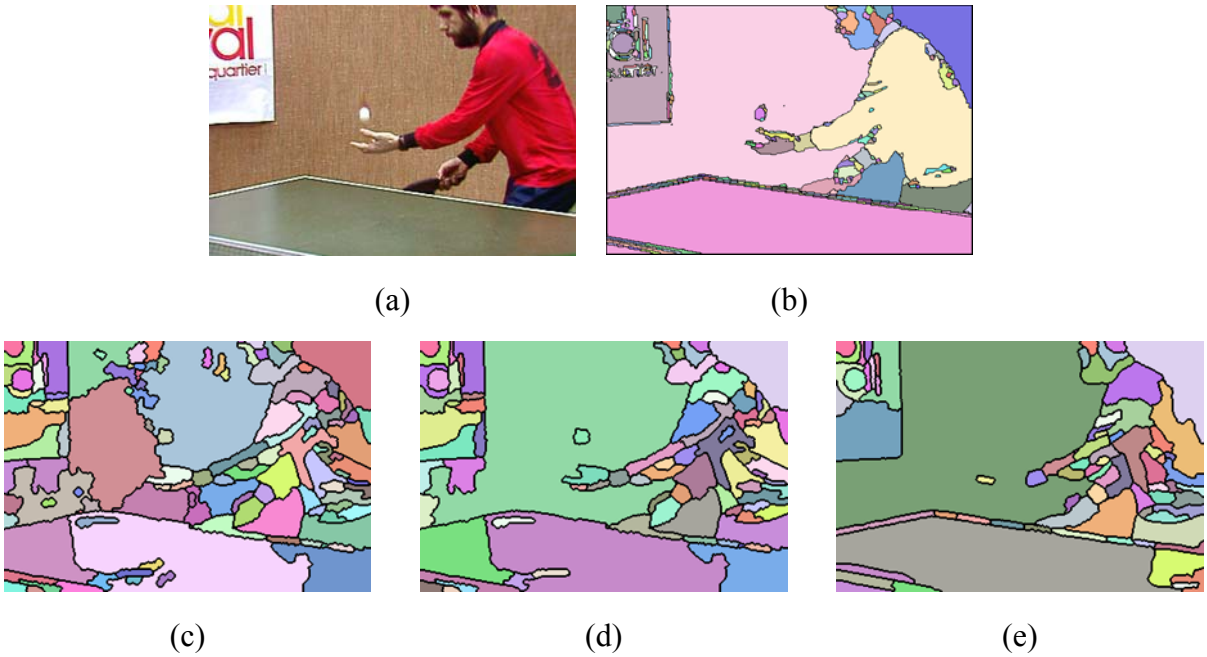

(a) (b)

(c) (d) (e)

Fig. 4.16 (a) Original image. (b) Segmentation result of the proposed algorithm, represented in pseudo-color, with $\sigma = 1.4$ and threshold = 23. (c)(d)(e) Segmentation results of the Deng and Manjunath's algorithm [15], represented in pseudo-color, with different threshold values.

In summary, in this section, we propose the use of contrast information for color image segmentation. We found that the contrast information is quite useful and reliable in detecting boundaries. To estimate the color contrast in a 2-D image, we use four directional operators to extract directional color contrast information. A single-threshold scheme is then applied over the estimated color contrast to detect directional boundaries. Finally, these directional boundaries are merged together via a connection and verification process to form 2-D boundaries. Based on the contrast definition, the simulation results demonstrate that this simple new algorithm is capable of providing reasonable and reliable results.

4.3.2 Color Segmentation Algorithm Based on Visible Color Difference

In image analysis and pattern recognition, color segmentation is a crucial step. So far, hundreds of color segmentation algorithms have already been developed to deal with various kinds of image-related applications. In our opinions, the development of color segmentation algorithm should be highly related to segmentation evaluation. In this section, we'll discuss how to apply previously proposed evaluation measures to facilitate the development of segmentation algorithms.

4.3.2.1 Modified Quantitative Visual Error Measures

In previous sections, to avoid directly measuring the subjectively perceived quality of color segmentation, we consider two objective visual quantities, the quantity of missing boundaries and the quantity of fake boundaries. Then, two quantitative measures, named intra-region visual error and inter-region visual error, are designed to measure the degrees of missing boundaries and fake boundaries, respectively. Given an $N \times M$ color image $f(x,y)$, we denote $ff(x,y)$ as a segmented result, with the color of each segmented region being filled with the average color of that region. Then the intra-region error is defined as

$$\mathrm{E}_{\mathrm{intra}}(I) = \frac{\sum_{x=1}^{N}\sum_{y=1}^{M} u(\left\| f(x,y) - ff(x,y) \right\|_{L^*a^*b^*} - th)}{N \times M}, \tag{4.16}$$

where $\| \|_{L^*a^*b^*}$ denotes the color difference in the CIE L*a*b* space, th denotes the threshold for visible color difference, and $u(.)$ denotes the step function. On the other hand, the inter-region visual error of a segmented image is defined as:

$$\mathrm{E}_{\mathrm{inter}}(I)=\frac{\sum_{i=1}^{R}\sum_{\substack{j=1\\ j\neq i}}^{R} w_{ij}\times u(th-\left\|ff_i-ff_j\right\|_{L^*a^*b^*})}{N\times M}, \tag{4.17}$$

where R denotes the number of segmented regions, and w_{ij} denotes the joined length between Region i and Region j. Here, w_{ij} is equal to zero if Region i and Region j are not connected.

In Section 4.2.1, a series of visual rating experiments had been made to demonstrate that the correlation between the intra-region visual error and the degree of missing boundaries is significant and the sign of the correlation is positive. Similarly, the correlation between the inter-region visual error and the degree of fake boundaries is verified to be significant and positive. In this section, two slightly modified measures, named "modified intra-region visual error" and "modified inter-region visual error", are proposed to further include the color distance values in the measures. The modified intra-region error is defined as:

$$\mathrm{ME}_{\mathrm{intra}}(I)=\frac{\sum_{x=1}^{N}\sum_{y=1}^{M}\left\{u(\left\|f(x,y)-ff(x,y)\right\|_{L^*a^*b^*}-th)\times(\left\|f(x,y)-ff(x,y)\right\|_{L^*a^*b^*}-th)\right\}}{N\times M} \tag{4.18}$$

In Table 4.13, for each of the 6 color images, we confirm that the correlation between the modified intra-region visual error and the perceived degree of missing boundaries in the visual rating experiments, which has been mentioned in Section 4.2.1, is significant at the 0.01 level and the sign of the correlation is positive. This implies that the modified intra-region visual error could also be an effective measure for the perceived degree of missing boundaries.

Table 4.13: Missing-boundary v.s. Modified Intra-region visual error

Correlation \ Color Image	Fruit	Lena	House	Tower	Room	Table Tennis
Missing-boundary vs. Intra-error	0.856**	0.962**	0.914**	0.961**	0.835**	0.950**

** correlation is significant at the 0.01 level (two-tailed) [59].

On the other hand, the modified inter-region error is defined as:

$$\mathrm{ME}_{\mathrm{inter}}(I)=\frac{\sum_{i=1}^{R}\sum_{\substack{j=1\\ j\neq i}}^{R}\left\{w_{ij}\times u(th-\left\|ff_i-ff_j\right\|_{L^*a^*b^*})\times(th-\left\|ff_i-ff_j\right\|_{L^*a^*b^*})\right\}}{N\times M} \quad (4.19)$$

In this section, we still set the threshold *th* in Equation (4.18) and Equation (4.19) to be 6, as mentioned in Section 4.1.2.

In Table 4.14, for each of the 6 color images, we confirm that the correlation between the modified inter-region visual error and the perceived degree of fake boundaries in the visual rating experiments is significant at the 0.01 level and the sign of the correlation is positive. This implies that the modified intra-region visual error could also be an effective measure for the perceived degree of fake boundaries.

Table 4.14: Fake-boundary v.s. Modified Inter-region visual error

Correlation \ Color Image	Fruit	Lena	House	Tower	Room	Table Tennis
Fake-boundary vs. Inter-error	0.961**	0.963**	0.978**	0.984**	0.968**	0.846**

** correlation is significant at the 0.01 level (two-tailed) [59].

Same as before, even though each of these two measures is image-dependent, the alliance of both measures may provide an effective way for the evaluation of color segmentation. As the given image is under-segmented, more boundaries are missing

and the modified intra-region visual error increases. On the contrary, as the image is over-segmented, more fake boundaries appear and the modified inter-region error increases. These two measures are complementary to each other. Therefore, we could combine the modified intra-region visual error and the modified inter-region visual error into a single measure, named the modified total visual error. That is,

$$\mathrm{ME}_{\mathrm{total}}(I) = M\mathrm{E}_{\mathrm{intra}}(I) + \lambda M\mathrm{E}_{\mathrm{inter}}(I). \tag{4.20}$$

Here, λ is set to be 5. In the following sections, based on these modified quantitative visual error measures, a color segmentation algorithm will be proposed.

4.3.2.2 Color Segmentation Algorithm Uniting with Quantitative Measures

In this section, we'll propose a color segmentation algorithm which unites with some quantitative visual measures. Given a color image, at the initial step, we produce an initial segmented image in which each pixel is regarded as an independent region. Then, for this initial segmented image, all the regions and the connection between any two adjacent regions are represented in a region adjacent graph (RAG) data structure. With the RAG, a merging process, consisting of a sorting procedure, a merging procedure, and an updating procedure, is used to further merge the segmented image. In the following subsections, the region adjacent graph data structure is introduced first and then the proposed color segmentation algorithm is presented.

4.3.2.2.1 Region Adjacent Graph

Region Adjacent Graph (RAG) data structure is a data structure consisting of two basic elements: nodes and edges [22]. Given a segmented result, each region can be denoted as a node and the connection between any two adjacent regions can be denoted as an undirected edge connecting two corresponding nodes. In mathematics, given a segmented result with R regions, the RAG is defined as an undirected graph G = (V, E), where V = {1, 2, …, R} and E denotes the set of undirected edges. Moreover, a weight e(i,j), with e(i,j) ∈ E if i, j ∈ V, is assigned to each edge to represent the connection relation. Here, the edge weight is assigned a nonzero value when the two regions are adjacent to each other. Fig. 4.17 shows an example to illustrate the relation between a segmented image and its corresponding RAG. Fig. 4.17(a) illustrates a segmented image containing five regions, R1, R2, R3, R4 and R5. Its corresponding RAG is shown in Fig. 4.17(b). In Fig. 4.17(b), the five nodes represent the five separate regions in Fig. 4.17(a), while the corresponding connections are denoted as the edges having the weights, e(1,2), e(1,3), …, and e(4,5).

Furthermore, after a merging process, the processed result of an RAG can also be represented with another RAG. For the RAG in Fig. 4.17(b), if the regions R4 and R5 are merged, the result can be described by another RAG, as shown in Fig. 4.17(c). Here, the weight e(4,5) between R4 and R5 is removed, and the weights related to R4 and R5, such as e(2,3) and e(3,4), are updated. As shown in Fig. 4.17(d), the merged result is represented in a new RAG. The merged node of R4 and R5 is denoted as R'4, while the updated edges, e(2,3) and e(3,4), are represented as e'(2,3) and e'(3,4), respectively.

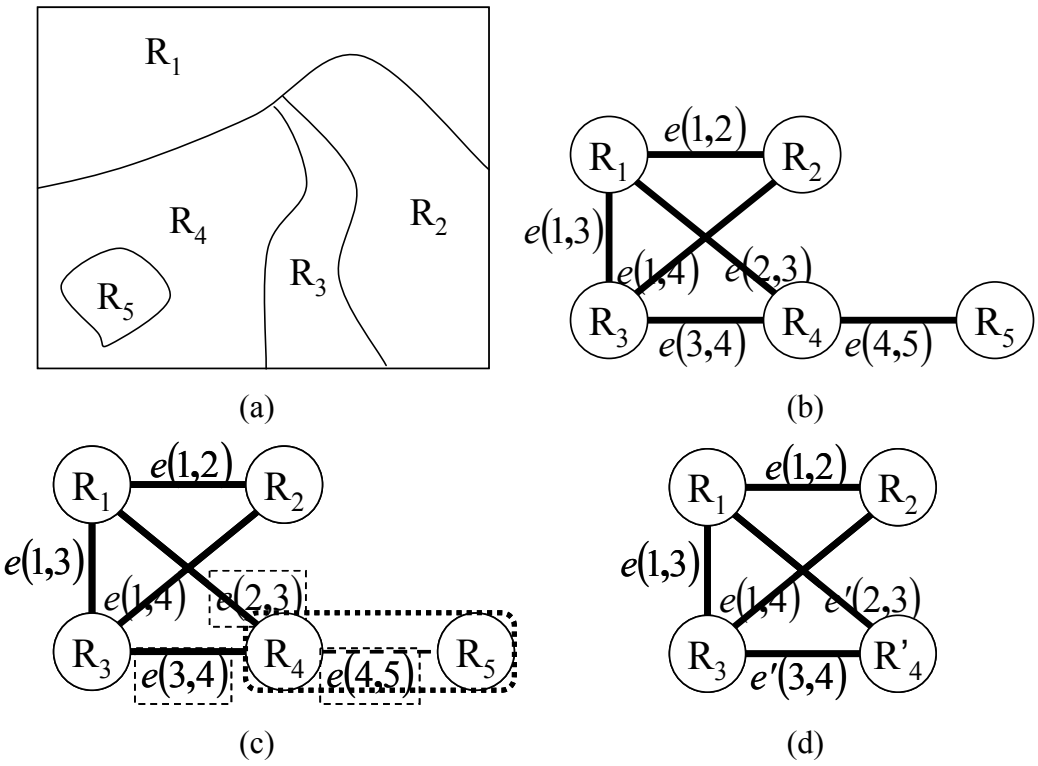

Fig. 4.17 An Image Segmentation of Five Regions and Its Corresponding RAG.

4.3.2.2.2 Color Segmentation Uniting with Quantitative Measures

The flowchart of the proposed color segmentation algorithm is shown in Fig. 4.18. Given a color image, at the initial step, each pixel is regarded as an independent region. This sets up an initial RAG. Here, the connection relation is referred to the cost if the corresponding two regions are to be merged into one region.

Based on the initial RAG, two regions are merged into one region each time. Within one iteration, there would be one sorting procedure, one merging procedure, and one updating procedure. For the sorting procedure, all the edge weights of the current RAG are sorted in an ascending order. Then, the two regions with the minimal edge weight are merged into one region in the merging procedure. The weights relating to the two regions are updated in the updating procedure and a new RAG is generated accordingly. The iterative process continues till some predefined stop

criterion is satisfied.

In the proposed segmentation algorithm, we define the edge weight of an edge as

$$e(i, j) = f_k(R_i, R_j), \tag{4.21}$$

where $f_k(R_i, R_j)$, with $k=1, 2, 3,$ denotes a cost function made of some quantitative measurements, like the modified total visual error, the F-function, or the PSNR function. This cost function denotes the cost produced by merging R_i and R_j into one region. For example, we may define the cost function to be

$$f_1(R_i, R_j) = PSNR(R_i) + PSNR(R_j) - PSNR(R_i, R_i); \tag{4.22}$$

$$f_2(R_i, R_j) = F(R_i, R_i) - F(R_i) - F(R_j); \tag{4.23}$$

or

$$f_3(R_i, R_j) = ME_{intra}(R_i, R_i) - ME_{intra}(R_i) - ME_{intra}(R_j) - \lambda\, ME_{inter}(R_i, R_j). \tag{4.24}$$

As mentioned above, for the PSNR function, the preferred segmented results are the images with larger PSNR values. Since the merging of two regions into one region usually decreases the PSNR value, the weight function in Equation (4.22) is assigned to be the subtraction of $PSNR(R_i, R_j)$ from the summation of $PSNR(R_i)$ and $PSNR(R_j)$. On the contrary, since the merging of two regions usually increases the value of the F-function, the weight function in Equation (4.23) is assigned the increased F-function value. On the other hand, for the modified total visual error, the merging process usually increases the modified intra error while decreases the modified inter error at the same time. Hence, the weight function in Equation (4.24) is assigned the summation of the increased modified intra-region error value and the decreased modified inter-region error value.

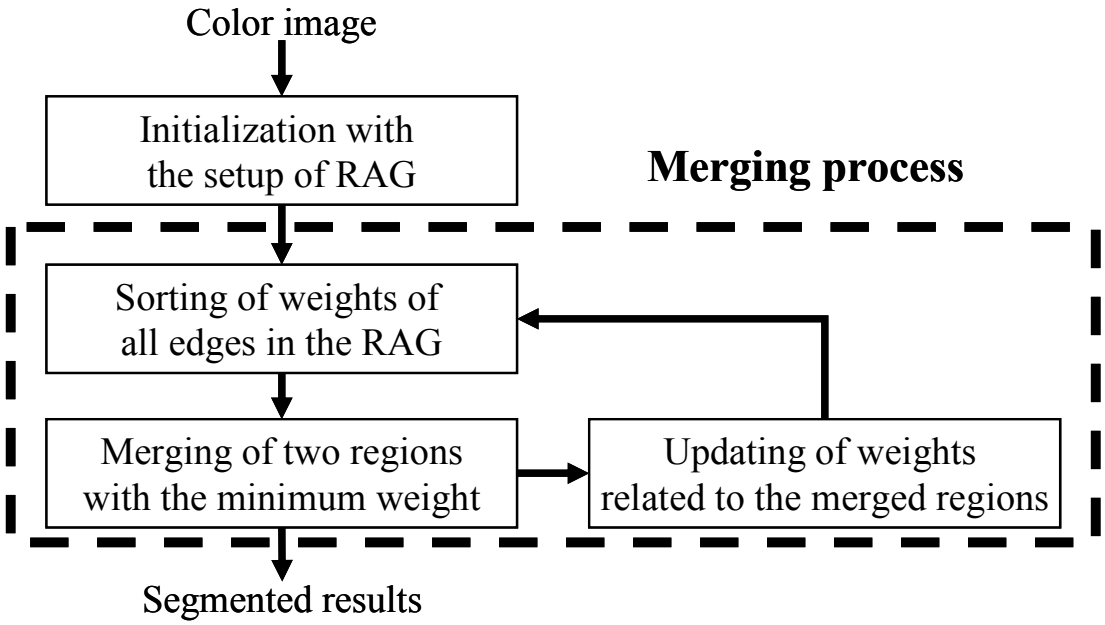

Fig. 4.18 Flowchart of the Proposed Color Segmentation Algorithm.

Assume we adopt the modified total error to define the edge weights, then a segmented result with a smaller modified total error is regarded as a better segmented result. During the merging process, the modified inter-region error decreases while the modified intra-region error increases. In our proposed algorithm, we actually define the stop criterion to be the point when the modified intra-region error reaches a threshold C_1. That is, the iterative process stops when $ME_{intra}(I) \geq C_1$. Here, C_1 is a application-dependent constant. The use of a threshold over the modified intra-region error is to allow some degree of under segmentation.

Figs. 4.19(a)-(f) show the results produced by using the proposed segmentation algorithm with use of the modified total error. Fig. 4.19(a) is an 84×128 color image named “Tower”. Fig. 4.19(b) is the segmented result which contains 700 segmented regions, with MEintra = 0.036 and MEinter = 0.012. In Fig. 4.19(b), it can be seen that pixels with invisible color difference are merged into regions while pixels with visible color difference are treated as image edges.

On the other hand, the segmented results with fewer details, like the segmented result in Fig. 4.19(d) and (e), are sometimes useful for many applications. To fit for different requirements, we may adjust the constant C_1 in the stop criterion. Figs. 4.19(c)(d)(e) show the segmented results with C_1 = 0.673, 1.63 and 2.24, respectively. Fig. 4.19(c) shows a finer segmented image containing 60 regions in total, while Fig. 4.19(d) and Fig. 4.19(e) show two coarser results containing 19 and 12 regions, respectively. In Fig. 4.19(c), we can see some finer detials, like grasses on the ground and clouds in the sky. On the contrary, the segmented result in Fig. 4.19(e) is much coarser.

Moreover, the plot of the modified intra error versus the modified inter error is given in Fig. 4.19(f). In this figure, the triangle, the square, and the circle denote the error pairs of Figs. 4.19(c), (d) and (e), respectively. It can be seen that by setting different threshold values over the modified intra-region error, we can obtain different segmentation results with different degrees of under-segmentation.

Figs. 4.20(a)-(i) show the comparison of the segmented results produced by the proposed algorithm uniting with the modified total visual error, the F function, and the PSNR function. Fig. 4.20(a) is a 128×88 color image, named “Tennis”. Fig. 4.20(b) shows the segmented results having 90 regions, with MEintra = 1.19 produced by the proposed algorithm. Fig. 4.20(c) shows the average color representation of Fig. 4.20(b). For the PSNR function, Figs. 4.20(d)(e)(f) show the segmented results having 1000, 90 and 30 regions, respectively. As mentioned above, the use of the PSNR function only measures the within-region color difference but not the color contrast between adjacent regions. Hence, over-segmented results are expected. For example, if compared with Fig. 4.20(b), some regions in Fig. 4.20(e), like the background regions, are over-segmented. On the other hand, Figs. 4.20(g)(h)(i) show the segmented results having 1000, 90 and 30 regions when the F-function is used in the

cost function. As mentioned above, the methods by using the F-function directly may generate both over-segmented regions and under-segmented regions at the same time. For example, even though some parts of the player's hand in Fig. 4.20(g) have already been mistakenly merged into the background, many small regions still exist in the segmented image.

In Figs. 4.21(a)-(c) and Figs 4.22(a)-(c), two more segmented results are shown. Fig. 4.21(a) shows a 128×100 image and Figs. 4.21(b)(c) show the segmented results containing 7 regions with MEintra = 2.16. Fig. 4.22(a) is a 56×128 image and Figs. 4.22(b)(c) are the segmented results containing 10 regions with MEintra = 2.49.

(a)

(b)

(c)

(d)

(e)

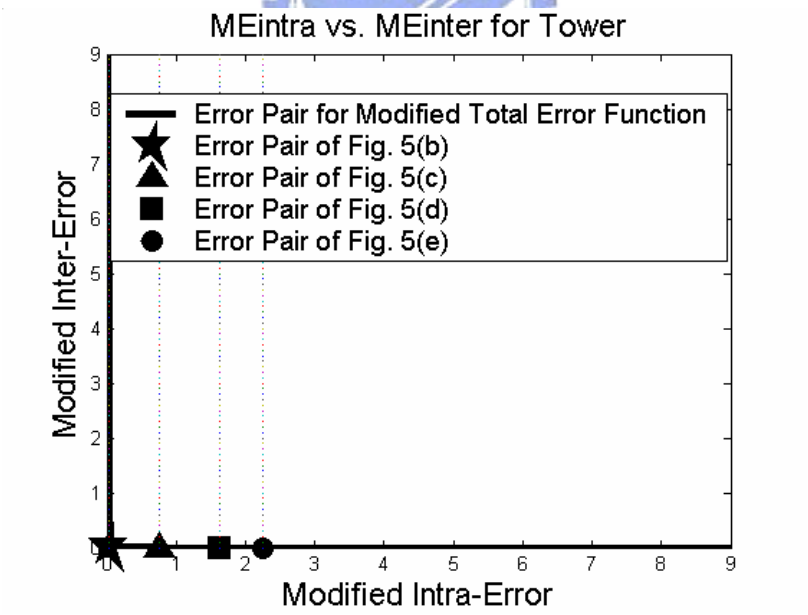

(f)

Fig. 4.19 Segmentation uniting with Modified Total Visual Error.

(a) Original Image.

(b) Segmented Results with minimum Modified Total Error.

(c)(d)(e) Segmented Results with MEintra = 0.763, 1.63, and 2.24.

(f) Plot of Modified Intra Error versus Modified Inter Error.

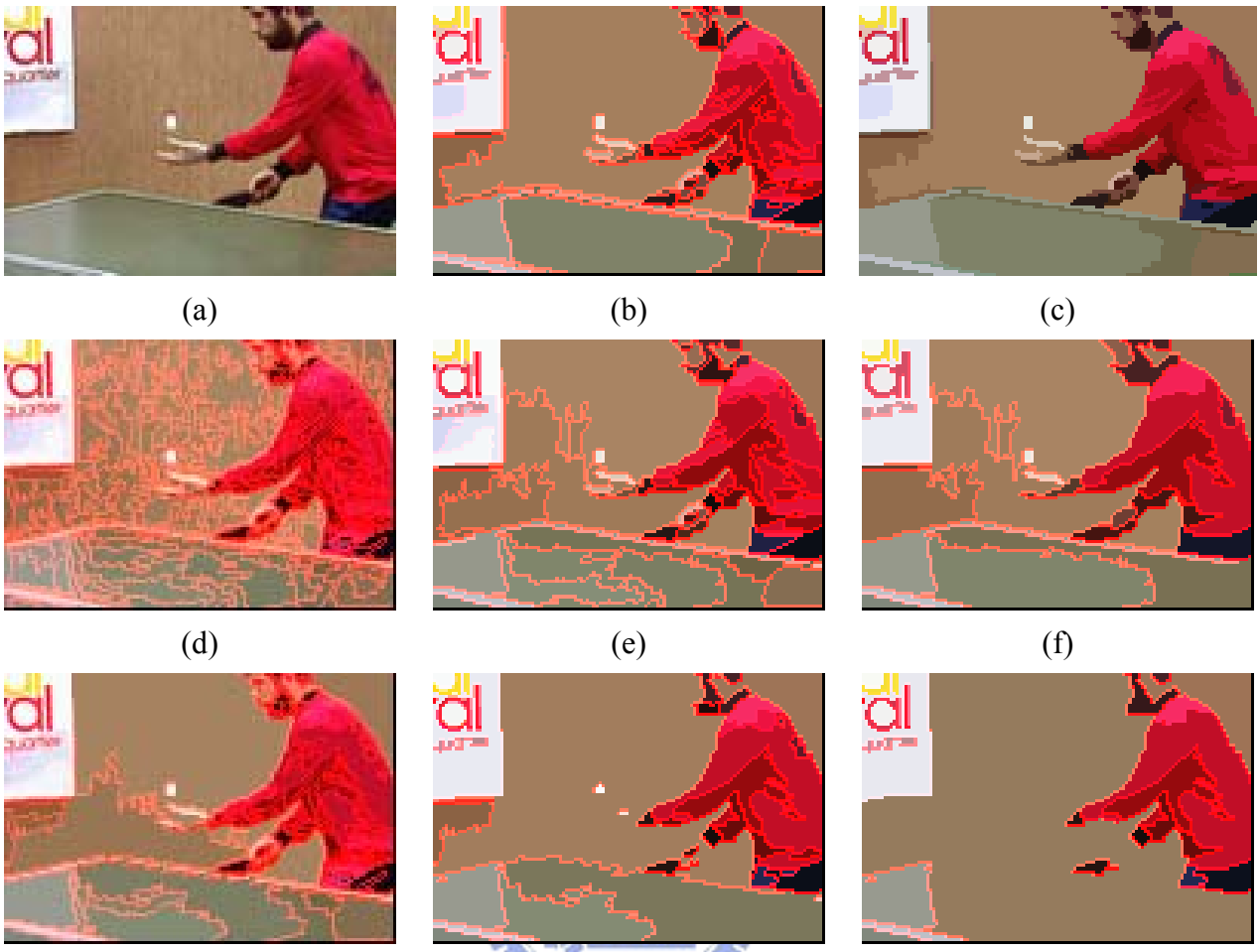

Fig. 4.20 Color Segmentation with Quantitative Measures for “Tennis” Image.

(a) Original Image.

(b) Segmented Result with MEintra=1.19 for the proposed algorithm.

(c) Averaged Color Representation of (b).

(d)-(f) Segmented Results for the PSNR Function.

(g)-(i) Segmented Results for the F Function.

(a) (b) (c)

Fig. 4.21 Segmentation for “Hand” Image.

(a) Original Image.

(b) Segmented Result with MEintra = 2.16.

(c) Averaged Color Representation of (b).

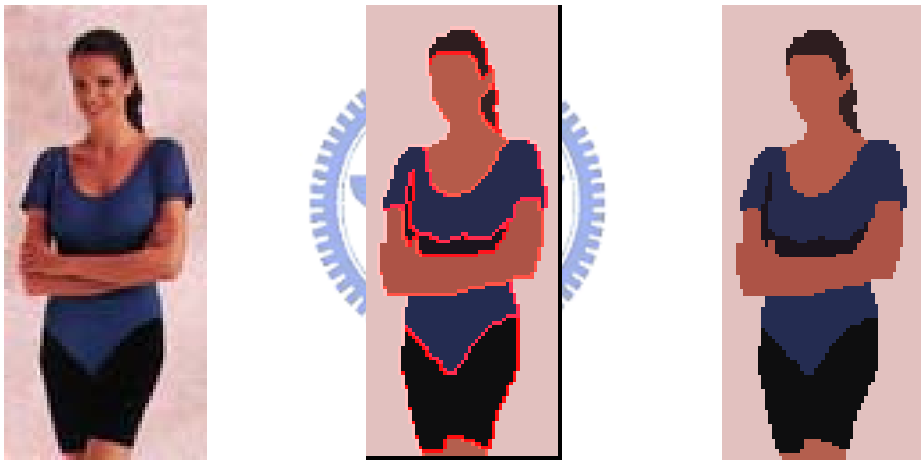

(a) (b) (c)

Fig. 4.22 Segmentation for “Woman” Image.

(a) Original Image.

(b) Segmented Result with MEintra = 2.49.

(c) Averaged Color Representation of (b).

CHAPTER 5

Conclusions

In this dissertation, image analysis techniques based on luminance/color contrast are presented. To mimic the way humans perform image analysis, we perform subjective experiments to deduce useful subjective visual quantities. Some suitable objective visual quantities are then designed to quantify these subjective visual quantities. In this dissertation, a few definitions of luminance/color contrast are especially used to quantify these visual quantities. Based on these objective visual quantities, effective and efficient quantitative measures are developed for various kinds of applications.

In this dissertation, we consider two image analysis applications: 1) automatic inspection for visual defects on LCD panels, and 2) color segmentation. In the problem of automatic defect inspection, we follow Mori's proposal to quantify the degrees of image defects, based on the luminance contrast and area size of visual defects. Based on Mori's subjective experiments, which were performed to relate human visual perception with the contrast and size of visual defects, and the SEMU formula, which was proposed by Mori et al for the quantitative measurement of visual

perception, we can effectively quantify the degrees of visual defects in terms of luminance contrast and defect size. In this dissertation, 2-D LOG operators and 1-D LOG operators are presented to detect Cluster Mura and V-Band Mura, respectively. Specifically, to detect round-type/rectangular-type cluster Mura defects, the use of 2-D round-type /rectangular LOG filters are suggested. Based on SEMU formula, we presented an optimal thresholding mechanism in the inspection of Cluster Mura. On the other hand, a curvature-based approach is proposed to detect V-Band Mura. In the curvature-based approach, a 1-D LOG filter is used to generate a smooth curve that represents the curvature tendency of the 1-D projected profile. With this smooth curve, V-Band Mura defects can be detected easily. In simulation, the results demonstrate the LOG filters, unifying with measures of visual quantities, are very useful in the inspection of Mura defects.

In the problem of color segmentation, we estimate the degrees of missing boundaries and fake boundaries, instead of directly evaluating the subjective quality of color segmentation. With the combination of these two quantities, we can well quantify the subjective evaluation of color segmentation. Moreover, based the definition of visible color difference, we design two measures, the intra-region visual error and inter-region visual error, to estimate the degrees of missing boundaries and fake boundaries, respectively. We found these two measures have significant correlation with the degree of missing boundaries and the degree of fake boundaries. With these two measures, an evaluation scheme is proposed to evaluate the segmentation results and to help the automatic selection of the parameters for a given segmentation algorithm. On the other hand, we also present a color segmentation algorithm uniting with quantitative visual measures. In this algorithm, two more quantitative measures, named modified intra-region visual error and modified inter-region visual error, are designed to measure the degrees of missing boundaries

and fake boundaries, respectively. Combing these two visual errors, the modified total visual error is used to measure the amount of visible errors for segmented results. With these quantitative visual measures, a merging process based on the region adjacent graph (RAG) data structure is adopted to generate segmentation results with small intra-region errors. The experiments demonstrate the proposed color segmentation algorithm does offer flexible and reasonable segmented results.

Bibliography

[1] P. Whittle, “The Psychophysics of Contrast Brightness,” In A. L. Gilchrist (Ed.), *Lightness, Brightness, and Transparency*, pp. 35-110. Hillsdale, NJ: Lawrence Erlbaum Associates, 1994.

[2] Semiconductor Equipment and Materials International (SEMI) Standard, “New Standard: Definition of Measurement Index (SEMU) for Luminance Mura in FPD Image Quality Inspection,” draft number: 3324, pp. 1-6, 2002.

[3] Y. Mori, R. Yoshitake, T. Tamura, T. Yoshizawa and S. Tsuji, “Evaluation and Discrimination Method of “Mura” in Liquid Crystal Displays by Just Noticeable Difference Observation,” Proceedings of SPIE (The International Society for Optical Engineering), Optomechatronic Systems III, vol. 4902, pp. 715-722, Oct. 2002.

[4] D. G. Lee, I. H. Kim, M. C. Jeong, B. K. Oh, and W. Y. Kim, “Mura Analysis Method by Using JND Luminance and The SEMU Definition,” Proceedings of SID (Society for Information Display), pp. 1467-1470, 2003.

[5] T. Tamura, M. Baba and T. Furuhata, “Effect of The Background Luminance on Just Noticeable Difference Contrast of ‘Mura’ in LCDs,” Proceedings of SID (Society for Information Display), pp. 1527-1530, 2003.

[6] R. S. Berns, “Billmeyer and Saltzman’s Principles of Color Technology, 3rd Edition,” John Wiley and Sons, 2000.

[7] http://cit.dixie.edu/vt/reading/gamuts.asp, “Illustration of The CIE L*a*b* Color Space”.

[8] K. N. Plataniotis and A. N. Venetsanopoulos, “Color Image Processing and Applications,” Springer, 2000.

[9] Video Electronics Standards Association (VESA): Flat Panel Display Measurements Standard, version 2.0.

[10] Y. Mori, K. Tanahashi, and S. Tsuji, “Quantitative Evaluation of Visual Performance of Liquid Crystal Displays,” Proceedings SPIE (The International Society for Optical Engineering), The Algorithms and Systems for Optical

Information Processing, vol. 4113, pp. 242-249, 2000.

[11] W. K. Pratt, S. S. Sawkar, and K. O'Reilly, "Automatic Blemish Detection in Liquid Crystal Flat Panel Displays," Proceedings of SPIE (The International Society for Optical Engineering), vol. 3306, pp. 2-13, 1998.

[12] V. Gibour and T. Leroux, "Automated, Eye-like Analysis of Mura Defects," Proceedings of SID (Society for Information Display), pp. 1440-1443, 2003.

[13] L. Lucchese and S. K. Mitra, "Color Image Segmentation: A State-of-The-Art Survey," Proc. The Indian National Science Academy (INSA-A), vol. 67, A, no.2, pp. 207-221, New Delhi, India, Mar. 2001.

[14] W. Y. Ma and B. S. Manjunath, "Edge Flow: A Technique for Boundary Detection and Image Segmentation," *IEEE Trans. Image Processing*, vol. 9, no. 8, pp. 1375-1388, 2000.

[15] Y. Deng, and B. S. Manjunath, "Unsupervised Segmentation of Color-texture Regions in Images and Video," *IEEE Trans. Pattern Anal. Mach. Intell.*, vol. 23, no. 8, pp. 800-810, Aug. 2001.

[16] J. Canny, "A Computational Approach to Edge Detection," *IEEE Trans. Pattern Anal. Machine Intell.*, vol. 8, no. 6, pp. 679-698, Nov. 1986.

[17] A. Cumani, "Edge Detection in Multispectral Images," *CVGIP: Graphical Models and Image Processing*, vol. 53, no. 1, pp. 40-51, Jan. 1991.

[18] W. Y. Ma and B.S. Manjunath, "Edge Flow: A Framework of Boundary Detection and Image Segmentation," Proc. IEEE Conf. on Computer Vision Pattern Recognition, pp. 744-749, June 1997.

[19] C. Xu and J. L. Prince, "Snakes, Shapes, and Gradient Vector Flow," *IEEE Trans. Image Processing*, vol. 7, no.3, pp. 359-369, Mar. 1998.

[20] L. Vincent and P. Soille, "Watersheds in Digital Space: An Efficient Algorithm Based on Immersion Simulations," *IEEE Trans. Pattern Anal. Machine Intell.*, vol. 13, no. 6, pp. 583-598, June 1991.

[21] S. C. Zhu and A. Yuille, "Region Competition: Unifying Snakes, Region Growing, and Bayes/MDL for Multiband Image Segmentation," *IEEE Trans. Pattern Anal. Machine Intell.*, vol. 18, no. 9, pp.884-900, Sep. 1996.

[22] K. Haris, S. N. Efstratiadis, N. Maglaveras, and A. K. Katsaggelos, "Hybrid Image Segmentation Using Watersheds and Fast Region Merging," *IEEE Trans. Image Processing*, vol. 7, no. 12, pp. 1684-1699, Dec. 1998.

[23] Y. Deng, B.S. Manjunath and H. Shin*, "Color Image Segmentation," Proc. IEEE Conf. on Computer Vision Pattern Recognition, vol. 2, pp. 446-451, June 1999.

[24] G. T. Herman, B. M. Carvalho, "Multiseeded Segmentation Using Fuzzy Connectedness," *IEEE Trans. Pattern Anal. Machine Intell.*, vol. 23, no. 5, pp.

460-474, May 2002.

[25] I. Vanhamel, I. Pratikakis, and H. Sahli, "Multiscale Gradient Watersheds of Color Images," *IEEE Trans. Image Processing*, vol. 12, no. 6, pp. 617-626, June 2003.

[26] M. A. Ruzon and C. Tomasi. "Edge, Junction, and Color Detection Using Color Distribution," *IEEE Trans. Pattern Anal. Machine Intell.*, vol. 23, no.11, pp. 1281-1295, Nov. 2001.

[27] D. Comaniciu and P. Meer, "Mean Shift: A Robust Approach toward Feature Space Analysis," *IEEE Trans. Pattern Anal. Mach. Intell.*, vol. 24, no. 5, pp. 603-619, May 2002.

[28] Y. Cheng, "Mean Shift, Mode Seeking, and Clustering," *IEEE Trans. Pattern Anal. Machine Intell.*, vol. 17, no. 8, pp. 790-799, Aug. 1995.

[29] J. Shi and J. Malik, "Normalized cuts and image segmentation," Proc. IEEE Conf. on Computer Vision Pattern Recognition, pp. 731-737, June 1997.

[30] D. Comaniciu and P. Meer, "Robust Analysis of Feature Spaces: Color Image Segmentation," Proc. IEEE Conf. on Computer Vision Pattern Recognition, pp. 750-755, June 1997.

[31] T. Hofmann, J. Puzicha, and J. M. Buhmann, "Unsupervised Texture Segmentation in a Deterministic Annealing Framework," *IEEE Trans. Pattern Anal. Machine Intell.*, vol. 20, no. 8, pp. 803-818, Aug. 1998.

[32] D. Comaniciu and P. Meer, "Mean Shift Analysis and Applications," Proc. IEEE Conf. on Intl. Conf. on Computer Vision, vol. 2, pp. 1197-1203, Kerkyra, Greece, Sep. 1999.

[33] M. A. Ruzon and C. Tomasi, "Color Edge Detection with The Compass Operator," Proc. IEEE Conf. on Computer Vision Pattern Recognition, vol. 2, pp. 160-166, June 1999.

[34] J. Shi and J. Malik, "Normalized Cuts and Image Segmentation," *IEEE Trans. Pattern Anal. Machine Intell.*, vol. 22, no. 8, pp. 888-905, Aug. 2000.

[35] H. D Cheng and Y. Sun, "A Hierarchical Approach to Color Image Segmentation Using Homogeneity," *IEEE Trans. Image Processing*, vol. 9, no. 12, pp. 2071-2082, Dec. 2000.

[36] T. W. Lee and M. S. Lewicki, "Unsupervised Image Classification, Segmentation, and Enhancement Using ICA Mixture Models," *IEEE Trans. Image Processing*, vol. 11, no. 3, pp. 270-279, Mar. 2002.

[37] Z. Tu and S. C. Zhu, "Image Segmentation by Data-Driven Markov Chain Monte Carlo," *IEEE Trans. Pattern Anal. Machine Intell.*, vol. 24, no. 5, pp. 657-673, May 2002.

[38] C. Carson, S. Belongie, H. Greenspan, and J. Malik , "Blobworld Image

Segmentation Using Expectation-Maximization and Its Application to Image Querying," *IEEE Trans. Pattern Anal. Machine Intell.*, vol. 24, no. 8, pp. 1026-1038, Aug. 2002.

[39] O. J. Tobias and R. Seara, "Image Segmentation by Histogram Thresholding Using Fuzzy Sets," *IEEE Trans. Image Processing*, vol. 11, no. 12, pp. 1457-1465, Dec. 2002.

[40] T. Gevers, "Adaptive Image Segmentation by Combining Photometric Invariant Region and Edge Information," *IEEE Trans. Pattern Anal. Machine Intell.*, vol. 24, no. 6, pp. 848-852, June 2002.

[41] H. D. Cheng, X. H. Jiang, Y. Sun, and J. Wang, "Color Image Segmentation: Advances and Prospects," *Pattern Recognit.*, vol. 34, no. 6, pp. 2259-2281, Dec. 2001.

[42] Y. J. Zhang, "A Survey on Evaluation Methods for Image Segmentation," *Pattern Recognit.*, vol. 29, no.8, pp. 1335-1346, Aug. 1996.

[43] Y. J. Zhang, "A Review of Recent Evaluation Methods for Image Segmentation," Proc. 6th Int. Symp. on Signal processing and its applications, pp. 148-151, Kuala Lumpur, Malaysia, Aug. 2001.

[44] M. D. Heath, S. Sarkar, T. Sanocki, and K. W. Bowyer, "A Robust Visual Method for Assessing The Relative Performance of Edge-detection Algorithms," *IEEE Trans. Pattern Anal. Mach. Intell.*, vol. 19, no. 12, pp. 1338-1359, Dec. 1997.

[45] A. Hoover, G. Jean-Baptiste, X. Jiang, P. J. Flynn, H. Bunke, D. B. Goldgof, K. Bowyer, D. W. Eggert, A. Fitzgibbon, and R. B. Fisher, "An Experimental Comparison of Range Image Segmentation Algorithms," *IEEE Trans. Pattern Anal. Mach. Intell.*, vol. 18, no. 7, pp. 673-689, July 1996.

[46] P. L. Correia and F. Pereira, "Objective Evaluation of Video Segmentation Quality," *IEEE Trans. Image Processing*, vol. 12, no.2, pp. 186-200, Feb. 2003.

[47] D. D. Martin, C. C. Fowlkes, D. Tal, and J. Malik, "A Database of Human Segmented Natural Images and Its Application to Evaluating Segmentation Algorithms and Measuring Ecological Statistics," Proc. IEEE Int. Conf. on Computer vision, vol. 2, pp. 416-423, Vancouver, Canada, July 2001.

[48] D. R. Martin, C. C. Fowlkes, and J. Malik, "Learning to Detect Natural Image Boundaries Using Local Brightness, Color, and Texture Cues," *IEEE Trans. Pattern Anal. Mach. Intell.*, vol. 26, no. 5, pp. 530-549, May 2004.

[49] J. Liu and Y. H. Yang, "Multiresolution Color Image Segmentation," *IEEE Trans. Pattern Anal. Mach. Intell.*, vol. 16, no. 7, pp. 689-700, July 1994.

[50] M. Borsotti, P. Campadelli, and R. Schettini, "Quantitative Evaluation of Color Image Segmentation Results," *Pattern Recognit. Letters*, vol. 19, no. 8, pp.

741-747, June 1998.

[51] Intel corp. patent, "Anti-Aliasing Diffractive Aperture and Optical System Using The Same," US. Patent: 5940217, Aug. 1999.

[52] "Aliasing Reduction in Discrete Imaging System Using Pupil Function Controlling," Proceedings of Acta Opt. Sin., vol. 19, no.3, pp.289-294, 1999.

[53] G. Wyszecki and W. Stiles, "Color Science: Concepts and Methods, Quantitative Data and Formulae, 2nd Edition," New York: John Wiley and Sons, 1982.

[54] International Electrotechnical Commission (IEC) 61966-2-1, http://www.iec.ch, "sRGB – Default RGB colour space," Oct. 1999.

[55] G. Sharma and H. J. Trussell, "Digital Color Image," *IEEE Trans. Image Processing*, vol. 6, no. 7, pp. 901-932, July 1997.

[56] J. Y. Hardeberg, "Acquisition and Reproduction of Colour Images: Colorimetric and Multispectral Approaches," PhD dissertation, Ecole Nationale Supérieure des Télécommunications', Paris, France, 1999.

[57] ITU-R Recommendation BT. 500-11, "Methodology for The Subjective Assessment of The Quality of Television Pictures", Geneva, 2002 (available at http://www.itu.org).

[58] S. Siegel, "Nonparametric Statistics for The Behavioral Sciences," McGraw-Hill Kogakusha Ltd., Tokyo, 1956.

[59] R. A. Ronald and F. Yates, "Statistical Methods for Research Workers, 14th Edition," Oliver and Boyd Ltd., Edinburgh, 1970.

Curriculum Vita

Name:

Hsin-Chia Chen (陳信嘉) Born on Sep. 7, 1976.

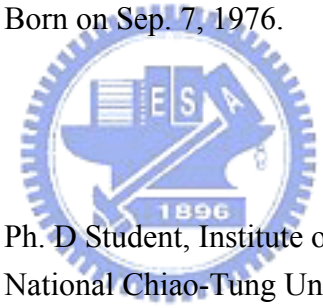

Education:

Sep. 2000 ~ June 2006	Ph. D Student, Institute of Electronics, National Chiao-Tung University, Hsin-chu, Taiwan
Sep. 1999 ~ June 2000	M.S. Student, Institute of Electronics, National Chiao-Tung University, Hsin-chu, Taiwan
Sep. 1995 ~ June 1999	B.S. Student, Institute of Electronics, National Chiao-Tung University, Hsin-chu, Taiwan

Work Experience:

Oct. 2004 ~ June 2006	Work in Pixart Imaging Inc. (原相科技)
Jan. 2004 ~ Oct. 2004	Cooperating with ITRI (工業技術研究院) for Project "Defect Inspection and Evaluation for LCDs".
July 1999 ~ Aug. 1999	Summer Job in Texas Instrument Corp. (德州儀器)

Publications:

Dissertation:

Ph. D Dissertation: A Study of Image Analysis Techniques Based on Luminance/Color Contrast
(以亮度／色彩對比為基礎的影像分析技術之研究)

Journal Papers:

[1] H. C. Chen, W. J. Chien, and S. J. Wang, "Contrast-Based Color Image Segmentation," *IEEE Signal Processing Letters*, vol. 11, no. 7, pp. 641-644, July 2004.

[2] H. C. Chen and S. J. Wang, "Visible Color Difference Based Quantitative Evaluation of Color Segmentation," in *IEE Proceedings – Vision, Image & Signal Processing*, 8 pages. (to be published)

Conference Papers:

[1] H. C. Chen, W. J. Chien, and S. J. Wang, "Contrast-Based Color Image Segmentation with Adaptive Thresholds," in IEEE Proceeding on International Conference Image Processing, vol. 2, pp. 73-76, Rochester, New York, USA, Sep. 2002.

[2] H. C. Chen and S. J. Wang, "The Use of Visible Difference in The Quantitative Evaluation of Color Image Segmentation," in IEEE Proceeding on Acoustics, Speech, and Signal Processing, vol. 3, pp. 593-596, Montreal, Quebec, Canada, May 2004.

[3] H. C. Chen, L T. Fang, Louis Lee, C. H. Wen, S. Y. Cheng, and S. J. Wang, "Log-Filter-Based Inspection of Cluster Mura and Vertical−Band Mura on Liquid Crystal Displays," Proceedings of the SPIE, Volume 5679, pp. 257-265, Jan. 2005.

[4] J. J. Tsai and H. C. Chen, "Predictive Block-Matching Discrepancy Based Rhombus Pattern Search for Block Motion Estimation," in IEEE Proceeding on International Conference Image Processing, Genoa, Italy, Sep. 2005.

[5] H. C. Chen and S. J. Wang, "Color Segmentation Uniting with Quantitative Visual Error Measures," in the 6th IEEE International Symposium on Signal Processing and Information Technology, Vancouver, Canada, Aug. 2006. (accepted)

Filed U.S. Patents:

[1] C. H. Lin, H. C. Chen, J. J. Tsai, Yi-Fang Lee, Hsuan-Hsien Lee and Tsai-Yi Chao, "Orientation Device and Method for Coordinate Generation Employed Thereby", Filing No.: 11/392,089, Filing Date: Mar. 28, 2006.

[2] C. H. Lin, H. C. Chen, J. J. Tsai, and T. Y. Chao, "Apparatus and Method for Audio Encoding", Filing No.: 11/391,752, Filing Date: Mar. 28, 2006.

[3] H. C. Chen and T. Y. Chao, "Method and Apparatus for Estimating Relative Motion Based on Maximum Likelihood and Its Application to Optical Mouse", Filing No.: 11/420,715, Filing Date: May 26, 2006.

[4] H. C. Chen, Y. F. Lee, and T. Y. Chao, "Displacement Estimation Device and Method for the Same" (filing).

Filed Taiwan Patents:

[1] 林志新、陳信嘉、蔡彰哲、李宜方、李宣賢、趙子毅，"指向裝置之指向點定位方及其裝置"，申請案號：94115044.0，申請日：94.05.11.

[2] 林志新、陳信嘉、蔡彰哲、趙子毅，"音訊編碼裝置及方法"，申請案號：94124914，申請日：94.07.22.

[3] 陳信嘉、李宜方、趙子毅，"位移估測方法與裝置"，申請案號：94147531，申請日：94.12.30.

[4] 魏守德、陳信嘉、趙子毅，"點陣型圖案的設計及其解碼方法與裝置"，申請案號：95107426，申請日：95.03.06.

[5] 趙子毅、吳孟聰、林志新、陳信嘉、黃昭荐、李宣賢、李宜方，"指向裝置方法及應用"，申請案號：95116011，申請日：95.05.05.

[6] 陳信嘉、趙子毅、李宜方、林俊煌、藍正豐，"用以估測訊號頻率的碰撞演算法及位移估測方法與裝置" (filing)